Swarm equilibria in domains with boundaries

by

Mitchell Anthony Kovacic

M.Sc., University of Ontario Institute of Technology, 2013
B.Sc., University of Ontario Institute of Technology, 2011

Thesis Submitted in Partial Fulfillment of the
Requirements for the Degree of
Doctor of Philosophy

in the
Department of Applied Mathematics
Faculty of Science

SIMON FRASER UNIVERSITY
Summer 2018

Approval

Name:	**Mitchell Anthony Kovacic**
Degree:	**Doctor of Philosophy (Mathematics)**
Title:	**Swarm equilibria in domains with boundaries**
Examining Committee:	**Chair:** Weiran Sun Assistant Professor
	Razvan Fetecau Senior Supervisor Associate Professor
	JF Williams Co-Supervisor Associate Professor
	Ralf Wittenberg Internal Examiner Associate Professor
	Andrew Bernoff External Examiner Professor Department of Mathematics Harvey Mudd College
Date Defended:	**August 13th, 2018**

Abstract

This thesis involves the study of a well-known swarming model with interaction and external potentials in one and two dimensions. We refer to this model as the plain aggregation model and later study the model with nonlinear diffusion, so-called the diffusive model here. Typically set in free space, one of the novelties of this thesis is the study of such swarming models in the presence of a boundary. We consider a no-flux boundary condition enforced in a particle context via a "slip" condition. Of particular relevance to the context of this thesis, the swarming model used here can be formulated as an energy gradient flow and thusly, one might expect equilibrium states to be minima of the energy.

In this work we demonstrate, through both analytical and numerical investigations, a continuum of equilibria of the plain aggregation model that are not minima of the energy. Furthermore, we show that these non-minimizing equilibria are achieved dynamically from a non-trivial set of initial conditions with a variety of interaction potentials and boundary geometries. Thus we show conclusively a deficiency with the plain aggregation model in domains with boundaries, namely that it appears to evolve into equilibria that are not minima of the energy.

Following this we then propose a rectification to this deficiency in way of nonlinear diffusion. This choice of nonlinear diffusion is especially attractive because it preserves compact states of the plain aggregation model. We showcase how the diffusive model approaches, but does not equilibrate at, the non-minimizing equilibria of the plain aggregation model. Furthermore we demonstrate how minimizers of the diffusive model do approach minimizers of the plain aggregation model in the zero diffusion limit.

Keywords: swarm equilibria, energy minimizers, gradient flow, attractors, nonsmooth dynamics, nonlinear diffusion, numerical methods

Dedication

I would like to dedicate this work to my parents, Gary Kovacic and Theresa Gallant, who always encouraged and supported me in my academic journey. The path has been long and difficult at times and without the support of Gary and Theresa, as well as various supervisors and friends, may simply have not been completed. Truly my parents' contributions and sympathetic voices cannot be overstated in enabling me to complete my academic journey.

Acknowledgements

I would first like to acknowledge my high school Math teachers who entertained my own investigations into Maths at that age. They also shared with me the projects they were working on which gave me slight insight into higher level Maths. Enabling my early studies at this age followed up into my next acknowledgement.

I would now like to acknowledge Dr. Pietro-Luciano Buono, a professor at UOIT that I came into contact with during my first year of my undergraduate degree. I actually started talking to him regarding my own investigations that I had started at the end of my high school life. This eventually lead into becoming an undergraduate research assistant with Dr. Buono that continued through most of my undergraduate degree. Ultimately Dr. Buono co-supervised me through my Masters degree and provided crucial guidance in getting me to where I am now.

I would be remiss not to acknowledge my other co-supervisor, Dr. Lennaert van Veen, during my Masters degree. Though certainly not as impactful as Dr. Buono, Dr. van Veen gave a more numerical perspective to my studies and contributed significantly to my completion of the Masters degree.

Now coming into the acknowledgements crucial to the completion of my current PhD studies, I would first like to note difficulties encountered during this period. During my PhD studies I encountered significant psychological issues stemming from a lack of confidence, overburdening myself, and then time pressure from initial troubles.

Dr. Williams was crucial to overcoming these problems at a time when I needed it most and they seemed most daunting. Without his sympathy and own personal experience giving insight into my problems, I do not believe I would have made it through to the completion of my studies. During my PhD studies, Dr. Fetecau provided the regular pushes to help guide me and ultimately lead me to completing the various projects. Of particular importance, it is Dr. Fetecau's guidance, contacts, and professional experience that I believe drove and enabled me to the completion, submission, and acceptance of my two papers.

Really though, I must acknowledge the patience and understanding of both my PhD supervisors. I was by no means an ideal student and at times things were understandably difficult. At times I seriously doubted my ability to produce something of value and the pride I feel with where I am now is without a doubt a result of the nature and personality of my supervisors.

Coming directly from Dr. Fetecau's connections, I'd also like to thank Dr. Ihsan Topaloglu for his significant contributions to the second paper. He provided analytical insight and results that really made the paper what it is, as just with my numerical portion it would certainly have lacked the impact it has now.

During my time doing my PhD studies I was fortunate enough to be accepted to two conferences. The first being a summer school hosted by the University of Bath during the Summer of 2014 which focused on swarming models and where I presented a poster on my Masters research. The second conference was a graduate summit hosted by PIMS at Jasper National Park, Alberta which again focused on swarming models where I presented a talk on my first paper "Swarming equilibria in domains with boundaries". The discussions and connections made during these conferences were invaluable to my academic career.

There were several visitors to the university that are either major influences in my research field and/or provided insightful conversations when they generously offered their time to speak with me. These were in no particular order: Dr. José Carrillo, Dr. Andrew Bernoff, Dr. Theodore Kolokolnikov, and Dr. Chris Budd. Speaking of important conversations, I'd also like to acknowledge peers and professors that either gave me insight, support, and/or friendship with regards to many different areas. These are in no particular order: Dr. Ralf Wittenberg, Dr. Brenda Davison, Dr. Joep Evers, Dr. Benjamin Goodman, Lee Safranek, Martin Ambrozic, Benny Wai, Jeremy Chiu, Avinash Kulkarni, Nathan King, Daniel Messenger, Ray Walsh, and Clinton Innes.

Finally I want to acknowledge Simon Fraser University for providing me scholarships for my research in way of a Special Entrance Scholarship, two Graduate Fellowships, and a PhD President's Scholarship. These scholarships enabled me to focus entirely on my research during these periods, easing the burden on myself and helping me stay in a positive frame of mind. Additionally I want to thank Simon Fraser University for two travel scholarships that enabled me to go to the two conferences acknowledged earlier.

Table of Contents

List of Tables

List of Figures

Chapter 1

Introduction

The patterns of flocks of birds as they fly, the potentially disastrous locomotion of locust swarms, or the sharp gradient of schools of fish as they are being herded by killer whales. The movement and grouping of bison on the plains or even the daily bustle of humans moving through a train station. It is simply astounding that essentially the same simple rules that can be used to describe one of these, in fact can describe them all [22]. In fact the rules found by many other researchers to describe these examples of agents swarming, can even be used to describe the self-organization of things that do not live or are entirely immaterial.

With such a broad range of applications, the area of mathematical research involved with self-organizing behaviour or swarming has been booming lately. Understanding these models have lead to insights into processes that seemed far too complex to even attempt to solve, in particular understanding how locusts swarm have enabled researchers to see the cues before they eat all in their paths. This is just one way in which study of swarming models ultimately benefits humanity and provides solutions to many of our problems.

A plain aggregation model that has attracted a great amount of interest recently is given by the following integro-differential equation in $\mathbb{R}^n$:

$$\rho_t + \nabla \cdot (\rho v) = 0, \quad \text{in } \mathbb{R}^n \times [0, T), \tag{1.1a}$$

$$v = -\nabla K * \rho - \nabla V, \tag{1.1b}$$

$$\rho(0) = \rho_0 \quad \text{in } \mathbb{R}^n. \tag{1.1c}$$

Here ρ represents the density of the aggregation, ρ_0 is the initial condition, K is an interaction potential, and V is an external potential. The asterisk $*$ denotes convolution, and T can either be finite (in the case of studying finite-time blow-up for instance) or infinite (in that one studies the behaviour of the model with $T \to \infty$). Typically, the interaction potential K models symmetric inter-individual social interactions such as long-range attraction and short-range repulsion, though this is but one example and the interaction potential certainly can model more than this. Solutions to (1.1) may be classical in some contexts but also may be composed either entirely or partially

of singular concentrations in others. One approach in the mathematical analysis of this model is based on the formulation of the model as a gradient flow on spaces of probability measures with finite second moment endowed with the Wasserstein metric, following theory in [1].

Study into the free space model (1.1) has been a topic of intense interest in recent years. The model appeared in various contexts related to swarming and social aggregations, such as biological swarms and pattern formation [35, 16, 13, 9, 44], granular media [63, 27], self-assembly of nanoparticles [49, 50], Ginzburg-Landau vortices [34, 33], robotics and space missions [37], molecular dynamics simulations of matter [48], and opinion dynamics [58]. There is an extensive literature on the mathematical properties of the model in free space, which includes studies on the well-posedness of solutions [18, 14, 11], the long-time behaviour of solutions [44, 43, 9], and blow-up (in finite or infinite time) by mass concentration [41, 11, 12]. An active area of research also includes research into connecting the continuum models here with discrete models. These continuum models can be shown as mean field limits of the discrete models in certain cases. We introduce the discrete models and discuss properties in the preliminaries.

Many different variations of model (1.1) have been considered in the literature. One can consider interaction potentials with a finite sensing distance, senses that can be directional, or senses that can be occluded by other agents [36, 59, 60, 55]. One can consider variations on the external potential V, to enforce a gravity-like or wind-like potential to study agents forced to motion, or one can study a confining potential that keeps agents from drifting from each other [10]. Finally one can consider an internal potential H that, among other things, can model diffusion among the agents [42, 29]. The generic version of (1.1) with an internal potential is given by:

$$\rho_t + \nabla \cdot (\rho v) = 0, \quad \text{in } \mathbb{R}^n \times [0,T), \tag{1.2a}$$

$$v = -\nabla H'(\rho) - \nabla K * \rho - \nabla V, \tag{1.2b}$$

$$\rho(0) = \rho_0 \quad \text{in } \mathbb{R}^n. \tag{1.2c}$$

Model (1.2) can be used to model linear diffusion, if $H(\rho) = \nu(\rho \log(\rho) - \rho)$, or nonlinear diffusion in the form of a power-law, if $H(\rho) = \frac{\nu}{m-1}\rho^m$ $(m > 1)$.

Linear diffusion has been extensively studied in the context of swarming as the continuum limit of random walk processes among discrete individuals [52, 32]. The authors of [65] study the zero diffusion limit of the linear diffusion model and [39] showcases how, with the addition of linear diffusion, states with multiple disconnected components lead to unique steady states. On the other hand, nonlinear diffusion is a natural outcome of mean-field treatments of some systems, particularly when volume exclusion effects are considered [53], although rigorous continuum limits are lacking. Despite this, the PDEs that come out of mean-field arguments tend to agree with simulations [42, 54].

Throughout the work here in this thesis, we consider only nonlinear diffusion in the form of a power-law, which is to consider the diffusive model:

$$\rho_t + \nabla \cdot (\rho v) = 0, \quad \text{in } \mathbb{R}^n \times [0, T), \tag{1.3a}$$

$$v = -\frac{\nu m}{m-1} \nabla \rho^{m-1} - \nabla K * \rho - \nabla V, \tag{1.3b}$$

$$\rho(0) = \rho_0 \quad \text{in } \mathbb{R}^n. \tag{1.3c}$$

Nonlinear diffusion models like (1.3) have also received a great deal of interest lately. In the context of modelling biological aggregations, model (1.3) (with $m = 3$) was investigated in [16]; showcasing its ability to exhibit equilibria with compact support and sharp edges that correspond to localized clumps of organisms. There is also extensive work on mathematical studies of these models (mostly set in free space), including well-posedness results [1, 17, 6], investigations into properties of the steady states [20, 43, 21, 56, 26], and studies of long-time behaviour of the solutions [19, 27, 29].

So far we have introduced models in free space, and indeed most of the current literature into swarming models has been in contexts with free space. Of course in real life there are situations that could be well modelled by an unbounded domain such as on the open plains. But if there are natural boundaries such as a river or a cliff, or if the area is confined such as in a building, then one must consider boundaries in the models to accurately represent the situation.

Despite the extensive literature on the plain aggregation model in free space, there are decidedly fewer works that consider the presence of boundaries [10, 62, 28]. These papers are motivated by physical/biological scenarios where the environment involves an obstacle or an impenetrable wall; in the locust model from [8] for example, such an obstacle is the ground. We assume in this work that the presence of boundaries limits the movement in the following way [62, 28]: once particles/individuals meet the boundary, they do not exit the domain, but move freely along it as a "slip, no-flux" boundary condition.

In particular consider a domain $\Omega \subset \mathbb{R}^n$ with a smooth C^1 boundary with outward unit normal vector n_x at $x \in \partial\Omega$. The boundary confines the movement of agents in the following way. If x is in the interior of Ω or if $x \in \partial\Omega$ and the velocity (1.1b) points inward ($v \cdot n_x \leqslant 0$), then the velocity remains unchanged. If $x \in \partial\Omega$ and the velocity points outward ($v \cdot n_x > 0$) then we instead consider the projection onto the tangent plane of the boundary at x . Thus when considering domains with boundaries, the plain aggregation model (1.1) is modified to:

$$\rho_t + \nabla \cdot (\rho v) = 0, \quad \text{in } \Omega \times [0, T), \tag{1.4a}$$

$$v = P_x(-\nabla K * \rho - \nabla V), \tag{1.4b}$$

$$\rho(0) = \rho_0 \quad \text{in } \Omega, \tag{1.4c}$$

where

$$P_x\xi = \begin{cases} \xi & \text{if } x \notin \partial\Omega \text{ or } x \in \partial\Omega \text{ and } \xi \cdot n_x \leqslant 0 \\ \Pi_{\partial\Omega}\,\xi, & \text{otherwise.} \end{cases} \tag{1.5}$$

Here $\Pi_{\partial\Omega}$ denotes the projection onto the tangent plane to the boundary.

The well-posedness of weak measure solutions of (1.4) has been investigated in [62, 28] in the framework of gradient flows in spaces of probability measures [1, 25]. The setting of *measure*-valued solutions in these works is absolutely essential in this thesis, for various reasons. First, mass accumulates on the boundary of the domain and solutions develop Dirac delta singularities there. Second, the measure framework is the appropriate setup for connecting the PDE model with its discrete/particle approximation. In regard to the latter, by approximating the initial density ρ_0 with a finite number of delta masses, (1.4) reduces to an ODE system, which then can be studied on its own. In [28], the authors establish several important properties of such particle approximations. One is the well-posedness of the approximating particle system where, due to the discontinuities of the velocity field at the boundary, the theory of differential inclusions [47, 31] is being employed. Another is the rigorous limit of the discrete approximation as the number of particles approach infinity; this limit is shown to be a weak measure solution of the PDE model (1.4).

Similarly, the diffusive model (1.3) when posed in domains with boundaries is given by:

$$\rho_t + \nabla \cdot (\rho v) = 0, \quad \text{in } \Omega \times [0,T), \tag{1.6a}$$

$$v = -\frac{\nu m}{m-1}\nabla\rho^{m-1} - \nabla K * \rho - \nabla V, \tag{1.6b}$$

$$v \cdot n_x = 0 \quad \text{on } \partial\Omega \times [0,T), \tag{1.6c}$$

$$\rho(0) = \rho_0 \quad \text{in } \Omega. \tag{1.6d}$$

Note that we opt to use a more standard boundary condition (1.6c) here as opposed to using $\Pi_{\partial\Omega}$ as in (1.4). In fact because we do not need to consider singular concentrations for the diffusive model, the standard no-flux boundary condition (1.6c) is the appropriate choice.

The focus of this thesis is on equilibrium configurations of model (1.4) and (1.6). A state $\bar{\rho}$ is an equilibrium of the plain aggregation model (1.4) if the velocity (1.4b) vanishes everywhere on its support:

$$P_x(-\nabla K * \bar{\rho} - \nabla V) = 0 \qquad \text{in } \operatorname{supp}(\bar{\rho}). \tag{1.7}$$

Similarly, a state $\bar{\rho}$ of the diffusive model (1.6) is an equilibrium if the velocity (1.6b) vanishes everywhere on its support:

$$-\nabla\frac{\nu m}{m-1}\bar{\rho}^{m-1} - \nabla K * \bar{\rho} - \nabla V = 0 \qquad \text{in } \operatorname{supp}(\bar{\rho}). \tag{1.8}$$

Concerning (1.7), we note that at points on the boundary, the unprojected velocity (1.1b) may not be zero; by (1.5) it can have a nonzero normal component pointing outward. This scenario is akin to a falling object hitting a surface, when there is still a force acting on it but there is nowhere to go.

Outline of this thesis

First we go over necessary knowledge in Chapter 2. Here we introduce the 2-Wasserstein metric and convergence in this sense. We then introduce the energies of the plain aggregation (1.4) and diffusive (1.6) models. As these models are formulated as gradient flows of these energies, they are integral to our understanding to come. Following [10], we then go over the characterization of equilibria and minimizers for both models. We will also introduce the main interaction potential that we investigate in this thesis, the quadratic attraction, Newtonian repulsion (QANR) potential, as well as several important properties that are fundamental to the results presented. To close off Chapter 2 we then go over the particle method used in the numerics for the plain aggregation model. Lastly we show a numerical implementation to calculate the 2-Wasserstein metric.

In Chapter 3 we consider the plain aggregation model in one dimension. Here we provide an extensive study of equilibria of the QANR potential with one boundary, showcasing a whole family of states that can be analytically found and verified to be equilibria according to (1.7) but which are not energy minima. This family of two-component equilibria consist of one swarm component on the boundary and another in the interior of the domain. These two-component equilibria can be further differentiated as connected and disconnected, depending on whether the two components are adjacent or not. We find that none of the disconnected equilibria are local minima of the energy. In contrast, one of the connected configurations can be shown to be a global energy minimizer.

Nevertheless, we show that starting from a large class of initial densities, solutions to (1.4) do evolve into such disconnected equilibria that are not local energy minimizers. While unusual, this behaviour has been observed in continuum mechanics systems wherein singularities form which act as barriers preventing further energy decrease [4, 5, 51]. Following this study of the QANR potential with one boundary, we then consider the QANR potential with two boundaries to study equilibria in a truly confined domain. Here we find a 2-parameter family of three-component equilibria and show, again, that these can be found analytically and shown to be equilibria, though almost all of these states are not local minima of the energy. Similar to the study with one boundary, we find that the only state that is an energy minimum is one that is connected in the sense that the free swarm connects to both boundaries.

Following this two boundary study of the QANR potential, we study a C^1-smoothed version of the QANR potential for which equilibria in free space are composed of multiple singular accumulations. In the presence of a boundary we find, again, states that can be shown to be equilibria but which are not local minima. In contrast to the QANR potential, we find that there is now a family of energy minima and explicitly calculate such equilibria. We then study a Morse-like potential and

again show explicit calculations of equilibria, similarly finding that most of them are not local minima of the energy. Finally, wrapping up Chapter 3 we go over a numerical implementation to find equilibria, though this is more a lead-up to the implementation to find equilibria in two dimensions since we could find explicit equilibria in every case studied in one dimension.

In Chapter 4 we consider the QANR potential in two dimensions with a single boundary. While explicitly computable equilibria are available only for the simplest cases, we do present dynamics from the particle method and compare them to a numerical implementation which solves for equilibria. Again we find that most of the equilibria found are not local minima of the energy yet are achieved dynamically. We then also present results with a confined domain; in particular, we study the problem with the domain taken as a circle. Finally we describe the numerical implementation used in two dimensions to solve for equilibria.

By this point in the thesis we have then demonstrated a number of different contexts in which non-minimizing equilibria are found. As the plain aggregation model (1.4) is technically formulated as a gradient flow over the energy, these results in Chapters 3 and 4 could be conceived as flaws of the model, namely that its solutions tend to evolve into unstable equilibria. In Chapter 5 then we attempt to rectify this degeneracy by considering the diffusive model (1.6).

In particular we consider first quadratic diffusion, which is the case $m = 2$ in the diffusive model, and show how the solutions of the diffusive model compare to those of the plain aggregation model in the zero diffusion limit. We find that solutions to the diffusive model seem to approach, but not converge to, unstable equilibria of the plain aggregation model. We also compare how minimizers of the diffusive model compare to the minimizers of the plain aggregation model, showing that they approach each other in the zero diffusion limit. Ultimately we provide strong numerical evidence that the diffusive model rectifies the aforementioned flaw of the plain aggregation model, in the sense that solutions of (1.6) bypass the unstable equilibria of model (1.4). Lastly in Chapter 5 we study general nonlinear diffusion, in particular with $m = 1.5$ and $m = 3$, showcasing similar findings to that of quadratic diffusion.

Finally in the final Chapter 6 we provide a discussion of our results. Additionally we discuss some possible future directions for research accompanied with some interesting things that were found.

Main accomplishments of this thesis

Initially this thesis conclusively demonstrates a deficiency in the plain aggregation model in domains with boundaries with the slip boundary condition. (1.4). We show through analytical and numerical arguments that the model achieves equilibria that are not energy minima, despite the model coming from an energy gradient formulation, with a variety of interaction potentials and boundary geometries in one and two dimensions. We then provide a method for numerically calculating equilibria in one and two dimensions, which one can use to study these unstable equilibria

when they are not explicitly available. We then offer a solution to the deficiency of the plain aggregation model by way of nonlinear diffusion. We find that the diffusive model with boundaries (1.6) approaches, but does not equilibrate at, unstable equilibria of the plain aggregation model. In this way, the diffusive model avoids the unstable equilibria found for the plain aggregation model while preserving compact swarms.

Chapter 2

Preliminaries

2.1 Analytical preliminaries

2.1.1 The 2-Wasserstein metric

The diffusive model (1.6) and the plain aggregation model (1.4) are energy gradient systems with respect to energy functionals we will introduce in the next subsection. An important preliminary to discuss, however, is the metric space in which solutions are measured and how convergence is characterized. We consider the space

$$\mathcal{P}_2(\Omega) := \left\{ \rho \in \mathcal{P}(\Omega) \colon \int_\Omega |x|^2 \, d\rho(x) < +\infty \right\} \tag{2.1}$$

of probability measures on Ω with finite second moments, endowed with the 2-Wasserstein metric. We recall this metric briefly below, along with some of its basic properties. For further background, we refer the reader to the books by Ambrosio, Gigli and Savaré [1] and Villani [64]. The 2-Wasserstein distance between $\mu, \sigma \in \mathcal{P}_2(\Omega)$ is given by

$$d_W(\mu, \sigma) := \left(\min \left\{ \int_\Omega \int_\Omega |x - y|^2 \, d\gamma(x, y) \colon \gamma \in \Gamma(\mu, \sigma) \right\} \right)^{1/2}, \tag{2.2}$$

where $\Gamma(\mu, \sigma)$ is the set of transport plans between μ and σ,

$$\Gamma(\mu, \sigma) := \{ \gamma \in \mathcal{P}(\Omega \times \Omega) \colon (\pi_1)_\# \gamma = \mu \quad \text{and} \quad (\pi_2)_\# \gamma = \sigma \} .$$

Here π_1, π_2 denote the projections $\pi_1(x, y) = x$ and $\pi_2(x, y) = y$. For $i = 1, 2$, $(\pi_i)_\# \gamma$ denotes the pushforward of γ defined by $(\pi_i)_\# \gamma(U) := \gamma(\pi_i^{-1}(U))$ for any measurable set $U \subset \Omega$.

The minimization problem (2.2) admits a solution, i.e., there exists an optimal transport plan $\gamma_0 \in \Gamma(\mu, \sigma)$ so that

$$d_W^2(\mu, \sigma) = \int_\Omega \int_\Omega |x - y|^2 \, d\gamma_0(x, y).$$

If σ is absolutely continuous with respect to the Lebesgue measure, then there is an optimal transport map $\mathbf{t}_\sigma^\mu : \Omega \to \Omega$ that transports σ onto μ (i.e., $\mathbf{t}_{\sigma\#}^\mu \sigma = \mu$) such that (see [57] for details):

$$d_W^2(\mu, \sigma) = \int_\Omega \left|\mathbf{t}_\sigma^\mu(x) - x\right|^2 d\sigma(x).$$

Moreover, $(\mathcal{P}_2(\Omega), d_W)$ is a complete and separable metric space, and convergence in $(\mathcal{P}_2(\Omega), d_W)$ can be characterized as follows:

$$\begin{aligned} d_W(\mu_n, \mu) \to 0 \quad &\iff \quad \mu_n \to \mu \text{ weak-}* \text{ in } \mathcal{P}_2(\Omega) \text{ and } \textstyle\int_\Omega |x|^2 \, d\rho_n(x) \to \int_\Omega |x|^2 \, d\rho(x), \\ &\iff \quad \textstyle\int_\Omega f(x) \, d\rho_n(x) \to \int_\Omega f(x) \, d\rho(x), \\ &\qquad \forall f \in C(\Omega) \text{ such that } |f(x)| \leqslant C(1 + |x - x_0|^2). \end{aligned}$$

We will refer to functions satisfying $|f(x)| \leqslant C(1 + |x - x_0|^2)$, for some $C > 0$ and $x_0 \in \Omega$, as functions with *at most quadratic growth*.

2.1.2 Well-posedness of solutions and the energy functionals

The well-posedness of weak measure solutions to model (1.4) has been established recently in [62] and [28]. The functional setup in these works is in the space $\mathcal{P}_2(\Omega)$ endowed with the 2-Wasserstein metric. Under appropriate assumptions on the domain Ω and on the potentials K and V, it is shown that the initial value problem for (1.4) admits a weak measure solution $\rho(t)$ in $\mathcal{P}_2(\Omega)$. We refer to [62, 28] for specific details on the well-posedness theorems and proofs, and only highlight here the facts that are relevant for our work.

It is a well-established result that the plain aggregation model in free space (model (1.1)) can be formulated as a gradient flow on the space of probability measures $\mathcal{P}_2(\Omega)$ equipped with the 2-Wasserstein metric [1]. A key result in [62, 28] is that such an interpretation exists for model (1.4) as well. Specifically, consider the energy functional associated with the plain aggregation model (1.4),

$$E[\rho] = \frac{1}{2} \int_\Omega \int_\Omega K(x - y)\rho(x)\rho(y) \, \mathrm{d}x \, \mathrm{d}y + \int_\Omega V(x)\rho(x) \, \mathrm{d}x \, \mathrm{d}t, \tag{2.3}$$

where the first term represents the interaction energy and the second is the potential energy[1].

The weak measure solution $\rho(x, t)$ to model (1.4) is shown to satisfy the following energy dissipation equality [28]:

$$E[\rho(t)] - E[\rho(s)] = -\int_s^t \int_\Omega |P_x(-\nabla K * \rho(x, \tau) - \nabla V(x))|^2 \rho(x, \tau) \, \mathrm{d}x \, \mathrm{d}\tau, \tag{2.4}$$

[1]Note that throughout this work $\int \varphi(x)\rho(x) \, \mathrm{d}x$ denotes the integral of φ with respect to the measure ρ, regardless of whether ρ is absolutely continuous with respect to the Lebesgue measure.

for all $0 \leqslant s \leqslant t < \infty$. Equation (2.4) is a generalization of the energy dissipation for the model in free space [25]. Characterization of equilibria of (1.1) as ground states of the interaction energy has been a very active area of research [2, 30, 23, 61].

The authors in [28] use particle approximations of the continuum model (1.4) as an essential tool to show the existence of gradient flow solutions. The method consists in approximating an initial density ρ_0 by a sequence ρ_0^N of delta masses supported at a discrete set of points. For N fixed, the evolution of model (1.4) with discrete initial data ρ_0^N reduces to a system of ordinary differential equations, for which ODE theory can be applied. The ODE system governs the evolution of the characteristic paths (or particle trajectories) which originate from the points in the discrete support of ρ_0^N. Hence, the solution $\rho^N(t)$ consists of delta masses supported at a discrete set of characteristic paths. The key ingredient in the analysis is to find a stability property of solutions ρ^N with respect to initial data ρ_0^N and show that in the limit $N \to \infty$, ρ^N converges (in the Wasserstein distance (2.2)) to a weak measure solution of (1.4) with initial data ρ_0. This is one of the major results established in [28].

One can also consider an energy functional associated with the diffusive model (1.6),

$$E_\nu[\rho] = \int_\Omega \frac{\nu}{m-1}\rho^m \,\mathrm{d}x + \frac{1}{2}\int_\Omega\int_\Omega K(x-y)\rho(x)\rho(y)\,\mathrm{d}x\,\mathrm{d}y + \int_\Omega V(x)\rho(x)\,\mathrm{d}x, \tag{2.5}$$

where the first term represents the internal energy, the second term represents the interaction energy, and the third is the potential energy. Similar to the dissipation result for the plain aggregation model (2.4), one can show that weak measure solutions admit a dissipation result for the diffusive energy (2.5), specifically

$$E_\nu[\rho(t)] - E_\nu[\rho(s)] = -\int_s^t \int_\Omega \left| -\nabla \frac{\nu m}{m-1}\rho^{m-1}(x,\tau) - \nabla K * \rho(x,\tau) - \nabla V(x) \right|^2 \rho(x,\tau)\,\mathrm{d}x\,\mathrm{d}\tau, \tag{2.6}$$

for all $0 \leqslant s \leqslant t < \infty$. The proof of (2.6) follows by beginning with (1.6a) and multiplying both sides by $\frac{\nu m}{m-1}\rho^{m-1} + K * \rho + V$ getting

$$\left(\frac{\nu m}{m-1}\rho^{m-1} + K * \rho + V\right)\rho_t = -\left(\frac{\nu m}{m-1}\rho^{m-1} + K * \rho + V\right)\nabla\cdot(\rho v).$$

Now simply integrating over Ω and after some elementary work and by-parts integration we get

$$\frac{d}{dt}E_\nu[\rho] = -\int_{\partial\Omega}\left(\frac{\nu m}{m-1}\rho^{m-1} + K * \rho + V\right)\rho\, v\cdot n_x \,\mathrm{d}x - \int_\Omega \rho\left|\nabla\left(\frac{\nu m}{m-1}\rho^{m-1} + K * \rho + V\right)\right|^2 \,\mathrm{d}x,$$

where n_x is the unit outward normal to $\partial\Omega$ at x. By (1.6c), the boundary term is zero. Then integrating the above equation in time, one gets the energy dissipation relation (2.6).

2.1.3 Characterization of equilibria and minimizers

Here we wish to lay out much of the theoretical framework as established by Bernoff and Topaz in [10]. This is used to study the energy functional (2.3) and find conditions for critical points to be energy minimizers. We find that with this framework we can characterize equilibria, and local and global minimizers. Additionally we also define minimizers with respect to *spatially* local perturbations. We present the ideas in the more general context of the energy functional (2.5) with $m = 2$ (quadratic nonlinear diffusion); one can simply take $\nu = 0$ to recover the results for the plain aggregation model.

First note that the dynamics of model (1.4) and model (1.6) conserve mass:

$$\int_\Omega \rho(x,t)\,\mathrm{d}x = M \qquad \text{for all } t \geqslant 0. \tag{2.7}$$

Hence, in what follows it is sufficient to consider zero-mass perturbations of a fixed equilibrium.

Single-component equilibria

Consider an equilibrium solution $\bar\rho$ with mass M and *connected* support $\Omega_{\bar\rho} \subset \Omega$, and take a small perturbation $\epsilon\tilde\rho$ of zero mass:

$$\rho(x) = \bar\rho(x) + \epsilon\tilde\rho(x),$$

where

$$\int_\Omega \bar\rho(x)\,\mathrm{d}x = M, \tag{2.8a}$$

$$\int_\Omega \tilde\rho(x)\,\mathrm{d}x = 0. \tag{2.8b}$$

Consider quadratic diffusion ($m = 2$) in the diffusive model (1.6) or the plain aggregation model (1.4). For convenience of notations (we are about to compute the first and second variations of the energy) we will drop momentarily the subindex ν in energy (2.5). Then, both energy functionals (2.3) and (2.5) (for $m = 2$) are quadratic in ρ and one can write:

$$E[\rho] = E[\bar\rho] + \epsilon E_1[\bar\rho,\tilde\rho] + \epsilon^2 E_2[\tilde\rho,\tilde\rho], \tag{2.9}$$

where E_1 denotes the first variation:

$$E_1[\bar\rho,\tilde\rho] = \int_\Omega \left[2\nu\bar\rho(x) + \int_\Omega K(x-y)\bar\rho(y)\,\mathrm{d}y + V(x)\right]\tilde\rho(x)\,\mathrm{d}x, \tag{2.10}$$

and E_2 the second variation:

$$E_2[\tilde{\rho}, \tilde{\rho}] = \int_\Omega \nu \tilde{\rho}^2(x)\,\mathrm{d}x + \frac{1}{2}\int_\Omega \int_\Omega K(x-y)\tilde{\rho}(x)\tilde{\rho}(y)\,\mathrm{d}x\,\mathrm{d}y. \tag{2.11}$$

Using the notation

$$\Lambda(x) = 2\nu\bar{\rho}(x) + \int_{\Omega_{\bar{\rho}}} K(x-y)\bar{\rho}(y)\,\mathrm{d}y + V(x), \qquad \text{for } x \in \Omega, \tag{2.12}$$

one can also write the first variation as

$$E_1[\bar{\rho}, \tilde{\rho}] = \int_\Omega \Lambda(x)\tilde{\rho}(x)\,\mathrm{d}x. \tag{2.13}$$

Before going further, let us discuss what perturbations we consider. For this purpose, following [10] we are going to define two classes of perturbations. The first class are perturbations that are supported in $\Omega_{\bar{\rho}}$. The second class of perturbations are those with arbitrary support. The first class is a subset of this second class, but the second class also includes perturbations that are physically impossible via the dynamics, such as mass making finite jumps away from the support of the equilibrium $\bar{\rho}$.

Perturbations of the first class. For the following we have that $\mathrm{supp}(\tilde{\rho}) = \mathrm{supp}(\bar{\rho})$ and as a consequence of the perturbation being zero-mass, it must either be identically zero or else take negative and positive values.

Since $\tilde{\rho}$ changes sign in $\Omega_{\bar{\rho}}$, for $\bar{\rho}$ to be a critical point of the energy, the first variation must vanish. From (2.13), given that perturbations $\tilde{\rho}$ are arbitrary and satisfy (2.8b), one finds that E_1 vanishes provided Λ is constant in $\Omega_{\bar{\rho}}$,

$$\Lambda(x) = \lambda, \qquad \text{for } x \in \Omega_{\bar{\rho}}. \tag{2.14}$$

The (Lagrange) multiplier λ is given a physical interpretation in [10]: it represents the energy per unit mass felt by a test mass at position x due to interaction with the swarm in $\bar{\rho}$ and the exogenous potential. Indeed this interpretation is valid for all points x by considering $\Lambda(x)$ as the energy per unit mass felt by a test mass at position x. This interpretation is critical for the study in [10], as well as for this present work.

Equation (2.14) represents a necessary condition for $\bar{\rho}$ to be an equilibrium. For $\bar{\rho}$ that satisfies (2.14) to be a local minimizer with respect to the first class of perturbations, the second variation (2.11) must be positive. In general, the sign of E_2 cannot be determined easily.

Perturbations of the second class. Consider now perturbations of the second class. Since perturbations $\tilde{\rho}$ must be non-negative in the complement $\Omega_{\bar{\rho}}^c = \Omega \setminus \Omega_{\bar{\rho}}$, it is shown in [10] that a necessary

and sufficient condition for $E_1 \geqslant 0$ is

$$\Lambda(x) \geqslant \lambda, \qquad \text{for } x \in \Omega_{\bar{\rho}}^c. \tag{2.15}$$

The interpretation of (2.15) is that transporting mass from $\Omega_{\bar{\rho}}$ into its complement $\Omega_{\bar{\rho}}^c$ increases the total energy [10].

Remark 2.1.1 (Equilibria, $\Lambda(x)$, and the velocity field)**.** *It is not surprising that $\Lambda(x)$ can be used to characterize equilibria. One can observe that the velocity, v, of the plain aggregation model can be written*

$$v = P_x(-\nabla\Lambda).$$

So the equilibrium condition (2.14) *corresponds with a zero velocity along the support of the equilibrium. The minimizer condition* (2.15) *corresponds with the velocity field within a neighbourhood of the support of the equilibrium pointing towards the support. Figure 2.1 shows examples of a stable and an unstable state with accompanying $\Lambda(x)$.*

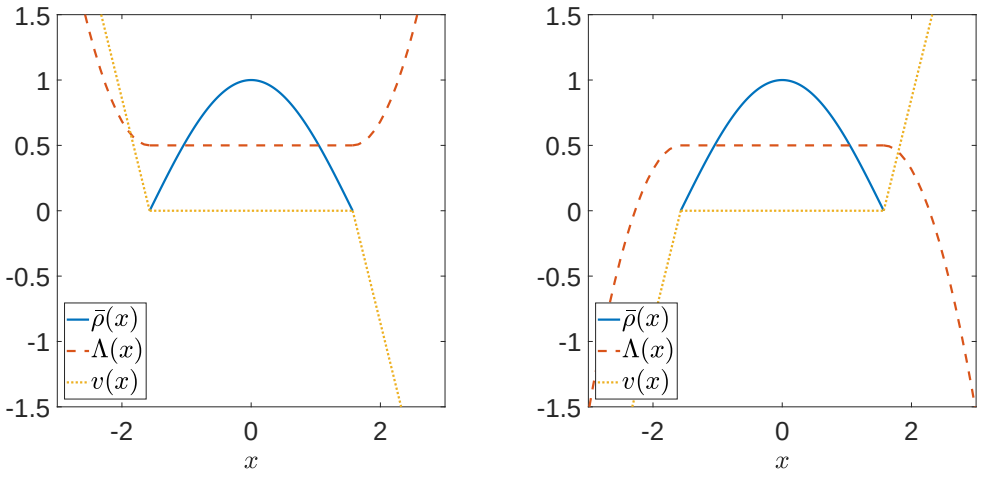

Figure 2.1: (a) An equilibrium that is stable and indeed an energy minimum. Notice that inside the support of $\rho(x)$ we see Λ is flat and so the velocity is zero there. Additionally we see that since $\Lambda(x)$ is greater on the complement of the support then the velocity field, calculated from $\Lambda(x)$, is directed towards the swarm. (b) An equilibrium that is unstable. While it still has zero velocity inside the support, since $\Lambda(x)$ decreases away from the support one can calculate the velocity field and find they point away from the swarm. Any infinitesimal perturbation that would move mass out of the support will be energetically favorable.

In summary, a critical point $\bar{\rho}$ for the energy satisfies the Fredholm integral equation (2.14) on its support. Also, $\bar{\rho}$ is a local minimizer (with respect to the general, second class perturbations) if it satisfies (2.15). Note however that the word *local* in this context refers to the small *size* of the perturbations, as the perturbations themselves are in fact allowed to be nonlocal in space.

Remark 2.1.2 (Formal variational framework)**.** *The minimization considerations above follow closely the* informal *setup and approach from [10]; for a mathematically complete and rigorous framework one needs to be more precise however. First, one has to set the space of densities over which the minimization of energy is considered (i.e., the space to which the equilibrium $\bar{\rho}$ and the perturbed equilibrium ρ belong to). We take the space of such admissible densities to be the set of Borel measures on Ω that have finite second moment and total mass M, endowed with the* 2*-Wasserstein metric. Apart from not having a density normalized to unit mass (which does not add any technical difficulties), this is the framework commonly used in rigorous variational studies of model* (1.1) *[2, 3, 25], including the recent work on domains with boundaries [62, 28].*

A rigorous derivation of the Euler-Lagrange equations within such formal setup is presented for instance in [2, Theorem 4]; note that while the derivation there is for equilibria in free space, it extends immediately to arbitrary domains Ω, as considered in this paper. As in [2], by considering various types of admissible perturbations to an equilibrium $\bar{\rho}$ (similar in fact to the first and second class perturbations from [10]), one finds that (2.14) *holds a.e. (with respect to the measure $\bar{\rho}$) within the support, while* (2.15) *holds at a.e. x. Hence, the necessary conditions* (2.14) *and* (2.15) *for a local minimum, as found through the informal approach in [10], could potentially be relaxed, by requiring to hold up to zero measure sets. Nevertheless, given the connected equilibria considered in this paper, working directly with* (2.14)-(2.15) *is simpler and makes no essential difference in our considerations.*

Multi-component equilibria. As discussed in [10], the support $\Omega_{\bar{\rho}}$ of an equilibrium density has in general multiple disconnected components. Assuming m disjoint, closed and connected components Ω_i, $i = 1, \dots, m$, one can write

$$\Omega_{\bar{\rho}} = \Omega_1 \cup \Omega_2 \cup \cdots \cup \Omega_m, \qquad \Omega_i \cap \Omega_j = \emptyset, \quad i \neq j. \tag{2.16}$$

In [10], a *swarm equilibrium* is defined as a configuration in which Λ is constant in every component of the swarm, i.e.,

$$\Lambda(x) = \lambda_i, \qquad \text{for } x \in \Omega_i, \quad i = 1, \dots, m. \tag{2.17}$$

Given the physical interpretation of $\Lambda(x)$, one can immediately observe that a multi-component equilibrium $\bar{\rho}$ that satisfies (2.17) cannot be a local minimizer unless all λ_i are equal to each other ($i = 1, \dots, m$). Indeed, for a swarm equilibrium with $\lambda_j > \lambda_k$, transferring mass from Ω_j to Ω_k would decrease the energy. However we will see in this thesis many examples of equilibria composed of multiple, disconnected components. While such equilibria cannot be minimizers with respect to

arbitrary perturbations, we investigate instead whether such equilibria are minimizers with respect to perturbations that are *local in space* [10].

Following [10], we define a *swarm minimizer* as a swarm equilibrium which satisfies

$$\Lambda(x) \geqslant \lambda_i, \qquad \text{in some neighbourhood of each } \Omega_i. \tag{2.18}$$

By the interpretation of Λ, (2.18) means that an infinitesimal redistribution of mass in a neighbourhood of Ω_i increases the energy. We should remark that a local minimizer would require

$$\lambda_i = \lambda, \quad i = 1, \dots, m.$$

Furthermore, to really check for global minimizers we would need to look to E_2 which, in general, is harder to characterize than E_1. The authors of [10] go into more detail.

Remark 2.1.3 (Equilibria of the plain aggregation model)**.** *We point out that condition* (2.17) *is only a* necessary *condition for $\bar{\rho}$ to be an equilibrium of* (1.4)*. Indeed, consider a density $\bar{\rho}$ that satisfies* (2.17) *and check whether it satisfies the equilibrium condition* (1.7)*. By* (2.17)*, equation* (1.7) *is indeed satisfied in every component Ω_i that lies in the interior of Ω (the projection plays no role there). However, consider a component Ω_i of the swarm that lies* on *the boundary of the physical domain Ω. The component Ω_i can be for instance a codimension one manifold, such as a line in $\mathbb{R}^2$; part of our investigation in Chapter 4 focuses on this example in fact. Since $\Lambda(x)$ is constant on $\Omega_i \subset \partial\Omega$, we infer that the tangential component to $\partial\Omega$ of $\nabla\Lambda$ is zero at any point $x \in \Omega_i$. Consequently, by* (2.12)*, we conclude that the unprojected velocity at x (c.f.,* (1.1b)*) is* normal *to $\partial\Omega$. For an equilibrium solution, this normal component must point away from the interior of Ω ($v \cdot n_x \geqslant 0$) – see* (1.4b) *and* (1.5)*; however, one cannot infer this condition from* (2.17)*. Chapter 4 provides examples where solutions to* (2.17) *do not yield equilibria, precisely because the velocity at some points on the boundary is directed toward the interior of Ω, and thus the steady state condition* (1.7) *fails.*

Remark 2.1.4 (Locality of perturbations)**.** *The word 'local' has appeared above in various instances with very different meanings. In the phrase 'local minimizer' the word* local *refers to the small* size *of the perturbations. On the other hand, for a multi-component swarm minimizer,* (2.18) *has to hold only in a* neighbourhood *of each component, which indicates that only perturbations $\tilde{\rho}$ that are* local in space *are considered. In other words, a swarm minimizer is a* local minimizer *of the energy with respect to admissible perturbations $\epsilon\tilde{\rho}$ (for precise terminology and formal variational setup see Remark 2.1.2) that are* local in space.

2.1.4 The quadratic attraction, Newtonian repulsion (QANR) potential and its equilibria in free space

Our studies mainly focus on a well known and well studied potential [41, 44, 43], which we introduce here. This is the quadratic attraction, Newtonian repulsion (QANR) potential,

$$K(x) = \phi(x) + \frac{1}{2}|x|^2, \tag{2.19}$$

where $\phi(x)$ is the free-space Green's function for the negative Laplace operator $-\Delta$:

$$\phi(x) = \begin{cases} -\frac{1}{2}|x|, & n = 1 \\ -\frac{1}{2\pi}\ln|x|, & n = 2. \end{cases} \tag{2.20}$$

A very important property of such potentials for us is that they lead to compactly supported equilibrium states of constant densities [41, 44] — as is rederived below.

We wish to quickly address assumptions for theoretical results for the model in domains with boundaries. While we use results to guide us (for example, [62, 28]), these require assumptions on K which the potential (2.19) does not satisfy. In particular, the interaction potential is required there to be C^1 and λ-geodesically convex. Consequently, the results in [62, 28] do not immediately apply to our study. Nevertheless we consider the framework developed in these papers, in particular the gradient flow and the energy dissipation (see (2.4)), and the particle approximation method which can be turned into a valuable computational tool. Indeed, to validate our equilibrium calculations we use a particle method to simulate solutions to (1.4). Additionally, we also investigate C^1- and C^2-smoothed versions of (2.19) later to provide results in line with the theoretical assumptions.

In the absence of an exogenous potential ($V = 0$), the aggregation model (1.1) with interaction potential (2.19) evolves into constant, compactly supported steady states. This can be inferred from a direct calculation using the specific form of the potential (2.19). Indeed, expand

$$\nabla \cdot (\rho v) = v \cdot \nabla\rho + \rho\nabla \cdot v,$$

and write the aggregation equation (1.1) as

$$\rho_t + v \cdot \nabla\rho = -\rho\nabla \cdot v. \tag{2.21}$$

From (1.1b) and (2.19), using $-\Delta\phi = \delta$ and the mass constraint (2.7), one gets

$$\begin{aligned} \nabla \cdot v &= -\Delta K * \rho \\ &= \rho - nM. \end{aligned} \tag{2.22}$$

This calculation shows that $\nabla \cdot v$ is a *local* quantity. By using (2.22) in (2.21), one finds that along characteristic paths $X(\alpha, t)$, defined by

$$\frac{d}{dt}X(\alpha, t) = v(X(\alpha, t), t), \qquad X(\alpha, 0) = \alpha, \tag{2.23}$$

$\rho(X(\alpha, t), t)$ satisfies:

$$\frac{D}{Dt}\rho = -\rho(\rho - nM). \tag{2.24}$$

The remarkable property of the interaction potential (2.19), as seen from equation (2.24), is that the evolution of the density along a certain characteristic path $X(\alpha, t)$ satisfies a decoupled, stand-alone, ordinary differential equation. Hence, as inferred from (2.24), $\rho(X(\alpha, t), t)$ approaches the value nM as $t \to \infty$, along *all* characteristic paths $X(\alpha, t)$ that transport non-zero densities. More specifically, it has been demonstrated in [15, 44] that solutions to equation (1.1), with K given by (2.19), approach asymptotically a radially symmetric equilibrium that consists in a ball of constant density nM.

In domains with boundaries, as the velocity is projected (see (1.4b) and (1.5)) at points on the boundary, the characteristic equations (and the evolution of the density along characteristic paths) should be considered in an extended, more general setup. In [28] for instance, the authors study particle approximations for model (1.4) within the framework of differential inclusions. We do not pursue here the idea of studying the characteristic equations for domains with boundaries. As the next calculation shows, for the purpose of studying the QANR potential, such extension is not needed in fact.

Indeed, consider an equilibrium solution $\bar{\rho}$ of model (1.4) that consists of a delta accumulation on the boundary and one or several swarms in the interior of the domain. Note that, unlike the problem in free space, the interior swarms are not expected to be radially symmetric. At any point x in the support of $\bar{\rho}$, the velocity $\bar{v}$ vanishes:

$$\bar{v} = P_x(-\nabla K * \bar{\rho}) = 0.$$

In particular, at an arbitrary point x in one of the interior swarms one has $\nabla \cdot \bar{v} = 0$ and hence, by a calculation similar to (2.22), one concludes that

$$\bar{\rho}(x) = nM \qquad \text{at any } x \in \text{supp}(\bar{\rho}) \cap \text{int}(\Omega). \tag{2.25}$$

This key observation is used in Chapter 3 and 4 to investigate equilibria for model (1.4).

Finally, in the presence of an external potential, calculation of $\nabla \cdot v$ from (1.1b) and (2.19) (see also (2.22)) yields:

$$\nabla \cdot v = \rho - nM - \Delta V.$$

Following similar considerations, for an equilibrium $\bar{\rho}$ of model (1.4), one has

$$\bar{\rho}(x) = nM + \Delta V \qquad \text{at any } x \in \operatorname{supp}(\bar{\rho}) \cap \operatorname{int}(\Omega). \tag{2.26}$$

Throughout this work the only non-zero exogeneous potential we consider is a linear gravitational potential V for which $\Delta V = 0$, so in fact whenever we consider the QANR potential, we have that all equilibria will have free swarms with constant densities, nM.

2.2 Numerical preliminaries

2.2.1 Particle method

Here we describe the particle method we used to evolve the plain aggregation model (1.4). Consider N particles with positions x_i and velocities v_i. In free space, the particle method for model (1.4) is simply implemented by numerically integrating

$$\frac{dx_i}{dt} = v_i, \tag{2.27a}$$

$$v_i = -\frac{M}{N} \sum_{j \neq i} \nabla K(x_i - x_j) - \nabla V(x_i), \tag{2.27b}$$

with $1 \leqslant i \leqslant N$. Recall that the discrete model here (2.27) is highly connected to the plain aggregation model (1.4). In some cases the continuum model can be shown to be the mean field limit of a discrete model such as this.

In domains with boundaries, one needs to consider the possibility of a particle meeting the boundary within a time step. Let Δt denote the time step used in simulations and consider an explicit Euler method for time integration. If within a time step, particle i meets the boundary, then, in accordance with (1.4b) and (1.5), from the moment of collision it only continues to move in the tangential direction to the boundary.

For instance, when considering the one dimensional problem on the half-line, this simply means that, had a particle at x_i with velocity v_i reached the origin within a time step Δt, then it should simply be placed at the origin at the end of the time step. The resulting integrating scheme is then given by

$$x_i(t + \Delta t) = x_i(t) + \Delta t \bar{P}_{x_i} v_i(t), \tag{2.28}$$

where the projection operator $\bar{P}_{x_i}$, a specific case of (1.5), is given by:

$$\bar{P}_{x_i} v_i = \begin{cases} v_i & \text{if } x_i + \Delta t v_i \geqslant 0 \\ -\Delta t^{-1} x_i & \text{otherwise.} \end{cases} \tag{2.29}$$

Similarly, when considering the two dimensional problem on the half-plane we have that the vertical velocity of a particle remains unchanged upon colliding with the wall. In this case, a particle $x_i = (x_{i,1}, x_{i,2})$ with velocity $v_i = (v_{i,1}, v_{i,2})$ updates its position according to (2.28), except that in two dimensions the discrete projection operator is

$$\bar{P}_{x_i} v_i = \begin{cases} (v_{i,1}, v_{i,2}) & \text{if } x_{i,1} + \Delta t v_{i,1} \geqslant 0 \\ (-\Delta t^{-1} x_{i,1}, v_{i,2}) & \text{otherwise.} \end{cases} \tag{2.30}$$

In order to investigate disconnected equilibria we used the particle method to evolve initial states that are concentrated (small support) and close, or adjacent to, the wall. This can either be done by randomly generating the particles on some segment of Ω or by generating equispaced particles on some segment of Ω. After seeing disconnected equilibria arise dynamically from such states, we also would manually move particles from the wall and placing them into the free swarm or vice versa. This allowed us to see representations of all disconnected equilibria.

Lastly we mention particular issues that can arise with regards to the choice of time step Δt. There are two phenomena that one can observe:

- If particles are very concentrated and/or Δt is too large then one can observe erratic dynamics where particles are sent far away from the free swarm.
- Related to the item above, particle methods applied in the manner described here tend to over-approximate the number of particles on the wall in their resultant steady states, though generally these errors are related to the time step size and one can see convergence as the time step is decreased. The error arises when multiple particles reach the wall within the same time step.

2.2.2 Calculation of the 2-Wasserstein distance

We describe here how to compute the 2-Wasserstein distance between a sum of deltas and a classical density which is continuous on its support. This is only when considering states in one dimension. This is used in Chapter 5.1 to compare solutions of the plain aggregation model (1.4) and the diffusive model (1.6) to understand how they approach each other in the zero diffusion limit ($\nu \to 0$).

For ρ_1, $\rho_2 \in \mathcal{P}_2^a(\Omega)$, which is to say that $\rho_1, \rho_2 \in \mathcal{P}_2$ and additionally are absolutely continuous measures, the 2-Wasserstein distance between them can be written as

$$d_W^2(\rho_1, \rho_2) = \inf_{\mathbf{t}} \int_{\mathbb{R}^d} |\mathbf{t}(x) - x|^2 \rho_1(x)\, dx, \tag{2.31}$$

where the infimum is taken over all maps $\mathbf{t}$ transporting ρ_1 to ρ_2. We say that a map $\mathbf{t} : \Omega \to \Omega$ transports ρ_1 into ρ_2 if

$$\int_{x\in A} \rho_2(x)\,\mathrm{d}x = \int_{\mathbf{t}(x)\in A} \rho_1(x)\,\mathrm{d}x \qquad \text{for all bounded subsets } A \text{ of } \Omega. \tag{2.32}$$

Then by a theorem due to Brenier (cf. [64, Theorem 2.12]) there exists a unique optimal transport map $\mathbf{t}_{\rho_1}^{\rho_2}$ which attains the infimum above, and it can be written as $\mathbf{t}_{\rho_1}^{\rho_2} = \nabla\psi$ for some convex function ψ. It is noted in [7] that in one-dimension the map $\mathbf{t}_{\rho_1}^{\rho_2}$ is non-decreasing by the convexity of ψ, and $\mathbf{t}_{\rho_1}^{\rho_2}$ can be determined entirely by the condition

$$\int_{x<\mathbf{t}_{\rho_1}^{\rho_2}(y)} \rho_2(x)\,\mathrm{d}x = \int_{x<y} \rho_1(x)\,\mathrm{d}x.$$

The considerations above also hold when one of the densities is a delta measure. To compute the 2-Wasserstein distance between a density function and a sum of Dirac deltas in one dimension we will proceed as in [7], and compute the optimal transport map $\mathbf{t}_\rho^\mu$ from a probability density ρ, compactly supported on $[0, L]$, into $\mu = \sum_{i=1}^n s_i\delta_{y_i}$. Since $\mathbf{t}_\rho^\mu$ is a non-decreasing function, using (2.32), we can find the optimal transport map by finding a partition $0 = x_0 < x_1 < \cdots < x_n = L$ of the interval $[0, L]$, where the weight of the Dirac mass at y_i is obtained by integrating the density ρ over the subinterval $[x_{i-1}, x_i]$:

$$s_i = \int_{[x_{i-1},x_i]} \rho(x)\,\mathrm{d}x \qquad \text{for all } i = 1, \ldots, N.$$

Then we define $y_i = \mathbf{t}_\rho^\mu(x)$ for $x \in [x_{i-1}, x_i]$ for all $i = 1, \ldots, N$. Returning to (2.31) we see that

$$d_W^2(\rho, \mu) = \int_{[0,L]} |\mathbf{t}_\rho^\mu(x) - x|^2\rho(x)\,\mathrm{d}x = \sum_{i=1}^N \int_{[x_{i-1},x_i]} |y_i - x|^2\rho(x)\,\mathrm{d}x.$$

Chapter 3

Plain aggregation in one dimension

In this chapter we begin to explore equilibria of (1.4) in one dimension and, in particular, investigate those equilibria which are not energy minima. We hope to give evidence that these unstable equilibria occur in a variety of contexts. First we focus on the well known potential involving quadratic attraction and Newtonian repulsion (QANR) where we provide a systematic and complete investigation of equilibria both on the half-line and on a bounded interval. Of these equilibria we differentiate between those that are energy minimizing and those that are not, then we showcase numerical and analytical results suggesting that the unstable equilibria occur from a non-trivial set of initial conditions. We will observe the unstable equilibria form a one parameter family with the unique (up to translation) minimizer occurring at the boundary of this continuum.

A similar study is then done on a bounded interval where we identify a 2-parameter family of unstable equilibria with the unique minimizer occurring on the boundary of this family. This study suggests that the dimensionality of the family of unstable equilibria may change depending on the boundary and has parallels to the results on the half-line though they are more complicated.

We then consider a C^1-smoothed version of the QANR potential and study equilibria again on the half-line, highlighting the equilibria which are not energy minima. This is a potential investigated in other works as well [43] whose contrasting feature is that instead of having the constant density free space equilibria of the QANR potential, it has equilibria composed of a sum of deltas. We will find in this study that again equilibria can be explicitly found, though an extensive study of all equilibria is not performed due to the branching complexity involved. Instead we study all equilibria that take the form of three deltas and use the general results to characterize the stability of a given state. Here we notice that a family of swarm minimizers can be found as a subset of the family of equilibria. Dynamical investigations then are used to argue that the unstable equilibria are dynamically achievable.

Finally we then showcase similar behavior for a different well known, Morse-like potential where we can find explicit forms of equilibria and differentiate those that are unstable. From the results of this chapter we argue convincingly that a generic feature of (1.4) in domains with boundaries is the formation of unstable equilibria through the dynamics of the system.

3.1 Quadratic attraction and Newtonian repulsion (QANR)

For this section we will consider the QANR interaction potential K given by (2.19)-(2.20). It has already been noted in Chapter 2.1.4 that the remarkable property of such potentials is that they lead to equilibria that are constant in the interior of the domain (see (2.25)). In the presence of an external potential, equilibria in the interior of the domain have the form (2.26). Note that (2.26) reduces to (2.25) for harmonic external potentials ($\Delta V = 0$), which is in fact the only case considered in this work.

3.1.1 On the half-line $[0, \infty)$

Here we consider the domain as the half-line $\Omega = [0, \infty)$ so that the boundary is at $x = 0$. We consider two cases: first we investigate without an external potential, $V(x) = 0$, and second we investigate a gravity-like potential, $V(x) = gx$ with $g > 0$, that acts to force agents towards the boundary. Note that $V''(x) = 0$ so regardless of whether we consider gravity or not, we assume a compact swarm away from the boundary with a constant density M.

To begin, we look for equilibria in the form of a delta accumulation of strength S at the origin and a constant density M in an interval $(d_1, d_1 + d_2)$, with $d_1 \geqslant 0$, $d_2 > 0$:

$$\bar{\rho}(x) = S\delta(x) + M\mathbb{1}_{(d_1, d_1+d_2)}. \tag{3.1}$$

The support $\Omega_{\bar{\rho}}$ of $\bar{\rho}$ consists of two (possibly disconnected) components:

$$\Omega_1 = \{0\} \quad \text{and} \quad \Omega_2 = [d_1, d_1 + d_2].$$

Note that we will generally refer to mass off the boundary as the free swarm and the mass on the boundary as the boundary swarm. Now we are going to impose the equilibrium condition (2.18) and see what results.

No external potential: $V(x) \equiv 0$

First observe that by the constant mass condition (2.8a), we have

$$S + Md_2 = M. \tag{3.2}$$

A necessary condition for $\bar{\rho}$ to be an equilibrium is to satisfy (2.17). Equation (2.17) is satisfied provided:

$$\Lambda(0) = \lambda_1, \quad \text{and} \quad \Lambda(x) = \lambda_2 \quad \text{in } [d_1, d_1 + d_2]. \tag{3.3}$$

The calculation of $\Lambda(x)$ from (2.12) yields:

$$\Lambda(x) = S\left(\frac{1}{2}x^2 - \frac{1}{2}x\right) + \int_{d_1}^{d_1+d_2}\left(\frac{1}{2}(x-y)^2 - \frac{1}{2}|x-y|\right) M\,\mathrm{d}y \tag{3.4}$$

for some constants λ_1 and λ_2. For $x \in (d_1, d_1+d_2)$, an elementary calculation of $\Lambda(x)$ gives

$$\begin{aligned}\Lambda(x) = \frac{1}{2}(S + Md_2 - M)x^2 + \frac{1}{2}\left(-S + M(2d_1+d_2)(1-d_2)\right)x \\ + \frac{M}{6}(3d_1^2d_2 + 3d_1d_2^2 + d_2^3) - \frac{M}{4}(2d_1^2 + 2d_1d_2 + d_2^2).\end{aligned}$$

The second condition in (3.3) is satisfied only if the coefficients of x^2 and x of the polynomial above are zero. Setting the coefficient of x^2 to zero yields the mass constraint condition (3.2), while the coefficient of x vanishes provided

$$S = M(2d_1 + d_2)(1 - d_2). \tag{3.6}$$

Combining the two conditions (3.2) and (3.6) we arrive at:

$$S = M(1-d_2), \qquad d_1 = \frac{1-d_2}{2}. \tag{3.7}$$

Hence, there is a family of solutions to (3.3) in the form (3.1). Note that $d_1 + \frac{d_2}{2} = \frac{1}{2}$, implying that for all the equilibria in this family, the centre of mass of the free swarm is at $\frac{1}{2}$.

Remark 3.1.1. *In the calculations so far we have set up d_2 to be the parameter that describes the family of solutions. We will choose to describe the family of solutions according to a more intuitive parameter, however. In particular we describe the family of solutions with the mass ratio r_M defined as the ratio of mass off the boundary to mass on the boundary. With* (3.1) *and* (3.7) *we would have, for instance:*

$$r_M = \frac{Md_2}{S}. \tag{3.8}$$

By expressing everything in terms of d_2 only, Λ takes the following values on the two components Ω_1 and Ω_2 of $\Omega_{\bar{\rho}}$, respectively:

$$\lambda_1 = -\frac{M}{24}(1-d_2)^3 + \frac{M}{8}(1-d_2)^2 - \frac{M}{12}, \tag{3.9a}$$

$$\lambda_2 = -\frac{M}{24}(1-d_2)^3 - \frac{M}{12}. \tag{3.9b}$$

Note that $\lambda_1 > \lambda_2$, unless $d_2 = 1$ ($d_1 = 0$), in which case $\lambda_1 = \lambda_2$. Based on this observation, we distinguish between two qualitatively different equilibria:

i) Disconnected equilibria ($d_1 > 0$). A generic disconnected solution to (3.3) of form (3.1) is shown in Figure 3.1(a); the solid line indicates the constant density in the free swarm and the circle on the vertical axis indicates the strength S of the delta-aggregation at the origin.

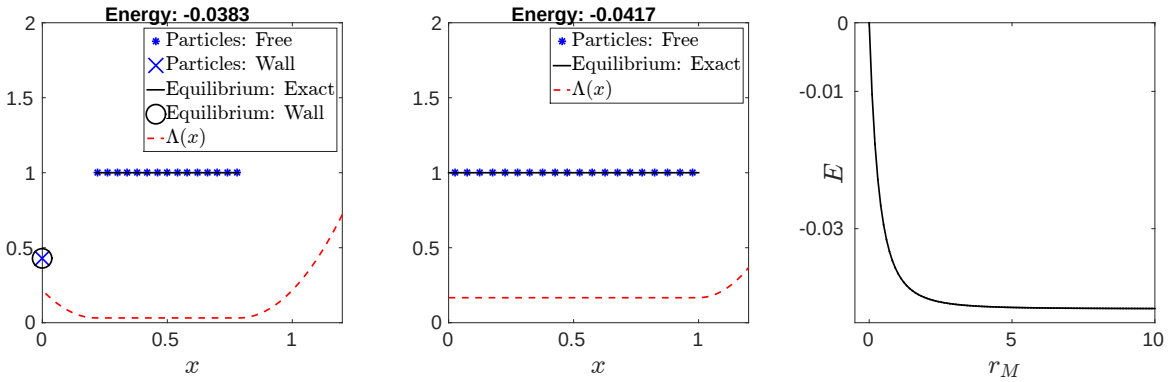

(a) (b) (c)

Figure 3.1: Equilibria (3.1) on half-line for $V = 0$ (no exogenous potential). (a) Disconnected equilibrium consisting in a free swarm of constant density and a degenerate concentration at the origin. (b) The unique (up to translation) minimizer composed of constant density 1 in $(0, 1)$. (c) Energy of equilibria (3.1) as a function of the mass ratio; the lowest energy state corresponds to the connected equilibrium ($r_M = \infty$). Note that for a better visualization $\Lambda(x)$ has been shifted and stretched vertically.

To verify that disconnected states as shown in Figure 3.1 are indeed equilibria, we must check that the velocity everywhere is zero. However because we have satisfied the equilibrium condition (2.14) we already have that the velocity is zero on the free swarm component. Then we focus on the velocity at the boundary and critically observe that the mass at the origin doesn't 'feel' itself. Any mass infinitesimally close to the origin will feel the mass concentrated at the origin, but as soon as we consider mass at the boundary there is no longer a contribution from the boundary itself. This highlights the discontinuous nature of the equilibria. Therefore, the velocity $v(0)$ calculated from (1.1b) reduces to an integral over Ω_2 only:

$$v(0) = P_0 \left(- \int_{\Omega_2} K'(-y)\bar{\rho}(y)\,\mathrm{d}y \right). \tag{3.10}$$

An elementary calculation, using $K'(y) = y - \mathrm{sgn}(y)$ and $\bar{\rho}(y) = M$ in $\Omega_2 = (d_1, d_1 + d_2)$, yields:

$$- \int_{\Omega_2} K'(-y)\bar{\rho}(y)\,\mathrm{d}y = \frac{M}{2} d_2(2d_1 + d_2 - 1). \tag{3.11}$$

Finally, by (3.7),

$$v(0) = P_0(0) = 0,$$

so the disconnected state is indeed an equilibrium. We now check whether the disconnected equilibria are energy minimizers. By an elementary calculation, we find from (3.4) (also using (3.7)):

$$\Lambda'(x) = M(x - d_1) \quad \text{for } x \in (0, d_1), \quad \text{and} \quad \Lambda'(x) = M(x - d_1 - d_2) \quad \text{for } x \in (d_1 + d_2, \infty).$$

Notice $\Lambda(x)$ is strictly decreasing in $(0, d_1)$ and strictly increasing in $(d_1 + d_2, \infty)$ so these disconnected equilibria do not satisfy the swarm minimizer condition (2.18) – see the dashed line representing the plot of $\Lambda(x)$ in Figure 3.1(a). All these disconnected equilibria are therefore not minima; however, as will be elaborated later, these states are asymptotically stable to certain perturbations and are dynamically achievable from a wide range of initial conditions.

ii) Connected equilibria. There are two possible connected equilibria. The first is a degenerate case of (3.1), where $d_1 = \frac{1}{2}$ and $d_2 = 0$, and all mass lies at the origin (or by translation, at any point in $(0, \infty)$):

$$\bar{\rho}(x) = M\delta(x). \tag{3.12}$$

While (3.12) is an equilibrium solution, it is not an energy minimizer, as can be inferred from the expression of Λ:

$$\Lambda(x) = -\frac{1}{2}M|x| + \frac{1}{2}Mx^2,$$

by noting that (2.15) is not satisfied for $x \in (0, 1)$. Any perturbation which does not create a delta accumulation in the interior of Ω, (from this trivial equilibrium) would result either in a disconnected state or in the second connected equilibrium, given by:

$$\bar{\rho}(x) = M\mathbb{1}_{(0,1)}, \tag{3.13}$$

or a translated version of it away from the boundary. This second connected equilibrium (shown in Figure 3.1(b)) can be shown to be an energy minimizer. It is, in fact, the global minimizer as shown by the remark below.

Remark 3.1.2 (States composed of more than two components)**.** *To conclude that the connected equilibrium is the global minimizer one needs to rule out other states as energy minima. We have already shown that disconnected equilibria of form* (3.1) *are not minimizers. One can also show that a multi-component free swarm is not an energy minimizer either. The argument essentially comes from [10] where we wish to show that $\Lambda(x)$ is convex between free swarm components, which is a sufficient condition to show it is not an energy minimizer as* (2.18) *does not hold.*

Assume a disconnected equilibrium of the form

$$\rho(x) = S\delta(x) + \sum_{i=1}^{m} \rho_i(x), \tag{3.14}$$

where ρ_i are supported on Ω_i (Ω_i are disjoint from each other and do not include the origin). Note that as mentioned in Remark 3.1.1, $\rho_i(x) = M$ for $x \in \Omega_i$, though this is not directly used below to show that equilibrium (3.14) *is not a minimizer.*

Then (2.12) *becomes*

$$\Lambda(x) = S\left(\frac{1}{2}x^2 - \frac{1}{2}x\right) + \sum_{i=1}^{m} \int_{\Omega_i} K(x-y)\rho_i(y)\,\mathrm{d}y,$$

and for $x \notin \cup\Omega_i$ one gets

$$\Lambda''(x) = S + \sum_{i=1}^{m} \int_{\Omega_i} \rho_i(y)\,\mathrm{d}y = M > 0.$$

Therefore, $\Lambda(x)$ is indeed convex between free swarm components and (3.14) *cannot be a minimizer. So then the only states we needed to consider were those with an accumulation on the wall and a single component as the free swarm, which is precisely what we considered at the onset* (3.1)*. Furthermore from* (2.26) *we know that we need only consider free swarm components with a constant density M, which is what we did consider.*

The energy corresponding to the equilibria (3.1) can be computed as:

$$E[\bar{\rho}] = \frac{1}{2}\int_{\Omega_{\bar{\rho}}} \Lambda(x)\bar{\rho}(x)\,\mathrm{d}x = \frac{\lambda_1}{2}\int_{\Omega_1} \bar{\rho}(x)\,\mathrm{d}x + \frac{\lambda_2}{2}\int_{\Omega_2} \bar{\rho}(x)\,\mathrm{d}x.$$

After a simple calculation, using the explicit expressions of λ_1 and λ_2 from (3.9), one finds:

$$E[\bar{\rho}] = \frac{M^2}{3}\left(d_1^3 - \frac{1}{8}\right) = \frac{M^2}{24}d_2(-3 + 3d_2 - d_2^2). \tag{3.15}$$

Note that $E[\bar{\rho}]$ has the lowest energy for $d_1 = 0$ (or equivalently, $d_2 = 1$), which corresponds to the global minimizer (3.13). Figure 3.1(c) shows the energy as a function of the mass ratio.

Linear exogeneous potential: $V(x) = gx$

We managed to find explicit forms of equilibria without an external potential present and were able to demonstrate that some of these states were not minima of the energy but yet were equilibria according to (1.7). Now we will consider a gravity-like potential that pushes towards the boundary, forcing mass closer to the boundary. We will again find unstable equilibria again with the connected minimizer having a non-zero mass delta accumulation on the boundary as similarly found in [10]. We take the same form as before (3.1) and seek to satisfy the necessary condition (2.17). By direct calculation,

$$\Lambda(x) = S\left(\frac{1}{2}x^2 - \frac{1}{2}x\right) + \int_{d_1}^{d_1+d_2} \left(\frac{1}{2}(x-y)^2 - \frac{1}{2}|x-y|\right) M dy + gx. \tag{3.16}$$

Then we note that the coefficient of x vanishes provided

$$S = M(2d_1 + d_2)(1 - d_2) + 2g.$$

Combine this equation with the mass constraint (3.2) to find

$$S = M(1 - d_2), \qquad d_1 = -\frac{g}{M(1 - d_2)} + \frac{1 - d_2}{2}. \tag{3.17}$$

Note that since $d_1 \geqslant 0$ and $0 < d_2 < 1$, then necessarily $g < \frac{M}{2}$ and $0 < d_2 \leqslant 1 - \sqrt{\frac{2g}{M}}$. In fact $g_c = \frac{M}{2}$ is a critical value for the system since if $g > g_c$ then all the mass is simply forced onto the boundary and the only equilibria are those with all mass on the boundary. These are not interesting and so we only study $g < g_c$ below.

By an elementary calculation, one can compute the values of $\Lambda(x)$ in each component of the support, Ω_1 and Ω_2, respectively:

$$\lambda_1 = -\frac{M}{24}(1 - d_2)^3 + \frac{M}{8}(1 - d_2)^2 - \frac{M}{12} + \frac{g^2}{2M}\frac{d_2}{(1 - d_2)^2}, \tag{3.18a}$$

$$\lambda_2 = -\frac{M}{24}(1 - d_2)^3 - \frac{M}{12} - \frac{g^2}{2M}\frac{1}{1 - d_2} + \frac{g}{2}. \tag{3.18b}$$

As in the zero gravity case, we find that $\lambda_1 > \lambda_2$, unless $d_2 = 1 - \sqrt{\frac{2g}{M}}$ (or equivalently, $d_1 = 0$), in which case $\lambda_1 = \lambda_2$.

i) Disconnected equilibria ($d_1 > 0$). Figure 3.2(a) shows an example of a disconnected equilibrium we found. Now we wish to check whether i) these states are equilibria, and ii) these states are energy minima. By a similar argument as in the zero gravity case (attractive and repulsive effects at the origin are only felt through interactions with the free swarm), the velocity $v(0)$ calculated from (1.7) reads:

$$v(0) = P_0\left(-\int_{\Omega_2} K'(-y)\bar{\rho}(y)dy - g\right). \tag{3.19}$$

By (3.11) and (3.17),

$$-\int_{\Omega_2} K'(-y)\bar{\rho}(y)dy = -g\frac{d_2}{1 - d_2},$$

and hence, from (3.19) and (1.5) we find that

$$v(0) = P_0(\underbrace{-\frac{g}{1 - d_2}}_{<0}) = 0.$$

The disconnected state is indeed an equilibrium.

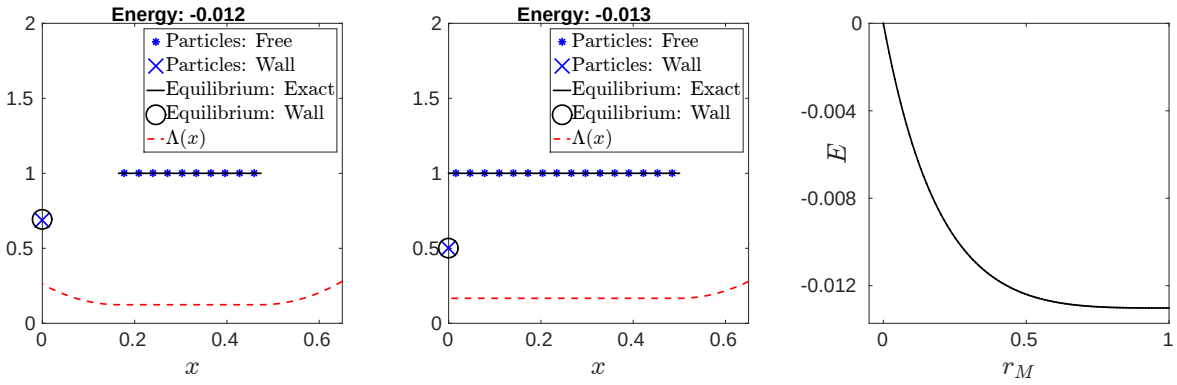

(a) (b) (c)

Figure 3.2: Equilibria (3.1) on half-line for $V(x) = gx$ (linear exogenous potential) with $g = 0.125$. (a) Disconnected state consisting in a free swarm of constant density and a delta aggregation at the origin. (b) Connected minimizer with a constant density in a segment adjacent to the origin and a delta aggregation at origin. (c) Energy of equilibria (3.1) as a function of the mass ratio; the lowest energy state corresponds to the connected equilibrium $\left(r_M = \sqrt{\frac{M}{2g}} - 1\right)$.

Again we check whether the disconnected equilibria are minimizers. By direct calculation, one can find from (3.16) and (3.17):

$$\Lambda'(x) = M(x - d_1) \quad \text{for } x \in (0, d_1), \quad \text{and} \quad \Lambda'(x) = M(x - d_1 - d_2) \quad \text{for } x \in (d_1 + d_2, \infty),$$

and hence, $\Lambda(x)$ is strictly decreasing in $(0, d_1)$ and strictly increasing in $(d_1 + d_2, \infty)$ – see Figure 3.2(a). Therefore these disconnected equilibria do not satisfy the condition (2.18) for a swarm minimizer.

ii) Connected equilibria. As with the results without an external potential, there are two connected states that are equilibria. One is with all the mass on the boundary and the second connected state is with mass off and on the boundary. First we consider the degenerate case with all mass on the boundary (see (3.12)). The calculation of Λ from (2.12) yields:

$$\Lambda(x) = -\frac{1}{2}M|x| + \frac{1}{2}Mx^2 + gx.$$

Since $\Omega_{\bar{\rho}} = \{0\}$, (2.14) trivially holds with $\lambda = 0$, while (2.15) is equivalent to

$$\left(-\frac{1}{2}M + \frac{1}{2}Mx + g\right) x > 0, \qquad \text{for all } x > 0. \tag{3.20}$$

The inequality above does not hold when $g < \frac{M}{2}$, hence the equilibrium (3.12) is not an energy minimizer when $g < g_c$.

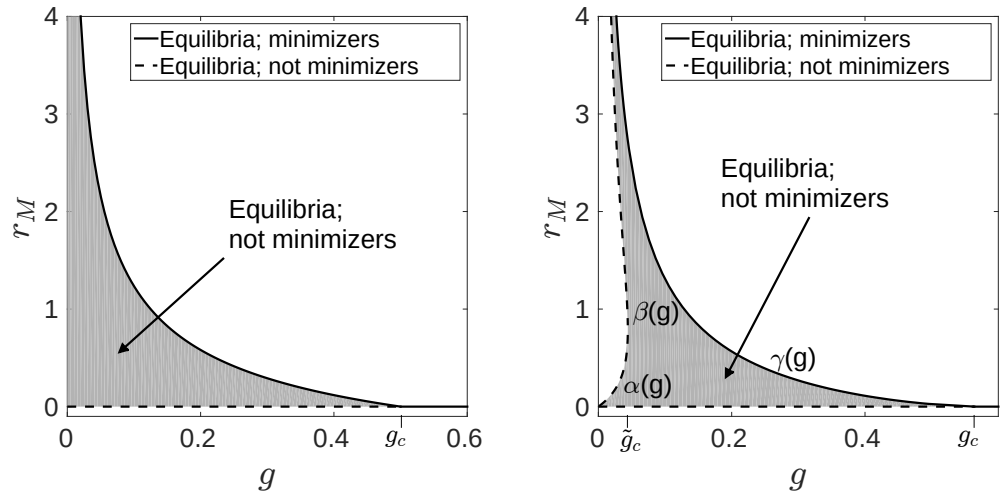

Figure 3.3: Existence and stability of connected and disconnected equilibria. Highlighted in grey are regions where equilibria exist but they are not minimizers. (a) One dimension, $V(x) = gx$, $g_c = 0.5$. For $0 < g < g_c$, disconnected equilibria in the form (3.1) exist for all mass ratios $r_M \in \left(0, \sqrt{\frac{g_c}{g}} - 1\right)$; these equilibria are not energy minimizers. The only stable equilibrium is the connected state with $r_M = \sqrt{\frac{g_c}{g}} - 1$ (solid line). For $g > g_c$, there exists no equilibrium in the form (3.1). The trivial equilibrium where all mass lies at the origin ($r_M = 0$) is unstable for $g < g_c$ (dashed line), but it is a global minimizer when $g \geqslant g_c$ (solid line). (b) Two dimensions, $V(x_1, x_2) = gx_1$, $\tilde{g}_c \approx 0.044$, $g_c \approx 0.564$. For $0 < g < \tilde{g}_c$ disconnected equilibria in the form (4.1) exist only for mass ratios $r_M \in (0, \alpha(g)) \cup (\beta(g), \gamma(g))$, while for $\tilde{g}_c < g < g_c$ disconnected equilibria exist for *all* mass ratios $r_M \in (0, \gamma(g))$; none of these disconnected equilibria are energy minimizers. The only stable equilibrium for $0 < g < g_c$ is the connected state with $r_M = \gamma(g)$ (solid line). For $g > g_c$, there exists no equilibrium in the form (4.1). The equilibrium that has all mass on the boundary ($r_M = 0$) is unstable for $g < g_c$ (dashed line), but it is a global minimizer when $g > g_c$ (solid line).

By computing the energy as a function of r_M, we find the second connected state, consisting of a delta at the boundary and a constant density free swarm, to be a minimizer. This equilibrium is shown in Figure 3.2(b), while Figure 3.2(c) shows the energy:

$$E[\bar{\rho}] = \frac{M^2}{24} d_2(-3 + 3d_2 - d_2^2) + \frac{g}{2} M d_2 - \frac{g^2}{2} \frac{d_2}{1 - d_2}. \tag{3.21}$$

The zero gravity calculation (3.15) can be obtained from (3.21) by setting g to zero. Also as expected, from (3.21) we find that the energy is decreasing with respect to d_2:

$$\frac{\partial E}{\partial d_2} = -\frac{1}{2}\left(\frac{M}{2}(d_2 - 1) - g\frac{1}{d_2 - 1}\right)^2 \leqslant 0.$$

Hence, among all equilibria in the form (3.1), the one that has the lowest energy is the connected state corresponding to $d_2 = 1 - \sqrt{\frac{2g}{M}}$. The family of equilibria above can be alternatively parametrized by the mass ratio r_M. The parameter d_2 ranges in $\left(0, 1 - \sqrt{\frac{2g}{M}}\right)$ for the disconnected equilibria, while $d_2 = 0$ and $d_2 = 1 - \sqrt{\frac{2g}{M}}$ correspond to the two connected equilibria discussed above. Hence, $r_M \in \left[0, \sqrt{\frac{M}{2g}} - 1\right]$, or equivalently $r_M \in \left[0, \sqrt{\frac{g_c}{g}} - 1\right]$. The results of this study have been summarized in Figure 3.3(a), where we have characterized the stability of each state.

Dynamic evolution

Reduced model

At this point we know that we can find explicit forms of equilibria and show analytically that some are indeed equilibria and not energy minima. However if these non-minimizing states are rarely, or never, seen from the dynamics of the system then these observations are not very useful. In this section we hope to understand the dynamics of the model in a way that will allow us to argue to the probability of ending up in a non-minimizing state. Though not rigorous, we give strong arguments for what the basin of attraction is for the connected minimizer when we have $g \equiv 0$ and ultimately argue that unstable equilibria occur from a non-trivial set of initial conditions.

We first examine a simplified model of (1.4) which we will see highlights what initial conditions leads to disconnected states. Then we go over a large-scale numerical test of many different random states that explicitly shows just how likely disconnected equilibria are. Finally we show that the model is decreasing the energy.

Consider a solution to (1.4) with a time-dependent density that has two distinct components:

$$\rho(x,t) = \rho_1(x) + \rho_2(x,t), \tag{3.22}$$

where $\rho_1(x) = S\delta(x)$ is a delta accumulation at the origin (with S fixed) and $\rho_2(x,t)$ is the density profile of the free swarm, with support $\Omega_2(t) = [a(t), b(t)]$. Here, $b(t) > a(t) > 0$ is assumed.

Let

$$M_2 = \int_{\Omega_2(t)} \rho_2(x,t)\,\mathrm{d}x \quad \text{and} \quad C_2(t) = \frac{\int_{\Omega_2(t)} x\rho_2(x,t)\,\mathrm{d}x}{M_2}, \tag{3.23}$$

be the mass and the centre of mass of the free swarm, respectively. Note that since the mass on the boundary is fixed, M_2 does not depend on t and we have $M_2 = M - S$. Solutions of form (3.22) satisfy the equation (1.4) in the weak sense. Note that (1.4) is an equation in conservation law form and its weak formulation is standard [38]. Assume that in the free swarm the solution $\rho_2(x,t)$ is smooth enough so that (1.4) holds in the classical sense. By a standard argument [38, Chapter 3.4] one can then derive the Rankine-Hugoniot conditions which give the evolution of the

two discontinuities $a(t)$ and $b(t)$. For instance, the evolution of the left end is given by

$$\frac{\mathrm{d}a}{\mathrm{d}t} = v(a,t), \tag{3.24}$$

and by (1.7) we calculate

$$\begin{aligned} v(a,t) &= -aS + \frac{S}{2} - \int_{\Omega_2} \left(a - y + \frac{1}{2}\right) \rho_2(y,t)\,\mathrm{d}y - g \\ &= -Ma + M_2\left(C_2 - \frac{1}{2}\right) + \frac{S}{2} - g. \end{aligned}$$

By a similar calculation,

$$\begin{aligned} \frac{\mathrm{d}b}{\mathrm{d}t} &= v(b,t) \\ &= -Mb + M_2\left(C_2 + \frac{1}{2}\right) + \frac{S}{2} - g. \end{aligned}$$

Finally, we derive the evolution of the centre of mass of ρ_2 and get a closed system. To simplify calculations to follow, we drop x and t dependencies when appropriate. Multiply (1.4) by x, integrate over Ω_2 and use integration by parts on the right-hand-side to get:

$$\int_{\Omega_2(t)} x(\rho_2)_t\,\mathrm{d}x = \left(x\rho_2(K*\rho_1 + K*\rho_2 + V)_x\right)\Big|_a^b - \int_{\Omega_2} \rho_2(K*\rho_1 + K*\rho_2 + V)_x\,\mathrm{d}x. \tag{3.25}$$

By an elementary calculation,

$$\frac{\mathrm{d}}{\mathrm{d}t}\int_{\Omega_2(t)} x\rho_2(x,t)\,\mathrm{d}x = \int_a^b x(\rho_2)_t\,\mathrm{d}x + \rho_2(b,t)b\frac{\mathrm{d}b}{\mathrm{d}t} - \rho_2(a,t)a\frac{\mathrm{d}a}{\mathrm{d}t}. \tag{3.26}$$

Combine (3.25) and (3.26) and use the evolution of $a(t)$ and $b(t)$ derived above. The boundary terms cancel and we find

$$M_2\frac{\mathrm{d}C_2}{\mathrm{d}t} = -\int_{\Omega_2} \rho_2(K*\rho_1 + K*\rho_2 + V)_x\,\mathrm{d}x. \tag{3.27}$$

By symmetry of K,

$$\int_{\Omega_2} \rho_2(K*\rho_2)_x\,\mathrm{d}x = 0,$$

and with (2.19) and $V(x) = gx$ we get

$$\begin{aligned} (K*\rho_1)_x &= S\left(x - \frac{1}{2}\right), \quad V_x = g, \\ \int_{\Omega_2} \rho_2(K*\rho_1 + V)_x\,\mathrm{d}x &= SM_2C_2 + M_2\left(g - \frac{S}{2}\right). \end{aligned}$$

Hence, from (3.27) one can derive the evolution of C_2, which together with the evolution of a and b, yields the following system of differential equations:

$$\frac{\mathrm{d}C_2}{\mathrm{d}t} = -SC_2 + \left(\frac{S}{2} - g\right), \tag{3.28a}$$

$$\frac{\mathrm{d}a}{\mathrm{d}t} = -Ma + M_2\left(C_2 - \frac{1}{2}\right) + \frac{S}{2} - g, \tag{3.28b}$$

$$\frac{\mathrm{d}b}{\mathrm{d}t} = -Mb + M_2\left(C_2 + \frac{1}{2}\right) + \frac{S}{2} - g. \tag{3.28c}$$

It is now an elementary exercise to solve (3.28) for $C_2(t)$, $a(t)$, and $b(t)$ given initial data $C_2(0)$, $a(0)$, and $b(0)$. One then gets

$$C_2(t) = \left(C_2(0) - \frac{1}{2} + \frac{g}{S}\right)e^{-St} + \left(\frac{1}{2} - \frac{g}{S}\right), \tag{3.29a}$$

$$a(t) = \left(C_2(0) - \frac{1}{2} + \frac{g}{S}\right)e^{-St} + \left(a(0) - C_2(0) + \frac{M_2}{2M}\right)e^{-Mt} + \left(\frac{S}{2M} - \frac{g}{S}\right), \tag{3.29b}$$

$$b(t) = \left(C_2(0) - \frac{1}{2} + \frac{g}{S}\right)e^{-St} + \left(b(0) - C_2(0) - \frac{M_2}{2M}\right)e^{-Mt} + \frac{1}{2MS}\left(M^2 - 2Mg - M_2^2\right). \tag{3.29c}$$

A first observation is that the equilibrium for (3.29) corresponds to the disconnected state found earlier. Indeed one can check that considering (3.29) as $t \to \infty$ yields, $a = d_1$, $b = d_1 + d_2$, and $C_2 = d_1 + \frac{d_2}{2}$, with d_1 and d_2 given in terms of S using (3.17). We finally mention we are only considering realistic cases ($C_2(0) \geqslant 0$, $a(0) \geqslant 0$).

Next we wish to use the reduced dynamics to determine under which perturbations the disconnected equilibria are asymptotically stable. By inspecting the profile of $\Lambda(x)$, we have already observed that these equilibria are unstable under infinitesimal perturbations which move mass off the boundary (see Figure 3.1(a)). Therefore we only seek to consider perturbations of the free swarm in this study. We consider a perturbation away from the boundary and then study the evolution of

$$\rho(x,t) = \bar{\rho}(x) + \tilde{\rho}_2(x,t), \tag{3.30}$$

where $\bar{\rho}$ is the disconnected equilibrium (3.1) and $\tilde{\rho}_2$ has support away from the origin and zero mass. Note that density (3.30) can also be written in the separated form (3.22), where

$$\rho_1(x) = S\delta(x) \qquad \text{and} \qquad \rho_2(x,t) = M\mathbb{1}_{(d_1,d_1+d_2)}(x) + \tilde{\rho}_2(x,t) \tag{3.31}$$

such that $\rho(x,t) = \rho_1(x) + \rho_2(x,t)$.

The reduced dynamics (3.28) can be used to track the dynamics of the centre of mass $C_2(t)$ and the support $[a(t), b(t)]$ of $\rho_2(x,t)$, provided:

(i) No mass leaves the origin; *and*

(ii) No mass transfers from ρ_2 to the origin.

We will quantify now when (i) and (ii) can happen. To address (i), one needs to inspect the velocity at the origin, which computed by (1.7) and (2.19) (see also (3.23)) gives:

$$\begin{aligned} v(0,t) &= P_0\left(\int_{\Omega_2(t)}\left(y-\frac{1}{2}\right)\rho_2(y,t)\,\mathrm{d}y - g\right) \\ &= P_0\left(M_2\left(C_2(t)-\frac{1}{2}\right)-g\right). \end{aligned}$$

We find that no mass leaves the origin ($v(0,t)=0$) provided

$$C_2(t) \leqslant \frac{1}{2} + \frac{g}{M_2}. \tag{3.32}$$

In particular, the initial perturbed state $\rho(\cdot,0)$ in (3.30) must satisfy this restriction. We note that once (3.32) holds at $t=0$, it holds for all times; this can be inferred from the monotonic evolution of $C_2(t)$ (see (3.29a)), and

$$\lim_{t\to\infty} C_2(t) = \frac{1}{2} - \frac{g}{S} < \frac{1}{2} + \frac{g}{M_2}.$$

For (ii) we note that mass transfer occurs when the left end of the support of the free swarm meets the boundary and pushes into it. This occurs when $a=0$ and $\frac{\mathrm{d}a}{\mathrm{d}t} < 0$ or, alternatively, if $a<0$ at any time. One can find a curve γ_{r_M} in $(a(0),\, C_2(0))$-space, dependent on r_M, where the solution (3.29) has $a(t) \geqslant 0$ for all $t \geqslant 0$ and $a(t)=0$ for some t. Furthermore one finds that the enclosed area under the curve represents the set of initial conditions where $a(t^*) < 0$ for some $t^* \geqslant 0$ and so the free swarm has collided with the boundary, which we believe would then lead to more mass concentrating on the boundary and r_M decreasing. It is observed from dynamical simulations that mass concentrating near the boundary ultimately leads to mass accumulating on the boundary and leading to disconnected states. Figure 3.4 shows some example solutions and relates them to these ideas of mass transfer and γ_{r_M}.

Then, one has that the region above γ_{r_M} represents states where the free swarm never contacts the boundary and so the mass ratio is constant. Since there is only one equilibrium for any given r_M then this region in fact represents the set of initial conditions with a mass ratio r_M that would dynamically approach the disconnected equilibrium with mass ratio r_M. This then allows visualizations of the following: (i) the set of perturbations one could make to a given disconnected

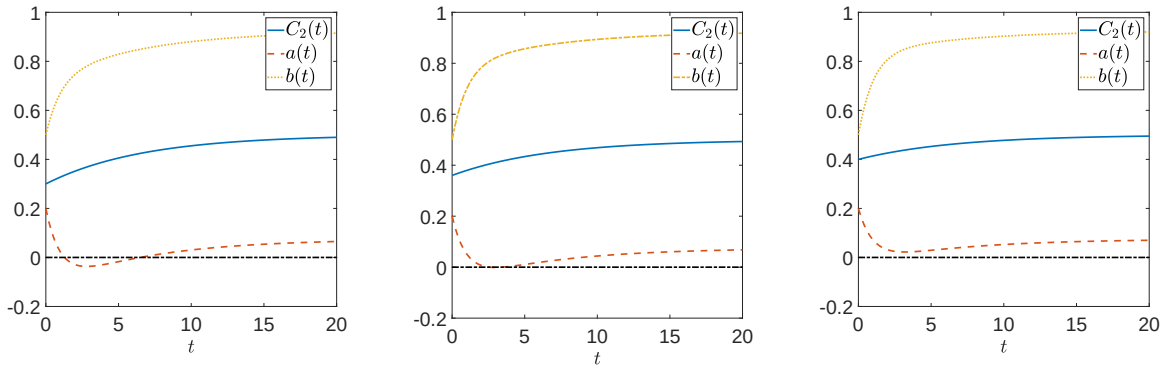

(a) (b) (c)

Figure 3.4: Solutions $(C_2(t), a(t), b(t))$ to the model (3.29) with $g = 0$ and $r_M = 5.66$. (a) Here $(C_2(0), a(0), b(0)) = (0.3, 0.2, 0.5)$ and we see $a(t)$ becomes negative for early times. The assumptions of the model break when this happens but suggests that mass is further accumulated on the wall, resulting in a state with a decreased mass ratio. (b) Here $(C_2(0), a(0), b(0)) \approx (0.36, 0.2, 0.5)$ and we see $a(t)$ becomes zero but does not become negative. This choice of initial condition lies on the curve γ_{r_M} (see the red solid line in Figure 3.5(a) associated with $r_M = 5.66$) . (c) Here $(C_2(0), a(0), b(0)) = (0.4, 0.2, 0.5)$ and we see $a(t)$ is always strictly positive and so mass transfer does not occur and the equilibrium will be disconnected with mass ratio $r_M = 5.66$.

equilibrium, and (ii) the basin of attraction among states with mass ratio r_M which are shown in Figure 3.5 without and with gravity.

Remark 3.1.3 (Interpreting Figure 3.5 and Observations)**.** *In order to identify the set of perturbations one could make to a given disconnected equilibrium, one considers where the disconnected equilibrium exists in the* $(a(0), C_2(0))$*-space. The location of the disconnected equilibrium within the set formed of states above* γ_{r_M} *and below* $C_2(0) = 1/2 + g/M_2$ *is how one determines stable perturbations. Taking, for example, Figure 3.5(b) with* $r_M = 0.875$*, then if the perturbed state had* $(a(0), C_2(0)) = (0.1, 0.2)$ *then it would be a stable perturbation. If the perturbed state had* $(a(0), C_2(0)) = (0.05, 0.1)$ *then it would be an unstable perturbation.*

A more striking example is in Figure 3.5(a) for $r_M = \infty$*. Recall that* $r_M = \infty$ *corresponds to the connected minimizer. Here, since* $\frac{1}{2} + \frac{g}{M_2} = \frac{1}{2}$ *and* γ_∞ *is also the line* $C_2(0) = \frac{1}{2}$ *then* $a(0) = 0$*, any perturbation that decreases the center of mass results in mass accumulating on the boundary and is thus an unstable perturbation of the connected minimizer. A perturbation that increases* $a(0)$ *or* $C_2(0)$ *then does not change the mass ratio and so the eventual final state will be the connected minimizer. This observation has been haphazardly summarized by the author in that* almost all states that interact with the boundary will result in disconnected equilibria.

Finally, it should be remarked that this result manages to encapsulate the basin of attraction of the connected minimizer of, at least, all initial conditions without any delta accumulations. One

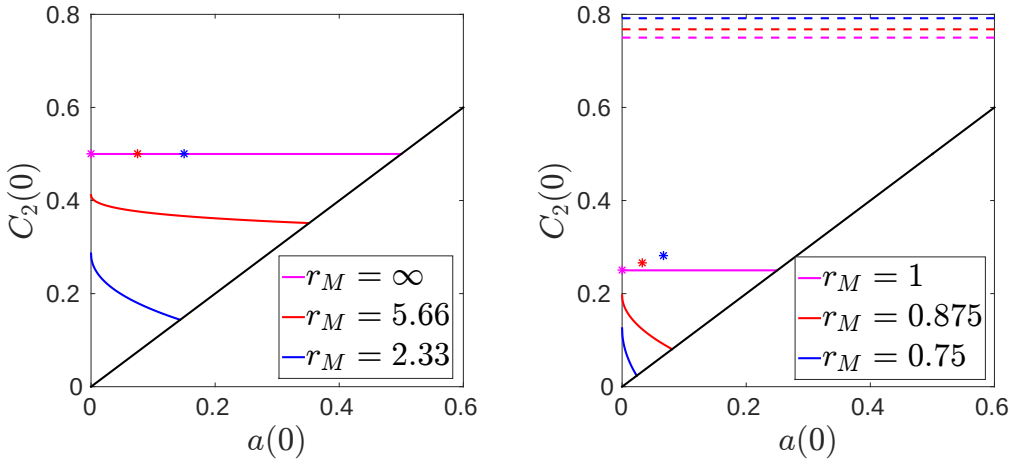

(a) (b)

Figure 3.5: Disconnected equilibria (3.1) are asymptotically attracting certain initial densities of type (3.22). Considered are three mass ratios, one of which being the mass ratio of the minimizer (magenta), for (a) $g = 0$ and (b) $g = 0.125$. A perturbed state $\rho(x,t)$ (see (3.30) and (3.31)) that has $a(0)$ and $C_2(0)$ in the region strictly above the solid curves, representing γ_{r_M}, and below the dashed lines, $C_2(0) = 1/2 + g/M_2$, will evolve dynamically to the disconnected equilibrium of the corresponding mass ratio. An initial condition with $(a(0), C_2(0))$ below the solid curves will evolve dynamically to an equilibrium of a smaller mass ratio. The dashed lines indicate the thresholds $1/2 + g/M_2$ above which mass on the boundary would lift off. Stars indicate the equilibrium for the mass ratio corresponding to its colour, which gives a sense of how much the center of mass or the left edge of the support can be perturbed.

could summarize this to a general result that any classical initial condition with $C_2(0) \geqslant \frac{1}{2}$ *and* $0 \leqslant a(0) \leqslant C_2(0)$ *will dynamically result in the connected minimizer.*

Remark 3.1.4. *There is an admission here of a lack of rigour. While the results above are attractive, it is necessary to point out that some key points of understanding require* $a(0) = 0$ *which means the free swarm is contacting with the boundary, violating an assumption that we initially built the reduced model from. In particular, considering* $r_M = \infty$ *goes against our assumptions. We believe by a continuity argument that one could consider the results discussed by taking* $r_M \to \infty$*. Additionally we support these results with large-scale numerical runs as explained in the next section.*

Non-trivial initial conditions leading to disconnected equilibria

In the previous arguments we presented evidence that disconnected states are perhaps commonly achieved through dynamic evolution of the model (1.4). However the arguments laid out do not necessarily hold once the free swarm contacts the boundary and so one would like more evidence.

To this end we consider initial states of particles with positions randomly generated from a uniform distribution on $(d_1^{(i)}, d_1^{(i)} + d_2^{(j)})$, where $1 \leqslant i, j \leqslant 10$, and

$$d_1^{(i)} = \frac{1}{20}(i-1), \quad d_2^{(j)} = \frac{1}{10}j, \quad \text{for} \quad g = 0, \tag{3.33}$$

$$d_1^{(i)} = \frac{1}{40}(i-1), \quad d_2^{(j)} = \frac{1}{20}j, \quad \text{for} \quad g = 0.125. \tag{3.34}$$

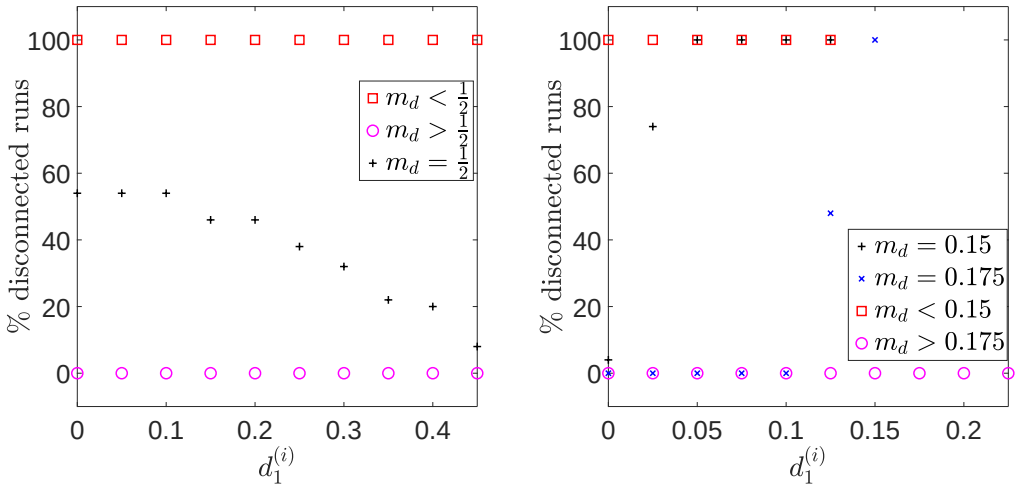

(a) (b)

Figure 3.6: Percentage of initial states which resulted in disconnected states for (a) $g = 0$ and (b) $g = 0.125$. Note that we find disconnected final states for a significant set of initial data.

We ran 50 particle simulations of $N = 1024$ particles for each interval $(d_1^{(i)}, d_1^{(i)} + d_2^{(j)})$, with $1 \leqslant i \leqslant 10$ and $1 \leqslant j \leqslant 10$. We evolved the particle simulations until the state is steady and calculated the mass ratio of the resultant state. For convenience of discussion later, denote the midpoint of the initial interval, by

$$m_d = \frac{1}{2}\left(d_1^{(i)} + \left(d_1^{(i)} + d_2^{(j)}\right)\right). \tag{3.35}$$

We mention here as well that the centre of mass of the initial swarm will likely be close to the midpoint as we have drawn particle positions from a uniform distribution. This is particularly important in comparing with the results of the reduced model, as the intervals $(d_1^{(i)}, d_1^{(i)} + d_2^{(j)})$ have been constructed in such a way that for $i = 11 - j$ we have $m_d = \frac{1}{2}$ for $g = 0$ and $m_d = \frac{1}{4}$ for $g = 0.125$, in consideration of Figure 3.5 and Remark 3.1.3.

We find that for the $g = 0$ case, all initial states with $m_d < \frac{1}{2}$ resulted in a disconnected state and all initial states with $m_d > \frac{1}{2}$ resulted in a connected state — see squares and circles in

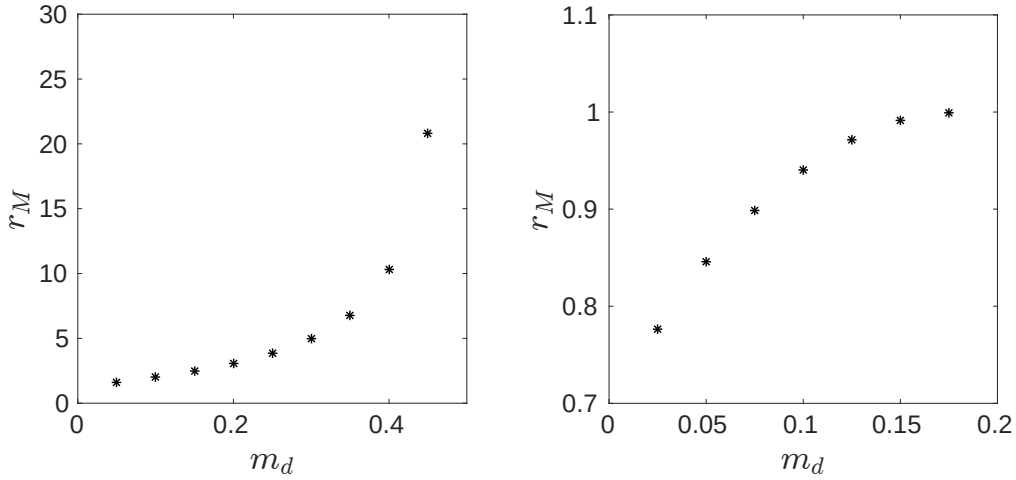

(a) (b)

Figure 3.7: Average mass ratios of resultant states for particular m_d for (a) $g = 0$ and (b) $g = 0.125$. $m_d = \frac{1}{2}$ has been neglected from (a) for clarity as the average is much larger (about 516).

Figure 3.6(a) indicating percentages of disconnected states. This is consistent with the observation made previously that any state with a centre of mass greater than one half results in the connected minimizer and any state with centre of mass less than one half results in a disconnected equilibrium.

For the case of $g = 0.125$ we find somewhat similar results. Figure 3.6(b) shows that for $m_d < 0.15$ we always get disconnected resultant states and for $m_d > 0.175$ we always get the connected equilibrium. For $m_d = 0.15$ and $m_d = 0.175$ the results can be mixed. We suspect in fact that there may be discrete numerical effects and that the true value of m_d where we observe variability in disconnected/connected resultant states is closer to $\frac{1}{4}$, but this cannot be substantiated confidently enough.

Discrete energy dissipation

Now, we have shown disconnected equilibria that are not energy minima. We have given arguments that they are achieved dynamically from a highly non-trivial set of initial conditions. Finally we supported those arguments with large-scale numerical tests showing these non-minimizing states are achieved, depending on the initial state. This seems to contradict the idea that model (1.4) is an energy gradient system as it appears to be possible to flow into an energy saddle point. One last sanity check of these results then is to look at whether the system is actually decreasing the energy throughout and whether it follows the expected dissipation formula (2.4). From our simulations we always check whether the energy is decreasing anyways, and in all simulations reported here the energies decrease monotonically.

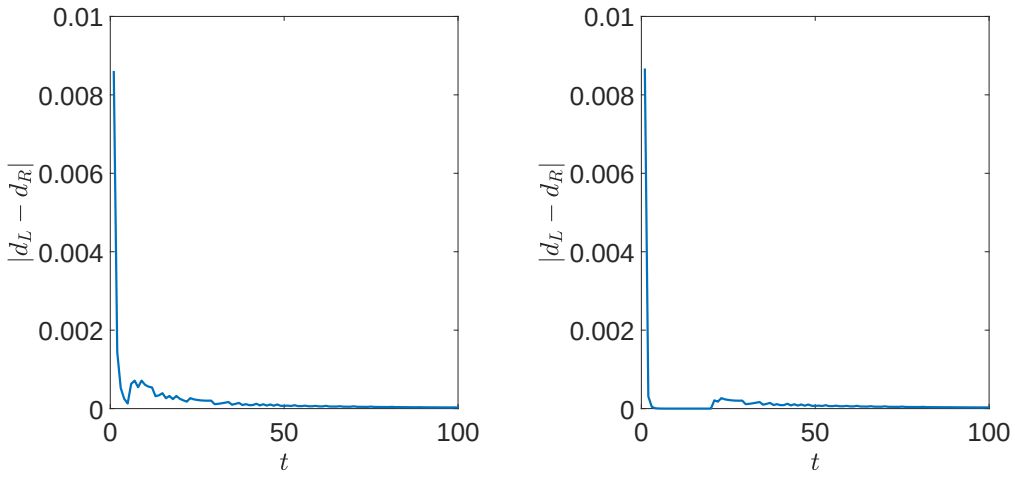

(a) (b)

Figure 3.8: The discrete energy dissipation formula appears to be validated during simulations even when interacting with the boundary. We take an initial configuration randomly uniformly distributed in $[0, 1/4]$ and evolve it with (a) $g = 0$ and (b) $g = 0.125$. Here we see the left-hand-side (3.38), d_L, and the right-hand-side (3.39), d_R of the discrete energy dissipation formula stay are close. We observe that this error decreases as either the number of particles N is taken larger or the time step Δt is taken smaller (see Table 3.1).

Let $s = n\Delta t$ and $t = (n+1)\Delta t$ for $n \geqslant 0$ be two successive times in (2.4). We then have, after dividing by Δt,

$$\frac{E[(n+1)\Delta t] - E[n\Delta t]}{\Delta t} = -\frac{1}{\Delta t}\int_{n\Delta t}^{(n+1)\Delta t}\int_{\Omega} |P_x(-\nabla K * \rho(x,\tau) - \nabla V(x))|^2 \rho(x,\tau)\,\mathrm{d}x\,\mathrm{d}\tau. \quad (3.36)$$

The discrete density is a superposition of delta accumulations at the particle locations:

$$\rho^N(x,t) = \frac{M}{N}\sum_{i=1}^{N}\delta(x - x_i(t)),$$

and the corresponding discrete energy (see (2.3)) is given by

$$E[\rho^N(t)] = \frac{M^2}{2N^2}\sum_{i=1}^{N}\sum_{j=1}^{N} K(x_i(t) - x_j(t)) + \frac{M}{N}\sum_{i=1}^{N} V(x_i(t)). \quad (3.37)$$

Note that $K(0) = 0$ in this context so we do not need to exclude the case of $i = j$ in the double sum representing social interaction. So then we calculate the discrete version of the left-hand-side

of (3.36) as

$$d_L = \frac{E[\rho^N((n+1)\Delta t)] - E[\rho^N(n\Delta t)]}{\Delta t}. \tag{3.38}$$

We approximate the right-hand side of (3.36) first by a right endpoint approximation. Then call $v_i(t)$ the velocity of particle $x_i(t)$ at time t. Note that $P_x(-\nabla K * \rho(x,\tau) - \nabla V(x))$ is the velocity. The discrete approximation to the right-hand-side of (3.36) is then given by

$$d_R = -\frac{M}{N}\sum_{i=1}^{N}\Big(v_i((n+1)\Delta t)\Big)^2. \tag{3.39}$$

Figure 3.8 shows the differences between d_L and d_R for a non-gravity and gravity case. We see they are quite close and get nearer as either the number of particles is increased or the time step is taken smaller. Table 3.1 gives some evidence for how this error depends on these.

	$\Delta t = 0.1$	$\Delta t = 0.01$	$\Delta t = 0.001$
$N = 2^8$	3.4264e−3	7.884e−4	4.3157e−4
$N = 2^9$	3.3459e−3	7.5446e−4	2.3621e−4
$N = 2^{10}$	3.3861e−3	6.9359e−4	1.5000e−4

Table 3.1: The maximum errors $|d_L - d_R|$ in the discrete energy dissipation formula for varied N and Δt. We see that decreasing the time step decreases the error more rapidly, likely due to a decreased time step more accurately capturing the joining of particles onto the wall. Larger time steps result in larger jumps in the mass on the wall.

We have then found there are indeed equilibria of models like (1.4) that are not minimizers of the energy but may be encountered dynamically at a non-insignificant probability, at least with the QANR potential. For the remainder of this chapter we wish to study variations of the study conducted here with different physical context or interaction potentials, the purpose being to showcase that unstable equilibria may be a generic feature of these models.

3.1.2 On the line segment $[-x^*, x^*]$

Previously we investigated equilibria in the presence of a single boundary point with an unbounded space away from it. The primary result was that disconnected equilibria existed that were not energy minimizers and these were dynamically being achieved from a non-trivial set of initial conditions. The bounded segment $[-x^*, x^*]$ has two boundary points and hence, based on the understanding gained from the one boundary study, more interaction with boundaries suggests more accumulation.

The boundary points are at $x = -x^*$ and at $x = x^*$. We will consider an exogeneous, gravitational force $V(x) = gx$ which we will first neglect ($g = 0$) and then turn it on later. We will first explicitly calculate equilibria and then see that the minimizer is again the state which has connected support. We will find that the length of the line segment is an important quantity and will find a critical segment length where equilibria change qualitatively.

There are a number of observations we can make here though:

- If $x^* \geqslant \frac{1}{2}$ then all the results from the one-boundary investigation carry over. In this way, the first critical segment length is 1.
  - In this case there is enough space in between the boundaries for the mass to simply form in the interior a constant density swarm. With $g > 0$, mass would accumulate on the left boundary but the free swarm never extends further than a distance of 1 away from the boundary (in fact one can find that $d_1 + d_2 \leqslant 1 - \sqrt{2g}$).
- For $x^* < \frac{1}{2}$ we should consider the one boundary results at times, but there will be the possibility for accumulation on both boundaries. We should be able to recover the one boundary results, in fact, except possibly when the one boundary free swarm would extend beyond the current boundaries.
  - One can get that if $\frac{1}{2} - \sqrt{\frac{g}{2}} \leqslant x^*$ then all one boundary equilibria should exist. This is a second critical segment length in this sense.
- For $\frac{1}{4} < x^* < \frac{1}{2}$ the boundaries exhibit attractive forces on each other and for $0 < x^* < \frac{1}{4}$ all forces become repulsive. This highlights the third and final critical segment length, $\frac{1}{4}$.

We are considering equilibria of the form,

$$\bar{\rho}(x) = S_1\delta(x + x^*) + M\mathbb{1}_{(d_1, d_1+d_2)} + S_2\delta(x - x^*). \tag{3.40}$$

The support $\Omega_{\bar{\rho}}$ of $\bar{\rho}(x)$ consists of three (possibly disconnected) components:

$$\Omega_1 = \{-x^*\}, \quad \Omega_2 = [d_1, d_1 + d_2], \quad \Omega_3 = \{x^*\}. \tag{3.41}$$

No external potential: $V(x) \equiv 0$

The calculations here are essentially the same as when studying the one boundary case, so we shorten when possible. As usual we have the mass constraint,

$$\int \rho(x)\,\mathrm{d}x = M, \tag{3.42}$$

which when using (3.40) we get

$$S_1 + Md_2 + S_2 = M. \tag{3.43}$$

We will also introduce the mass ratio

$$r_M = \frac{Md_2}{S_1 + S_2} \tag{3.44}$$

and the balance ratio

$$r_S = \frac{S_1}{S_2}. \tag{3.45}$$

For illustration and understanding here are some examples:

- $r_M = \infty$: This corresponds to a connected state where all the mass is off the boundaries (note that this state is never an equilibrium if $x^* < \frac{1}{2}$);
- $r_M = 0$, $r_S = 0$ ($r_S = \infty$): This corresponds with a connected state where all the mass is on the right (left) boundary;
- $r_M = \frac{2x^*}{1-2x^*}$, $r_S = 1$: This corresponds with a connected state where the interior swarm touches both boundaries. Note that this only makes sense for $x^* < \frac{1}{2}$ and is in fact the minimizer in this case.

As we did in the one boundary case, the next step is to consider

$$\Lambda(x) = \int K(x-y)\bar{\rho}(y)dy \tag{3.46}$$

which with the equilibrium (3.40) gives

$$\Lambda(x) = S_1 K(x+x^*) + M\int_{d_1}^{d_1+d_2} K(x-y)dy + S_2 K(x-x^*). \tag{3.47}$$

One can then consider this for $x \in [d_1, d_1+d_2]$ and directly extract the coefficients of the x^2 and x terms. Recall that we are seeking a state with $\Lambda(x) = \lambda_1$ for $x = -x^*$, $\Lambda(x) = \lambda_2$ for $x \in [d_1, d_1+d_2]$, and $\Lambda(x) = \lambda_3$ for $x = x^*$. Therefore setting the x^2 and x coefficients to zero would ensure we get this. The x^2 coefficients end up being the mass constraint and setting the x coefficients to zero gives us a further condition

$$S_1\left(x^* - \frac{1}{2}\right) + M\left(-\frac{1}{2}d_2^2 + \frac{1}{2}d_2 + d_1 - d_1 d_2\right) + S_2\left(\frac{1}{2} - x^*\right) = 0. \tag{3.48}$$

Note that we began with S_1, S_2, d_1, and d_2 as variables to describe the state and we have the mass condition (3.43) and the additional condition (3.48). We will find a family of solutions described by 2 parameters which we choose to represent in terms of r_M and r_S.

We will neglect the calculations, but writing everything in terms of r_M and r_S we get

$$S_1 = \frac{r_S M}{(r_S+1)(r_M+1)}, \tag{3.49a}$$

$$S_2 = \frac{M}{(r_S+1)(r_M+1)}, \tag{3.49b}$$

$$d_1 = \frac{r_S - 2r_M - 1 - 2(r_S-1)(r_M+1)x^*}{2(r_S+1)(r_M+1)}, \tag{3.49c}$$

$$d_2 = \frac{r_M}{r_M+1}. \tag{3.49d}$$

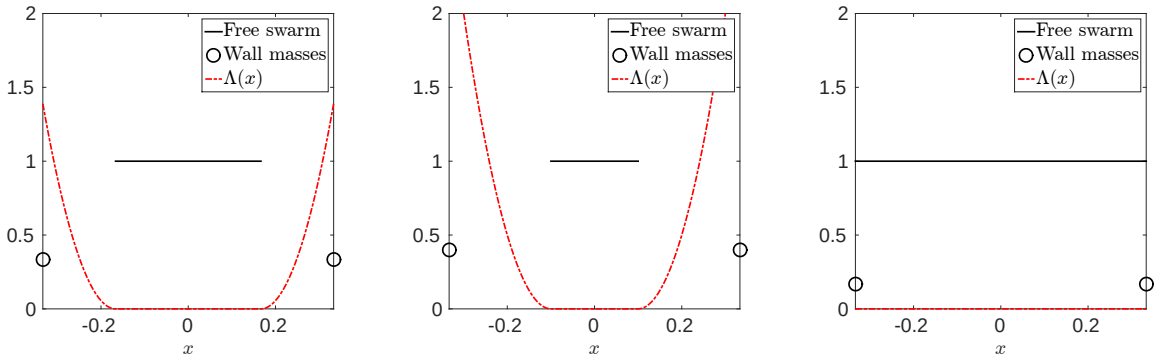

Figure 3.9: $x^* = \frac{1}{3}$: Three states with a characterization of their stability. (a) A symmetric, disconnected equilibrium with $r_M = 0.5$ and $r_S = 1$. (b) A state that satisfies the necessary equilibrium condition (2.17) but where the velocities at the boundaries point inwards at both boundaries. Here $r_M = 0.25$ and $r_S = 1$. (c) The global minimizer of the energy with $r_M = 2$ and $r_S = 1$.

In most of the calculations and results to follow the equations get very messy, so we have simplified the results and neglected to show the algebra.

The first thing we can address is when we get realistic solutions, that is we want $d_1 \geqslant -x^*$ and $d_1 + d_2 \leqslant x^*$. Respectively, we get borderline cases $d_1 = -x^*$ and $d_1 + d_2 = x^*$ as

$$r_S = 2(1 - 2x^*)r_M + (1 - 4x^*), \quad r_S = (2(1 - 2x^*)r_M + (1 - 4x^*))^{-1}. \tag{3.50}$$

The next thing to address is identifying when (3.40) with (3.49) is not an equilibrium. In particular we look for when the velocity at either boundary points into the interior. Recall that we have the unprojected velocity as:

$$v(x) = -\int K'(x - y)\bar{\rho}(y)dy, \tag{3.51}$$

and then recalling that mass on the boundary does not 'feel' itself then we can get

$$v(-x^*) = \frac{(4r_M x^* - 2r_M + 4x^* - 1)M}{2(r_S + 1)(r_M + 1)} = -\frac{v(x^*)}{r_S}. \tag{3.52}$$

Notice that since their signs are opposite, if the velocity at $-x^*$ would take mass off the boundary, then mass would necessarily leave the boundary at x^*. So to have an equilibrium we only require $v(x^*) \geqslant 0$ which then gives us the condition

$$r_M \geqslant \frac{1 - 4x^*}{2(2x^* - 1)}, \tag{3.53}$$

where we assumed $x^* < \frac{1}{2}$. Figure 3.9 shows three states of the form (3.40) with $x^* = \frac{1}{3}$ and Figure 3.10 shows three states with $x^* = \frac{1}{6}$. Figure 3.11 summarizes the results by visualizing where in (r_M, r_S)-space states are equilibria, minima, or neither. Additionally we draw contours of the energy and see that the contours decrease towards the energy minimum at the black star.

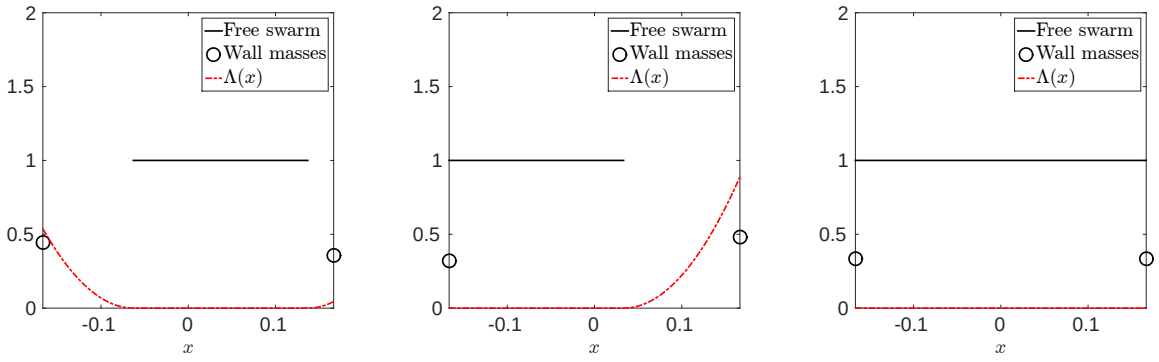

(a) (b) (c)

Figure 3.10: $x^* = \frac{1}{6}$: Three states with a characterization of their stability. (a) A non-symmetric, disconnected equilibrium with $r_M = 0.25$ and $r_S = 1.25$. (b) A non-symmetric equilibrium with $r_M = 0.25$ and $r_S = \frac{2}{3}$ where the free swarm connects with the left boundary but stays disconnected from the right boundary. (c) The only minimizer of equilibria of form (3.40). Notice the minimizer is connected to both boundaries now and is symmetric. Here $r_M = 0.5$ and $r_S = 1$.

Next we want to determine which states are minimizers by examining the energy. Solving for critical points of the energy as a function of r_M and r_S, we find

$$r_S{}^* = 1, \quad r_M{}^* = \frac{2x^*}{1 - 2x^*}. \tag{3.54}$$

Unfortunately, the second derivative test doesn't give us anything conclusive and in fact this is for good reason. This critical point is actually a saddle point but the direction in which it decreases is unrealistic (in the sense that if we did decrease the energy then the state wouldn't fit in the segment). In fact this was also the case with QANR on the half-line. Notice as well that $r_M = \frac{2x^*}{1-2x^*}$ is the largest value one can have for r_M, with as much mass in the interior as possible; $r_S = 1$ then prescribes equally balanced boundary masses.

Linear exogeneous potential: $V(x) = gx$

Most of the same process applies here. We assume the same form as in (3.40) and we go through the same process of taking the mass condition along with the condition from the coefficients of the x terms in $\Lambda(x)$ canceling to zero for $x \in [d_1, d_1 + d_2]$. And we will neglect the calculations, but

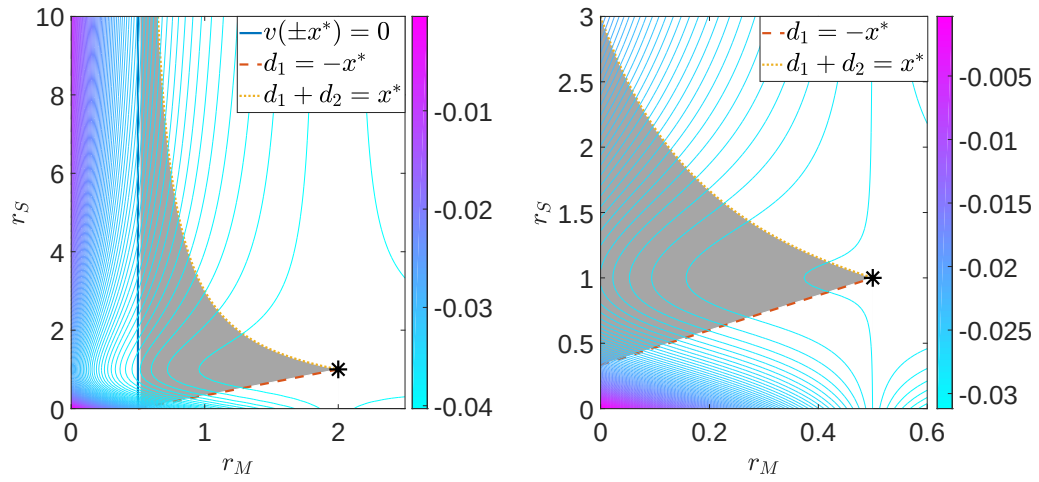

(a) (b)

Figure 3.11: Summarizing results of the two boundary case without an external potential. In each figure the shaded region depicts states that are equilibria. Also shown is a contour plot of the energy as a function of r_M and r_S as well as a black star corresponding to the global minimizer. (a) Here we consider $x^* = \frac{1}{3}$. Additionally, equilibria also exist along two lines; one given by $(r_M, 0)$ and another given by (r_M, ∞) where $r_M \in [0, \frac{1-4x^*}{2(2x^*-1)}]$ for both. These actually correspond to the one boundary equilibria. (b) Here we consider $x^* = \frac{1}{6}$. Additionally the points $(0, 0)$ and $(0, \infty)$ are also equilibria.

satisfying these and writing everything in terms of r_M and r_S we get

$$S_1 = \frac{r_S M}{(r_S+1)(r_M+1)}, \tag{3.55a}$$

$$S_2 = \frac{M}{(r_S+1)(r_M+1)}, \tag{3.55b}$$

$$d_1 = \frac{1}{2M(r_S+1)(r_M+1)}\big(-2g(r_S+1)r_M^2 + ((-2r_S x^* + 2x^* - 2)M \ldots \tag{3.55c}$$
$$- 4g(r_S+1))r_M + ((-2x^*+1)r_S + 2x^* - 1)M - 2g(r_S+1)\big),$$

$$d_2 = \frac{r_M}{r_M+1}, \tag{3.55d}$$

In many of the calculations and results to follow the equations get very messy and non-intuitive so we may neglect to show them completely.

The first thing we can address is when we get reasonable solutions, that is we want $d_1 \geqslant -x^*$ and $d_1 + d_2 \leqslant x^*$. Looking at borderline cases, we get $d_1 = -x^*$ as

$$r_S = \frac{2gr_M^2 + (4g + (2 - 4x^*)M)r_M + 2g + (1 - 4x^*)M}{M - 2gr_M^2 - 4gr_M - 2g}, \tag{3.56}$$

and $d_1 + d_2 = x^*$ as

$$r_S = \frac{-2(r_M + 1)^2 g - M}{2gr_M^2 + (4g + (4x^* - 2)M)r_M + 2g + (4x^* - 1)M}. \tag{3.57}$$

The next thing to address is identifying when (3.40) with (3.55) is not an equilibrium. In particular we look for when the velocity at either boundary points into the interior. If we consider the borderline case of $v(-x^*) = 0$ one gets

$$r_S = \frac{-2gr_M^2 + ((4x^* - 2)M - 4g)r_M + (4x^* - 1)M - 2g}{2(r_M + 1)^2 g}, \tag{3.58}$$

and then considering the borderline case of $v(x^*) = 0$ we get

$$r_S = \frac{-2(r_M + 1)^2 g}{2gr_M^2 + (4g + (4x^* - 2)M)r_M + 2g + (4x^* - 1)M}. \tag{3.59}$$

We note that the gravity breaks the sign symmetry we used to have for the velocity at the boundaries.

Figure 3.12 shows three states of the form (3.40) with $x^* = \frac{1}{3}$ and Figure 3.13 shows three states with $x^* = \frac{1}{6}$. Highlighted among the figures are unstable equilibria, states that fail to be equilibria at all, and the one minimizer of the energy. Also notice that for the larger of these two choices of x^*, we see the minimizer as the one boundary minimizer.

One can again compute when the energy is minimized and one finds that for $x^* = \frac{1}{3}$ the minimizer is a one boundary minimizer from the previous study. If $x^* = \frac{1}{6}$ then the critical point is $(r_M, r_S) \approx (0.5, 3.6)$. Figure 3.14 summarizes the findings with the external potential. In particular notice the contours of the energy corresponding to the state (3.40) satisfying the swarm minimizer condition for the respective mass and balance ratio.

In general, it appears that when we are in a truly confined domain the family of disconnected equilibria becomes more varied. Additionally there appears to be a critical domain size, distinguished mainly in that if the domain is short enough then all interactions are repulsive in effect. As the domain increases in size we see attractive effects arise. Most notably we see this in how the boundary masses, S_1 and S_2 in this case, will attract each other.

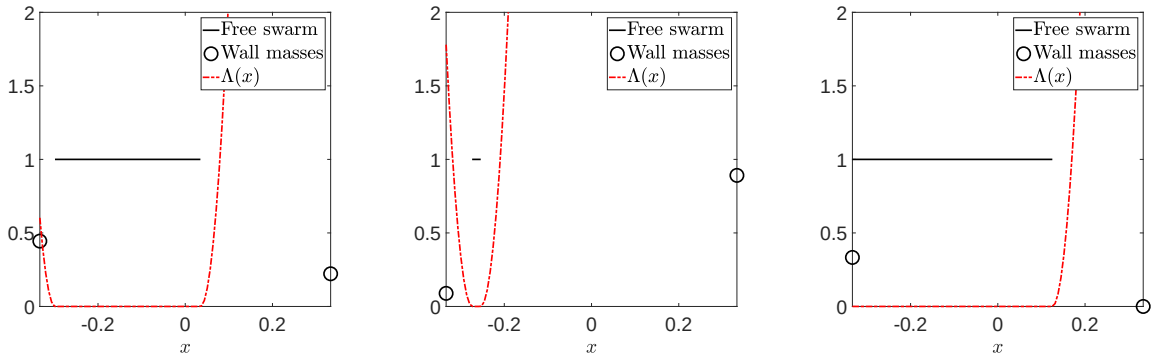

(a) (b) (c)

Figure 3.12: $x^* = \frac{1}{3}$: Three states with a characterization of their stability. (a) A disconnected equilibrium with $r_M = 0.5$ and $r_S = 2$. (b) A state that satisfies the necessary equilibrium condition (2.17) but where the velocity at the right boundary points inwards. Here $r_M = 0.02$ and $r_S = 0.1$. (c) The minimizer of the energy with $r_M = 1$ and $r_S = \infty$.

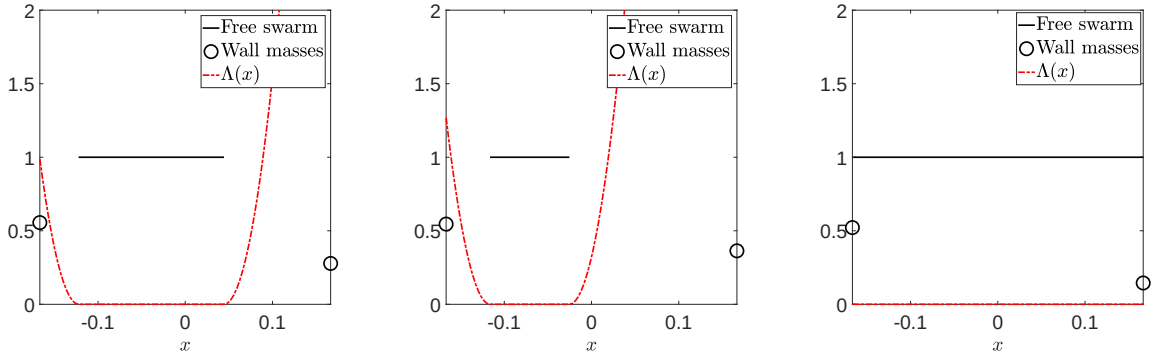

(a) (b) (c)

Figure 3.13: $x^* = \frac{1}{6}$: Three states with a characterization of their stability. (a) A disconnected equilibrium with $r_M = 0.1$ and $r_S = 2$. (b) A state that satisfies the necessary equilibrium condition (2.17) but where the velocity at the right boundary points inwards. Here $r_M = 0.1$ and $r_S = 1.5$. (c) The minimizer of the energy with $r_M = 1/2$ and $r_S \approx 3.6$. Notice the minimizer is connected to both boundaries now.

3.2 C^1-Smoothed QANR potential

Now that we have extensively studied the QANR potential, we would like to study a smoothed version. This base of knowledge may be useful in a later chapter when we revisit this system, but additionally there is a fundamental difference between the QANR potential and a C^1-smoothed

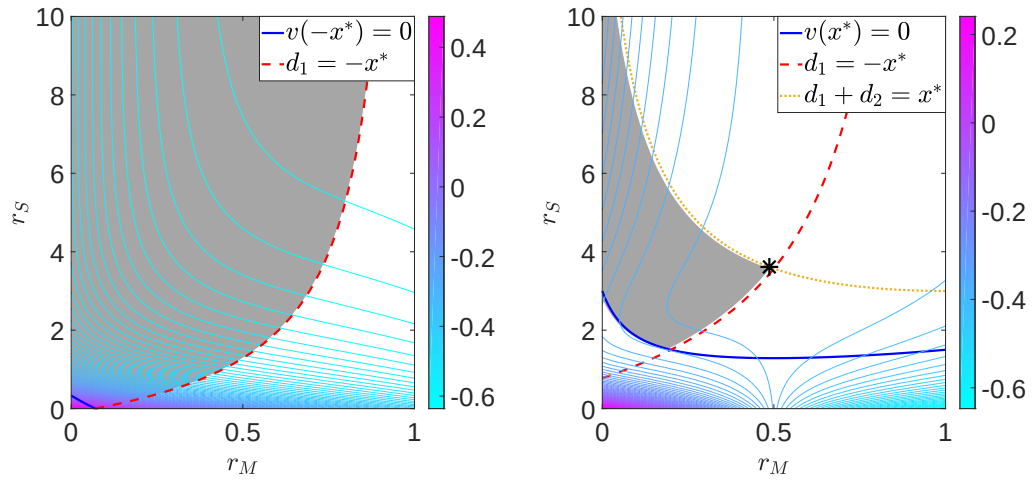

(a) (b)

Figure 3.14: Summarizing results of the two boundary case with an external potential. In each figure the shaded region depicts states that are equilibria. Also shown is a contour plot of the energy as a function of r_M and r_S as well as a black star where the one minimizer exists. (a) Here we consider $x^* = \frac{1}{3}$. The minimizer in this case is actually at the point $(r_M, r_S) = (1, \infty)$ and there is a wide range of possible equilibria. (b) Here we consider $x^* = \frac{1}{6}$. Now the space of equilibria has shrunk considerably and the minimizer can now be seen at $(r_M, r_S) \approx (0.5, 3.6)$. Additionally in both cases the points $(0, 0)$ and $(0, \infty)$ are also equilibria.

version. That is, since the QANR potential is C^0 (in 1D) we find that there is finite slope for infinitesimal distances. This means that as particles come closer to each other, in the limit of the particles completely overlapping, they experience finite and non-zero repulsion. A smoothed version of the QANR potential necessarily has infinitesimal slope at infinitesimal distances and so as particles move to overlap they experience zero repulsion in the limit. As studied in [41] for instance, equilibria in free space with the C^1-smoothed QANR potential are composed of a sum of deltas. First we do our own study in free space to get an idea of our procedure applied here.

In particular we consider a quadratically smoothed version of the QANR interaction potential investigated so far,

$$K_1^\epsilon(r) = \frac{1}{2}r^2 - \frac{1}{2}|r|_{\epsilon,1} \tag{3.60}$$

with

$$|r|_{\epsilon,1} = \begin{cases} \frac{1}{2\epsilon}r^2 + \frac{1}{2}\epsilon & r \leqslant \epsilon, \\ |r| & r > \epsilon. \end{cases} \tag{3.61}$$

So then we begin by assuming the form of equilibria as a state of a number of delta accumulations,

$$\bar{\rho}(x) = \sum_{i=1}^{N} S_i \delta(x - x_i). \tag{3.62}$$

We can make the assumption $x_1 < x_2 < \ldots < x_N$. Again to establish whether the state is an equilibrium, we have to consider,

$$\Lambda(x) = \int K_1^{\epsilon}(|x - y|)\bar{\rho}(y)\,\mathrm{d}y,$$

which for states in the form (3.62), becomes:

$$\Lambda(x) = \sum_{i=1}^{N} K_1^{\epsilon}(|x - x_i|)S_i.$$

Additionally the energy in this case is:

$$E = \frac{1}{2}\sum_{j=1}^{N}\sum_{i=1}^{N} K_1^{\epsilon}(|x_j - x_i|)S_i S_j,$$

or

$$E = \frac{1}{2}\sum_{j=1}^{N} \Lambda(x_j)S_j.$$

As before we want to characterize the stability of a given state. In this light we have the following requirements: For (3.62) to be

(i) a steady state we require $\Lambda'(x_i) = 0$ for all delta positions x_i.

(ii) a swarm minimizer we require *(i)* and furthermore; $\Lambda(x) \geqslant \Lambda(x_i)$ for $x \in (x_i - \epsilon_i, x_i + \epsilon_i)$ for some $\epsilon_i > 0$ for each delta position.

(iii) a local minimizer we require *(i)*, *(ii)*, and $\Lambda(x_i) = \lambda$ for all i and some $\lambda \in \mathbb{R}$. Or equivalently we might want to consider $\Lambda(x_i) = \Lambda(x_{i+1})$ for $i = 1, \ldots, N-1$.

In conjunction with the conditions above there is also the mass condition

$$M = \sum_{i=1}^{N} S_i.$$

We fix one of the particle positions, since for $V(x) \equiv 0$ any equilibrium in one position will also be an equilibrium if translated. For this point we choose,

$$x_1 = 0.$$

Therefore there are $2N-1$ variables defining a given state.

Note for our case we have

$$\Lambda(x) = \frac{1}{2}\sum_{i=1}^{N} S_i(x-x_i)^2 - \frac{1}{4\epsilon}\sum_{|x-x_i|\leqslant\epsilon} S_i\left((x-x_i)^2+\epsilon^2\right) - \frac{1}{2}\sum_{|x-x_i|>\epsilon} S_i|x-x_i|,$$

$$\Lambda'(x) = \sum_{i=1}^{N} S_i(x-x_i) - \frac{1}{2\epsilon}\sum_{|x-x_i|\leqslant\epsilon} S_i(x-x_i) - \frac{1}{2}\sum_{|x-x_i|>\epsilon} S_i\text{sign}(x-x_i),$$

$$\Lambda''(x) = \sum_{i=1}^{N} S_i - \frac{1}{2\epsilon}\sum_{|x-x_i|\leqslant\epsilon} S_i.$$

Thus we first consider the set of equations for (3.62) to be a steady state. This is the system

$$\Lambda'(x_j) = 0, \quad j = 1,\dots,N$$

or

$$\sum_{i=1}^{N} S_i(x_j-x_i) = \frac{1}{2\epsilon}\sum_{|x_j-x_i|\leqslant\epsilon} S_i(x_j-x_i) + \frac{1}{2}\sum_{|x_j-x_i|>\epsilon} S_i\text{sign}(x_j-x_i), \quad j = 1,\dots,N.$$

So notice that this constitutes N conditions so one might expect a $N-1$ parameter family of steady states.

For the condition for swarm minimizers we can consider $\Lambda''(x_i) \geqslant 0$. Therefore the conditions for a swarm minimizer are simply

$$\Lambda''(x_i) \geqslant 0, \quad i = 1,\dots,N$$

or

$$2\epsilon M \geqslant \sum_{|x_j-x_i|\leqslant\epsilon} S_i, \quad j = 1,\dots,N.$$

Now these are a set of inequalities so do not necessarily restrict the number of parameters defining the family of swarm minimizers. These essentially define a subset of the space of equilibria wherein the equilibria are also swarm minimizers. So the space of swarm minimizers with this potential has the same dimensionality as the space of equilibria.

The conditions for a local minimizer are simply

$$\Lambda(x_i) = \Lambda(x_{i+1}), \quad i = 1,\dots,N-1,$$

which constitute $N-1$ conditions. Therefore there is a 0-parameter family of local minimizers. Equivalently, there is only one local minimizer for each choice of N. One can find these local minimizers all have the same spacing between deltas and the same delta strengths when the deltas

are at least ϵ apart from each other. (Consider $x_i = \Delta(i-1)$ and $S_i = S$ for $i = 1, \dots, N$, $\Delta > 0$, and $S > 0$)

Remark 3.2.1 (Maximum mass of a delta)**.** *The condition for a swarm minimizer gives the most immediate result. For instance if we consider a state with $|x_j - x_i| > \epsilon$ for $i, j \in 1, \dots, N$ except $i = j$ then the swarm minimizer condition becomes*

$$S_i \leqslant 2\epsilon M, \quad i = 1, \dots, N,$$

which gives an explicit limit on how much mass can be in any given delta before the state could not be a minimizer. Also it speaks to the possibility of steady states that are not swarm minimizers since if $S_i = 2\epsilon M$ for some i then within a range of that delta $\Lambda(x)$ will be flat.

Remark 3.2.2 (Maximum mass of deltas within an ϵ)**.** *Considering no assumptions on the spacing of deltas, the swarm minimizer condition is sufficiently satisfied if*

$$\sum_{|x_j - x_i| \leqslant \epsilon} S_i \leqslant 2\epsilon M.$$

Immediately one notices that if all the particles were inside an ϵ ball then this would become

$$M \leqslant 2\epsilon M,$$

which certainly cannot hold for any $\epsilon < \frac{1}{2}$. Additionally though this limits how much mass can be within an ϵ ball for the state to be a swarm minimizer.

We are going to do a quick example of how the explicit solutions can be found. First we assume $N = 3$. Notice that various values of ϵ imply different things for what we can find. For instance:

- If $\epsilon = 0.1$ then there can be no swarm minimizers with 3 deltas since we would require, at the very least, $S_i \leqslant \frac{1}{5}M$ for $i = 1, 2, 3$ but also require $S_1 + S_2 + S_3 = M$; the borderline case is $\epsilon = \frac{1}{6}$ (in general $\epsilon = \frac{1}{2N}$).
- If $\epsilon = 0.2$ then if we can find a steady state then we can find swarm minimizers since we would require, at the very least, $S_i \leqslant \frac{2}{5}M$ for $i = 1, 2, 3$ so for instance $S_i = \frac{1}{3}$ then they sum to M and satisfy the swarm minimizer condition. However none of the deltas could be within 0.2 of each other since then the two that are within 0.2 could not have more than a combined mass of $\frac{2}{5}$ but the third delta also cannot have more than $\frac{2}{5}$ mass.
- If $\epsilon = 0.25$ then we can still find swarm minimizers and in fact we could perhaps find a swarm minimizer with 2 deltas within 0.25 of each other since we could take $S_1 = \frac{1}{2}M$ and then we would require $S_2 + S_3 \leqslant \frac{1}{2}M$ so $S_2 = S_3 = \frac{1}{4}$. In fact any ϵ less than 0.25 would give that we

couldn't find any deltas that are within ϵ and also swarm minimizers. So in general it appears that the space of minimizers and equilibria can change depending on ϵ.

In order to find explicit solutions we have to assume the spacing of the three deltas.

Deltas are not within ϵ of each other

The steady state conditions then are

$$\sum_{i=1}^{3} S_i(x_j - x_i) = \frac{1}{2} \sum_{|x_j - x_i| > \epsilon} S_i \text{sign}(x_j - x_i), \quad j = 1, \ldots, 3.$$

If we solve these three conditions and the mass condition at this point with $M = 1$ we find

$$S_1(x_2, x_3) = 2x_2 - 2x_3 + 1, \quad S_2(x_2, x_3) = 2x_3 - 1, \quad S_3(x_2, x_3) = -2x_2 + 1.$$

So we have a 2-parameter family of steady states. Now for any $\epsilon < x_2$ and $x_2 + \epsilon < x_3$ these states are steady states for any $\epsilon > 0$. To be realistic ($S_i > 0$) we further require $x_2 < \frac{1}{2}$, $x_3 > \frac{1}{2}$, and $x_3 - x_2 < \frac{1}{2}$.

To be a swarm minimizer we would have to consider only solutions to the inequalities

$$S_1(x_2, x_3) \leqslant 2\epsilon, \quad S_2(x_2, x_3) \leqslant 2\epsilon, \quad S_3(x_2, x_3) \leqslant 2\epsilon$$

or written out

$$2x_2 - 2x_3 + 1 \leqslant 2\epsilon, \quad 2x_3 - 1 \leqslant 2\epsilon, \quad -2x_2 + 1 \leqslant 2\epsilon.$$

This can be simplified to give

$$\frac{1}{2} - \epsilon \leqslant x_2, \quad x_3 \leqslant \frac{1}{2} + \epsilon, \quad \frac{1}{6} \leqslant \epsilon$$

which is the same borderline case found earlier. So then we have swarm minimizers for $\min\left(\epsilon, \frac{1}{2} - \epsilon\right) \leqslant x_2 \leqslant \frac{1}{2}$, $x_2 + \frac{1}{2} - \epsilon \leqslant x_3 \leqslant \frac{1}{2} + \epsilon$, and $\frac{1}{6} \leqslant \epsilon \leqslant \frac{1}{4}$.

To be a local minimizer we consider

$$\Lambda(x_1) = \lambda, \quad \Lambda(x_2) = \lambda, \quad \Lambda(x_3) = \lambda.$$

We get the solution

$$x_2 = \frac{1}{3}, \quad x_3 = \frac{1}{3}, \quad \lambda \approx -0.074,$$

and then find

$$S_1 = \frac{1}{3}, \quad S_2 = \frac{1}{3}, \quad S_3 = \frac{1}{3}.$$

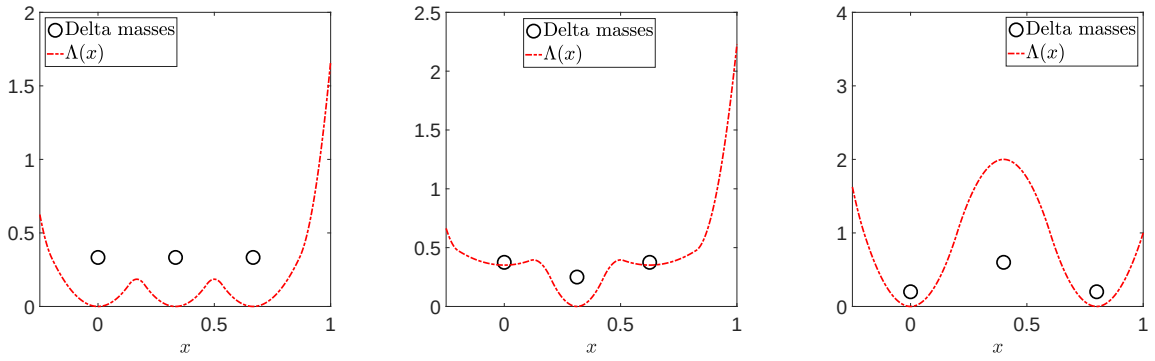

Figure 3.15: Showcasing a few of the states found with a characterization of their stability. (a) An example of a local minimizer as found above. Notice that all the values of $\Lambda(x)$ at each delta position are the same. (b) An example of a swarm minimizer as found above. Notice that the state is stable to spatially infinitesimal perturbations but is not an energy minimum with regard to perturbations that can 'teleport' mass. (c) An example of an unstable equilibrium. Notice that while $\Lambda'(x) = 0$ at each delta position, the second delta has a λ value larger than all neighbours and so this state cannot be a swarm minimizer. Here $\epsilon = 0.2$.

This is just one case of one choice of N particles with one ϵ. To complete the study with three particles we would need to consider only two of the particles within ϵ of each other and then consider if all three of the particles are within ϵ of each other. To complete the study for the chosen ϵ we would have to consider all possible choices of numbers of particles that give equilibria. Figure 3.15 gives an example of an equilibrium, a swarm minimizer, and a local minimizer as just found. Figure 3.16 completes the picture for 3 deltas not within ϵ of each other. Here we can see a continuum of equilibria and swarm minimizers, yet we still have only one local minimizer.

Ultimately, one could characterize every possible equilibrium, swarm minimizer, and local minimizer by fixing the number of deltas then running through all the possibilities of their relative distances to each other. So again we find equilibria that are explicitly calculated and can characterize their stability. Though we have calculated these without explicitly enforcing a boundary, our dynamic simulations have shown no classical initial conditions that flow into non-minimizing states in free space. With a wall, our dynamics do find non-minimizing equilibria as we will elaborate on now.

Domains with boundaries

So far we have not necessarily enforced a boundary, although all of the results found so far should hold even if there was a boundary at $x = 0$. Indeed the only difference to this scheme to find equilibria in the presence of a boundary is that the equilibrium condition which required $\Lambda'(x_i) = 0$

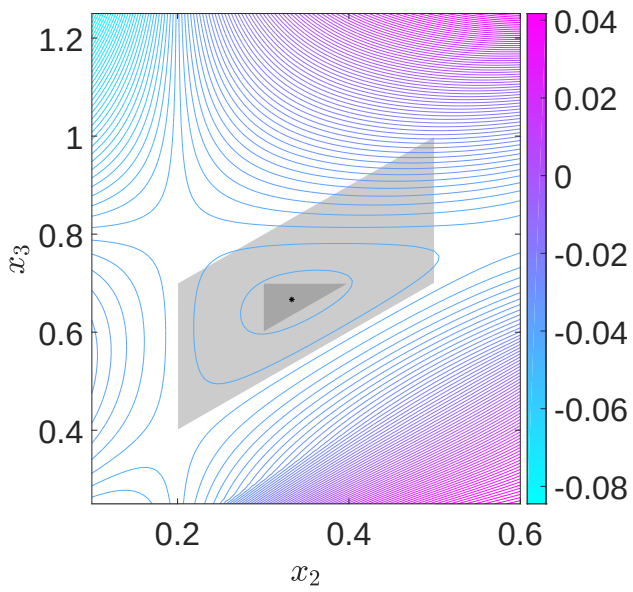

Figure 3.16: A representation of equilibria composed of 3 particles not within ϵ of each other, using the C^1-smoothed QANR potential. The black star at $(x_2, x_3) = (\frac{1}{3}, \frac{2}{3})$ represents the local minimizer while the dark grey triangular region represents a continuum of swarm minimizers. The lighter grey region represents the continuum of equilibria and finally we have included contours of the energy corresponding to the state. Notice that the contours decrease towards the local minimizer. Here $\epsilon = 0.2$.

for each delta position x_i could potentially be relaxed for x_1, the delta at the boundary. At this position we could potentially have $\Lambda'(x_1) \geqslant 0$ and still be in equilibrium as this would mean the velocity at x_1 points into the wall.

To investigate non-minimizing equilibria and also address whether they can be achieved dynamically, we perform some simulations with the particle method. Figure 3.17 showcases three such simulations, with different initial densities and their approximate steady states at $t = 200$. Similar to what we found with the QANR potential in Section 3.1, we find that the more concentrated the initial swarm is towards the boundary, the greater the final energy of the system is. There is, however, a difference that we would like to comment on: it appears that $\Lambda'(0) = 0$ from the figures. This is in contrast to the QANR potential where $\Lambda(x)$ appeared to be strictly increasing towards the boundary (see Figure 3.1(a)). Thinking more carefully here, this is actually expected since the smoothed QANR no longer has a discontinuity at zero distance. This means there is no discontinuous behaviour observed in the velocity when considering exactly at a particle's position and infinitesimally close by.

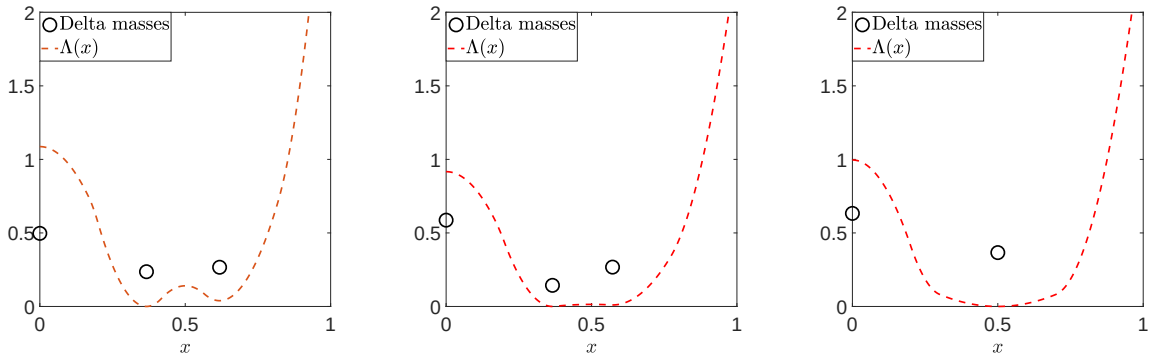

(a) (b) (c)

Figure 3.17: Dynamic simulations using the particle method showing approximate steady states with the C^1-smoothed QANR potential and $\epsilon = 0.2$. $\Lambda(x)$ is shown, though it has been vertically shifted and magnified for clarity. (a) Evolution from a uniformly randomly generated state in the region $[0, 0.25]$. We see the observed steady state is composed entirely of deltas and by inspection of $\Lambda(x)$, this state is not a swarm minimizer. (b) Evolution from a uniformly randomly generated state in the region $[0, 0.125]$. Note that the boundary seems to have more mass accumulated on it than in (a), though the state is still not a swarm minimizer. (c) Evolution from a uniformly randomly generated state in the region $[0, 0.0625]$. Here we see that the observed steady state has only two deltas now with even more mass accumulated on the boundary.

From the tests in Figure 3.17 we see evidence of non-minimizing equilibria achieved through dynamics with the C^1-smoothed QANR potential. We have shown that equilibria that are a sum of deltas can be analytically understood at least in free space, and hinted at how it might change in the presence of a boundary. In fact, our understanding of equilibria composed of 3 deltas in free space can be compared here with the dynamics. Figure 3.18 shows where the equilibria in Figures 3.17(a)&(b) can be found in the summary of 3 delta states in Figure 3.16 where their characterization was already predicted.

3.3 Morse potential

Up to now we have shown unstable equilibria in a variety of contexts, but only with the QANR potential and a smoothed version of it. Now we bring up the question of what happens if we choose a different potential altogether: do we still observe unstable equilibria? To this end we consider the Morse-type potential investigated in [9, 10]:

$$K(x) = -GLe^{-|x|/L} + e^{-|x|}. \tag{3.63}$$

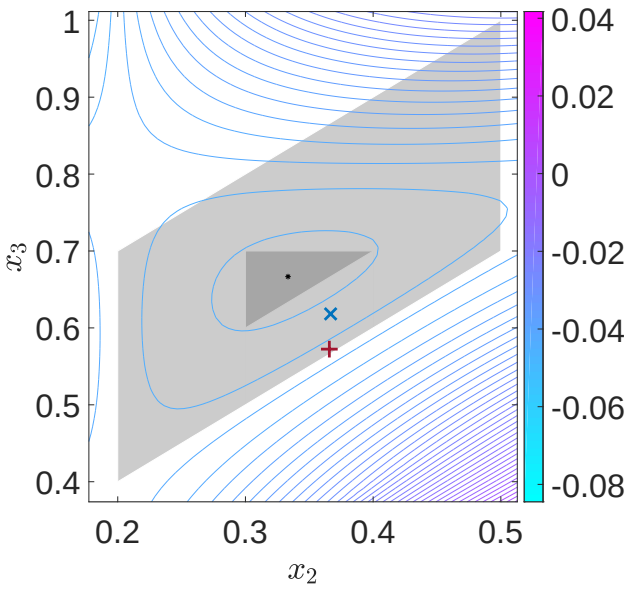

Figure 3.18: A close-up of the summary depicted in Figure 3.16 with the two 3 delta equilibria found dynamically pictured. The red cross corresponds to the observed steady state in Figure 3.17(b) and the blue X corresponds to the observed steady state in Figure 3.17(a). Observe that the characterization found analytically and depicted here matches what is observed from dynamics as both are found in the light grey region depicting the region of 3 delta, non-minimizing equilibria.

We consider the case of $G = 0.5$ and $L = 2$ throughout this section as these values were one of the cases highlighted in [10].

One can find explicit forms for the equilibria for the Morse potential in just the same way as we found explicit forms for the potential (2.19)-(2.20). We assume the solution form

$$\bar{\rho}(x) = S\delta(x) + \rho_*(x)\mathbb{1}_{(d_1, d_1+d_2)}, \tag{3.64}$$

with

$$\begin{aligned} \rho_*(x) =& C\cos(\mu x) + D\sin(\mu x) - \frac{\lambda_2}{\epsilon}, \\ \mu = \sqrt{\frac{\epsilon}{\nu}}, &\quad \epsilon = 2(GL^2 - 1), \quad \nu = 2L^2(1-G). \end{aligned} \tag{3.65}$$

The density ρ_* of the free swarm comes from the free space solution found in [10] and is an assumption we make without concrete argument in this context with boundaries.

Now in order for this state to be an equilibrium it needs to satisfy the equilibrium condition (3.3) and the mass condition (2.8a), i.e.,

$$\Lambda(0) = \lambda_1, \qquad \Lambda(x) = \lambda_2 \quad \text{for } x \in [d_1, d_1 + d_2], \qquad S + \int_{d_1}^{d_1+d_2} \rho_*(x)\,\mathrm{d}x = M. \tag{3.66}$$

The Appendix shows the system of equations that arise from these conditions. We end up with four equations from requiring $\Lambda(x) = \lambda_2$ for $x \in [d_1, d_1 + d_2]$ as the non-constant terms comprise four linearly independent terms in x:

$$-GL\exp\left(-\frac{x}{L}\right), \quad \exp(-x), \quad -GL\exp\left(\frac{x}{L}\right), \quad \exp(x). \tag{3.67}$$

In fact one finds that the constant component of $\Lambda(x)$ for $x \in [d_1, d_1 + d_2]$ is λ_2 by choice of the form (3.65). Together with $\Lambda(0) = \lambda_1$ and the mass constraint then, this yields a system of six equations for seven unknowns (C, D, S, d_1, d_2, λ_1, and λ_2), hinting to a one-parameter family of equilibria, which is the same as the results with the QANR potential on the half-line. The resulting system of equations do not have an explicit solution so we instead solved the system numerically. In order to capture all states in a given run we chose to use S as the free parameter instead of the mass ratio, though we still report results in the familiar mass ratio notation. This process involved the numerical continuation of C, D, d_1, d_2, λ_1, and λ_2 as functions of S starting from the known solution when $S = 0$ as we have the free space solution as in [10].

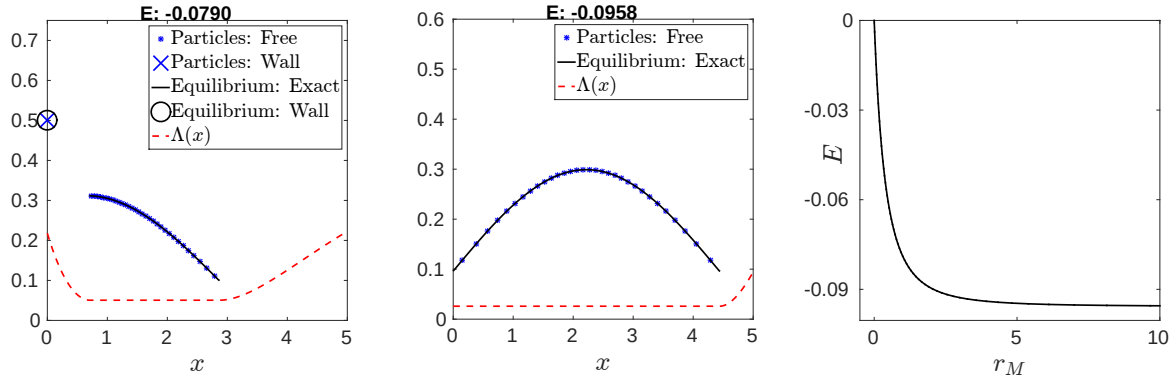

(a) (b) (c)

Figure 3.19: Equilibria (3.64) on half-line for $V(x) = 0$ (no exogenous potential). The interaction potential is given by (3.63), where $G = 0.5$ and $L = 2$. (a) Disconnected state. (b) Connected state with no aggregation at the origin; this is the same as the free space solution from [10]. (c) Energy of equilibria as a function of the mass ratio; the lowest energy state corresponds to the connected equilibrium $r_M = \infty$.

Remark 3.3.1. *The author would like to quickly comment on the assumed form* (3.64) *of the equilibrium solutions. For the QANR potential and its smoothed version we had arguments that supported the free swarm form. Here we simply assumed without reason the free space form found in [10] and it seems to have been a successful assumption. It would be an interesting study to see if other potentials showcase this behaviour.*

Remark 3.3.2. *Though we have only reported henceforth on three different potentials, the author has explored other polynomial, Morse, and Gaussian potentials, finding unstable equilibria just as reported here.*

3.4 Equilibria solver in 1D

We briefly describe here a numerical implementation to solve the equilibrium condition (2.17). Though this is unnecessary in one dimension because we have explicit solutions, in two dimensions we will find that we cannot find explicit solutions anymore and so rely on a numerical solver to find equilibria.

Here we assume a solution of the form (3.1) where we now treat S, d_1, and d_2 as variables to be determined by satisfying (3.3). Furthermore we also focus on the disconnected state, so λ_1, λ_2 are also variables. We use the term *observers* in this context to describe points along the boundary of $\Omega_{\bar{\rho}}$ at which we evaluate $\Lambda(x)$. In one dimension we only require 3 observers - see Figure 3.20. Finally, we consider the mass constraint (3.2) and the mass ratio (3.8); in general we keep r_M and M fixed.

Then our system of equations encompasses (3.2), (3.8), and

$$\Lambda(0) = \lambda_1, \quad \Lambda(d_1) = \lambda_2, \quad \Lambda(d_1 + d_2) = \lambda_2, \tag{3.68}$$

for a total of 5 equations for 5 unknowns. We also mention that if one fixes the mass ratio to be that of the minimizer for a given gravity g, then the result from solving the system of equations is one with $|\lambda_2 - \lambda_1|$ and d_1 below the tolerance of the solver and so effectively recovering the connected solution.

Though we only highlighted finding states here for the QANR potential, a similar scheme works for a general interaction potential. A more general implementation requires more variables however, since we cannot in general assume constant density in the free swarm. A general implementation would require discretizing the profile of the free swarm and including observers on the interior of the free swarm.

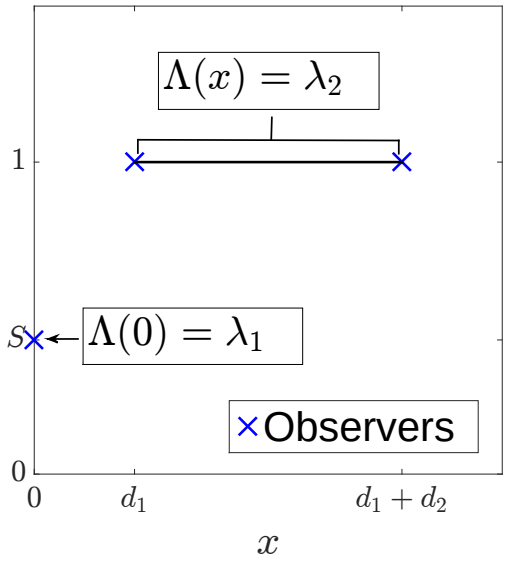

Figure 3.20: Abstracted solution presumed in the numerical solver in one dimension showing locations of observers where we solve $\Lambda(x)$ to be a constant. Variables for the system are d_1, d_2, S, λ_1, and λ_2 as shown in the figure.

Chapter 4

Plain aggregation in two dimensions

We have so far seen that model (1.4) can exhibit equilibria that are energetically unstable in one dimension. Now we wish to extend this study to two spatial dimensions. For this purpose we only investigate the QANR potential as it has the simplest free space forms, that is a constant density of $2M$ in two dimensions. Though it should be noted that we only report on the QANR potential in two dimensions here, we have explored other potentials and found similar results.

4.1 On the half-plane $[0, \infty) \times (-\infty, \infty)$

In this section we consider model (1.4) with $n = 2$ and Ω taken as the half-plane $[0, \infty) \times (-\infty, \infty)$ such that the boundary $\partial\Omega$ is given by $x_1 = 0$. To begin, we search for an equilibrium that consists of a constant density $2M$ in a bounded domain D that lies off the wall ($x_1 > 0$) and a Dirac delta accumulation on $\partial\Omega$. For consistency of notations with the study in one dimension, we take the horizontal extent of the free swarm D to be $d_1 < x_1 < d_1 + d_2$, with $d_1 \geqslant 0$, $d_2 > 0$. Also, we assume symmetry in the vertical direction, and take the vertical extent of D to be given by the lower and upper free boundaries $x_2 = -g(x_1)$ and $x_2 = g(x_1)$, respectively.

No external potential: $V(x) \equiv 0$
Specifically, let

$$D = \{(x_1, x_2) \mid d_1 < x_1 < d_1 + d_2, -g(x_1) < x_2 < g(x_1)\},$$

then the equilibrium we look for has the form:

$$\bar{\rho}(x_1, x_2) = f(x_2)\delta_{\partial\Omega}(x_1, x_2) + 2M\, \mathbb{1}_D(x_1, x_2), \tag{4.1}$$

where the density profile $f(x_2)$ on the wall is assumed to have support $[-L, L]$.

The support $\Omega_{\bar{\rho}}$ of $\bar{\rho}$ consists of two components:

$$\Omega_1 = \{0\} \times [-L, L] \qquad \text{and} \qquad \Omega_2 = \bar{D}, \tag{4.2}$$

where the bar indicates the closure of the set.

Again we seek to satisfy the mass condition (2.8a) and the equilibrium condition (2.17). In two dimensions it should be noted that solving these is now entirely non-trivial and we can only solve them numerically. To be specific, denote the area of D by $|D|$. By the mass constraint (2.8a) we find

$$\int_{-L}^{L} f(x_2)\,\mathrm{d}x_2 + 2M|D| = M. \tag{4.3}$$

Calculate $\Lambda(\mathbf{x})$ for $\mathbf{x} = (x_1, x_2) \in \Omega_{\bar{\rho}}$ using (2.12), where K is given by (2.19)-(2.20) and $V = 0$. A generic point $\mathbf{y} = (y_1, y_2) \in \Omega_{\bar{\rho}}$ can lie either on the wall or in D, along with its free boundary. Consequently, $\Lambda(\mathbf{x})$ consists of two terms:

$$\begin{aligned}\Lambda(\mathbf{x}) = &\int_{-L}^{L} \left(-\frac{1}{2\pi} \ln \sqrt{x_1^2 + (x_2 - y_2)^2} + \frac{1}{2}\left(x_1^2 + (x_2 - y_2)^2 \right) \right) f(y_2)\,\mathrm{d}y_2 \\ &+ 2M \iint_D \left(-\frac{1}{2\pi} \ln |\mathbf{x} - \mathbf{y}| + \frac{1}{2}|\mathbf{x} - \mathbf{y}|^2 \right) \mathrm{d}\mathbf{y}.\end{aligned} \tag{4.4}$$

For an equilibrium, $\Lambda(\mathbf{x})$ has to be constant in each component of $\Omega_{\bar{\rho}}$:

$$\Lambda(\mathbf{x}) = \lambda_1 \quad \text{in } \{0\} \times [-L, L], \qquad \text{and} \qquad \Lambda(\mathbf{x}) = \lambda_2 \quad \text{in } \bar{D}. \tag{4.5}$$

Solving (4.5) numerically would be very expensive. However, our interaction potential has a particular property we can use. Indeed, calculate the Laplacian of Λ from (4.4):

$$\begin{aligned}\Delta\Lambda(\mathbf{x}) &= 2\int_{-L}^{L} f(y_2)\,\mathrm{d}y_2 + 2M\left(-1 + 2\iint_D \mathrm{d}\mathbf{y} \right) \\ &= 2\left(\int_{-L}^{L} f(y_2)\,\mathrm{d}y_2 - M + 2M|D| \right),\end{aligned} \tag{4.6}$$

where for the first equality we used $\Delta\left(-\frac{1}{2\pi} \ln |\mathbf{x}| \right) = -\delta$; in particular, the logarithmic term in the single integral $\int_{-L}^{L}$ is harmonic for $\mathbf{x} \in D$.

Using the mass constraint (4.3), one can infer from (4.6) that Λ is harmonic in D:

$$\Delta\Lambda(\mathbf{x}) = 0, \qquad \text{for all } \mathbf{x} \in D. \tag{4.7}$$

As L is a harmonic function then, its function values in the interior are completely determined by the values on $\partial\Omega$. This observation greatly simplifies the problem of solving (4.5) since then (4.5)

reduces to solving

$$\Lambda(\mathbf{x}) = \lambda_1 \quad \text{in } \{0\} \times [-L, L], \qquad \text{and} \qquad \Lambda(\mathbf{x}) = \lambda_2 \quad \text{on } \partial D. \tag{4.8}$$

We solve numerically equation (4.8) to find d_1, d_2, λ_1, and λ_2 as well as the profiles f and g of the wall aggregation and the free boundary, respectively. Details on the numerical implementation are given at the end of the chapter.

As in one dimension, we find disconnected and connected equilibria and choose to parametrize them by the mass ratio, r_M, which is the ratio of the mass M_2 of the free swarm to the mass M_1 of the aggregation on the wall:

$$r_M := \frac{M_2}{M_1} = \frac{2M|D|}{\int_{-L}^{L} f(x_2)dx_2}. \tag{4.9}$$

Disconnected equilibria ($d_1 > 0$). We were successfully able to find disconnected solutions to (4.8) in the form (4.1) for any $r_M \in (0, \infty)$. We believe that there is a unique equilibrium for a given mass ratio with the limiting cases where either all mass is off the wall or all mass is on the wall being the connected states (see discussion below).

Again to check whether the states we found are equilibria we compute numerically the velocity field at points on Ω_1 which is the support of the mass on the wall. In fact we find from our numerical investigations that for any choice of mass ratio that isn't either of the connected states ($r_M = 0, \infty$), there will be $(x_1, x_2) \in \Omega_1$ where the velocity points inwards. Therefore in contrast to the results in one dimension, without an external potential we find that the only equilibrium that is not a minimizer is the connected state with all mass on the wall.

The author seeks to remark briefly on why we see this in two dimensions and predict what may be observed in higher dimensions. Attractive forces occur for larger distances than repulsive forces, so if one imagines the region of space swept out by an arc of a given radius of sufficient size then the relative size of the attractive area to the repulsive area increases as the dimension increases. This means there will be generally more attractive interactions in higher dimensions.

Connected equilibria. The first type of connected equilibria correspond to aggregations that lie entirely on the wall (no free swarm, $r_M = 0$). This is a degenerate case of densities of the form (4.1), where D is the empty set. The equilibrium in this case has the form of a delta-aggregation on the wall:

$$\bar{\rho}(x_1, x_2) = f(x_2)\delta_{\partial\Omega}(x_1, x_2). \tag{4.10}$$

We find the density profile $f(x_2)$ on the wall and its support $[-L, L]$ by solving numerically (2.14) in $\Omega_{\bar{\rho}} = \{0\} \times [-L, L]$. Note that the mass constraint (2.8a) implies:

$$\int_{-L}^{L} f(x_2)dx_2 = M, \tag{4.11}$$

while in our case (2.14) reduces to:

$$\int_{-L}^{L} \left(-\frac{1}{2\pi} \ln |x_2 - y_2| + \frac{1}{2}(x_2 - y_2)^2 \right) f(y_2) dy_2 = \lambda, \qquad \text{for all } x_2 \in [-L, L]. \tag{4.12}$$

We solve numerically (4.11) and (4.12) to find f, L and λ. This equilibrium is shown in 4.1(a), where both the solution to (4.12) is shown and a particle result, showing agreement. This is quite a degenerate equilibrium as it can only be achieved if all mass is initially on the boundary.

With this numerically computed solution we then checked (2.15), which here reads:

$$\int_{-L}^{L} \left(-\frac{1}{2\pi} \ln \sqrt{x_1^2 + (x_2 - y_2)^2} + \frac{1}{2} \left(x_1^2 + (x_2 - y_2)^2 \right) \right) f(y_2) \, \mathrm{d}y_2 \geqslant \lambda, \qquad \text{for all } (x_1, x_2) \in \Omega_{\bar{\rho}}^c.$$

Note that $\Omega_{\bar{\rho}}^c$ is the disjoint union of the two semi-infinite vertical lines $\{0\} \times (-\infty, -L)$ and $\{0\} \times (L, \infty)$, with the open half-plane $(0, \infty) \times \mathbb{R}$. A coloured contour plot of $\Lambda(x)$ is shown in Figure 4.1(a) showing that $\Lambda(x)$ decreases away from the wall, indicating that it is not a minimizer.

The second type of connected equilibria correspond to swarm equilibria in free space, and consist of a constant aggregation of density $2M$ in a disk of radius $\frac{1}{\sqrt{2\pi}}$ corresponding to the limiting case $r_M \to \infty$. This is numerically verified to be a minimizer by checking the contour plots of $\Lambda(x)$, as shown in Figure 4.1(b). Translations of this minimizer away from the wall would also yield another minimizer.

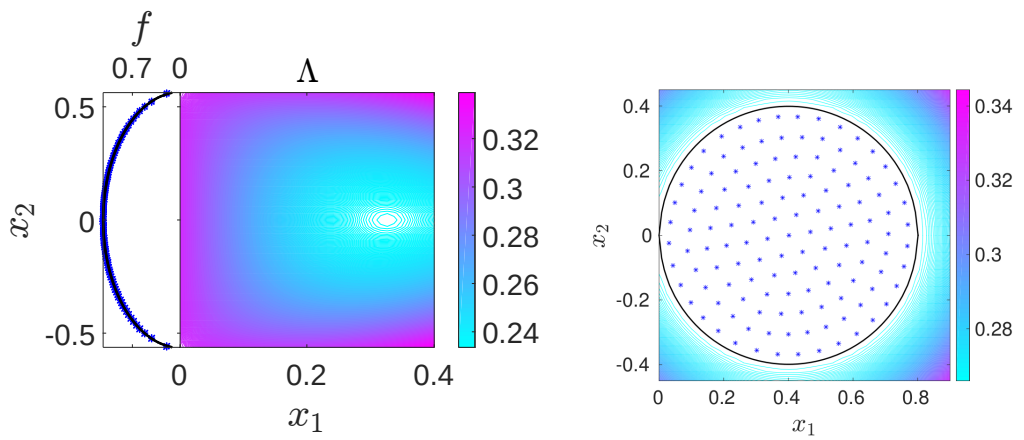

Figure 4.1: Equilibria on half-plane in two dimensions for $V = 0$ (no exogenous potential). (a) Equilibrium aggregation that lies entirely on the wall ($r_M = 0$). The solid line represents the density profile f on the wall as solved from (4.11) and (4.12). Note the excellent agreement with the particle simulations (blue stars). The equilibrium is not an energy minimizer, as indicated by the contour plot of Λ (shown on right). (b) Free swarm equilibrium ($r_M = \infty$) of constant density $2M$ in a disk of radius $\frac{1}{\sqrt{2\pi}}$. The contour plot of Λ, shown in the figure, demonstrates that this equilibrium is an energy minimizer. Note that there are no disconnected equilibria of form (4.1) in this case.

Linear exogeneous potential: $V(x_1, x_2) = gx_1$

We now consider an exogenous gravitational potential $V(x_1, x_2) = gx_1$, with $g > 0$. The domain is the same as above, the half-plane $\Omega = [0, \infty) \times \mathbb{R}$, so the exogenous forces are acting (horizontally) towards the wall. Note that $\Delta V = 0$ and by using this observation in (2.26) we infer that away from the wall the equilibrium densities are constant (equal to $2M$) on their support.

We search for equilibria in the form (4.1), which consist in a delta aggregation on the wall and a constant density free swarm. The same variables and setup from the non-exogeneous case are being used here as well. In particular, the support $\Omega_{\bar{\rho}}$ of the equilibrium is given by (4.2) and mass conservation leads to (4.3). We solve numerically the necessary condition for equilibrium (4.5), with $\Lambda(\mathbf{x})$ given by

$$\begin{aligned}\Lambda(\mathbf{x}) = &\int_{-L}^{L} \left(-\frac{1}{2\pi} \ln \sqrt{x_1^2 + (x_2 - y_2)^2} + \frac{1}{2} \left(x_1^2 + (x_2 - y_2)^2 \right) \right) f(y_2)\, \mathrm{d}y_2 \\ &+ 2M \iint_D \left(-\frac{1}{2\pi} \ln |\mathbf{x} - \mathbf{y}| + \frac{1}{2} |\mathbf{x} - \mathbf{y}|^2 \right) \mathrm{d}\mathbf{y} + gx_1.\end{aligned} \tag{4.13}$$

Note that since the gravitational potential has zero Laplacian, then Λ is still harmonic in D and so we can solve (4.8) with Λ given by (4.13). Again we solve this numerically to find approximations for L, d_1, d_2, and the profiles f and g of the wall aggregation and the free boundary.

We will begin to go over solutions found, though we note there are now two critical gravities that can be observed. There is still a critical gravity g_c such that the external potential is simply too strong and forces all mass against the wall. Additionally we will find a second critical gravity $\tilde{g}_c$ where below this value, we will find solutions to the equilibrium condition (2.14) that are no minimizers.

i) $g_c \leqslant g$

As remarked before, in this case the gravity is too strong and so all mass is on the wall. In fact the calculated equilibrium here is the same as was calculated in Figure 4.1(b), though the contour plot of $\Lambda(x)$ is of course different and increases away from Ω_1.

(ii) $\tilde{g}_c \leqslant g < g_c$

Disconnected equilibria. In this case we are able to numerically calculate a family of solutions to (4.8) for mass ratios in the interval $(0, \gamma(g))$ where $\gamma(g) = \sqrt{\frac{g_c}{g}} - 1$ denotes the maximal value that the mass ratio of the two components can take for that particular g. This curve γ can be seen in Figure 3.3(b). A typical disconnected solution is shown in Figure 4.2(a) with $g = 0.064$. Now when we check the velocity along Ω_1 we find these states have horizontal velocity's that are into the boundary and so are equilibria, though these disconnected equilibria are not minimizers as can be checked by the contour plot of Λ (also shown in Figure 4.2(a)). We have also visualized the energy as a function of mass ratio in Figure 4.2(c) where we see that the connected state is the minimizer.

Connected equilibria. For this case of gravity (and in fact, as we will find also with $g < \tilde{g}_c$), there are two connected equilibria: one that corresponds to all mass on the wall ($r_M = 0$) and another that corresponds to the maximal mass ratio $r_M = \gamma(g)$. The first is again the same as in the case without an external potential.

The second kind of connected equilibrium is supported on both the wall and the interior of Ω. These are achieved as the free component of the disconnected state touches the wall in the limit $r_M \to \gamma(g)$. Figure 4.2(b) shows an example of a connected equilibrium of the second kind as computed numerically and compared with particle simulations. As can be confirmed by the contour plot of Λ, this equilibrium is in fact a minimizer.

Figure 4.3 suggests how the disconnected equilibria approaches the connected minimizer as we limit the mass ratio towards that of the connected minimizer. An interesting result is that the free swarm seems to establish contact with the boundary over an *entire* vertical segment and not just a single point.

(iii) $g < \tilde{g}_c$

In this case the connected equilibria are the same two as described above. The differentiating character of the disconnected equilibria in this case is that they do no longer exist for all $r_M \in (0, \gamma(g))$. Now, if $0 < r_M \leqslant \alpha(g)$ or $\beta(g) \leqslant r_M < \gamma(g)$ then the solution found from (4.8) is

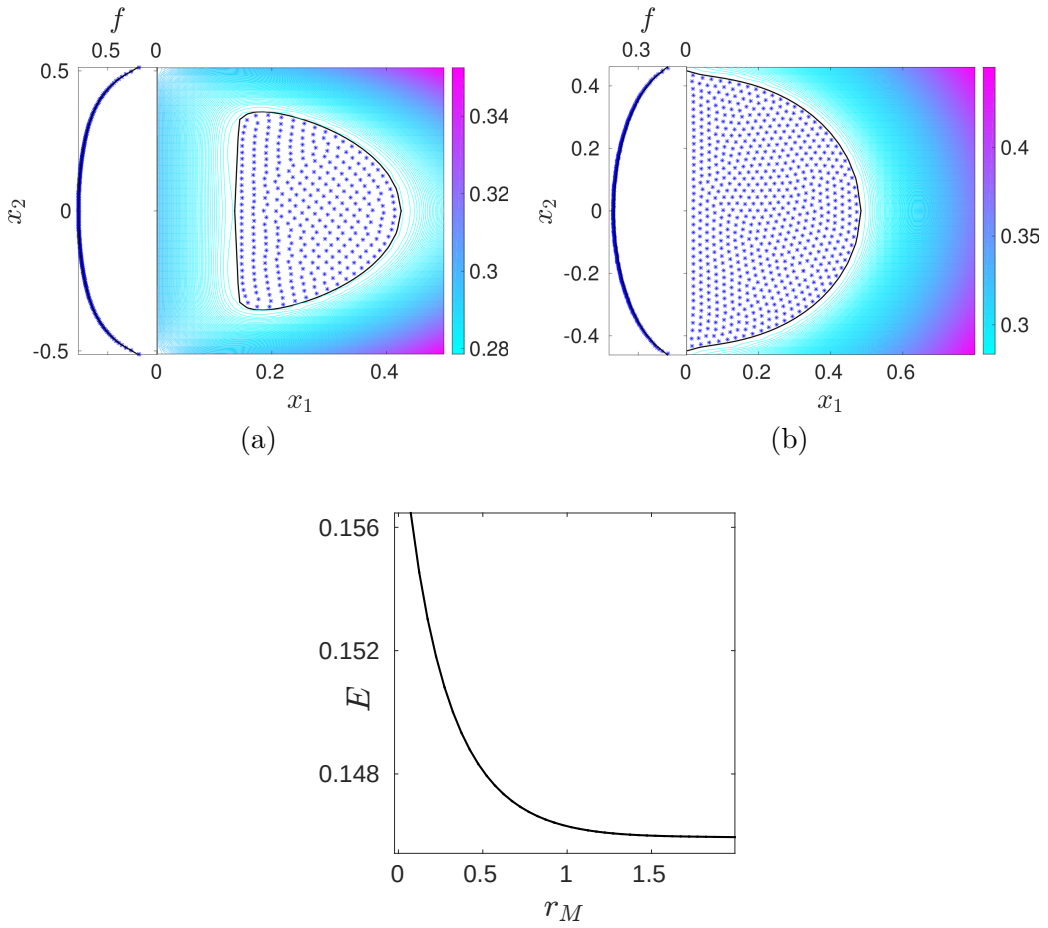

Figure 4.2: Equilibria (4.1) on half-plane for $V(x_1, x_2) = gx_1$ (linear exogenous potential) with $g = 0.064$. (a) Disconnected state consisting in a free swarm of constant density and a delta aggregation on the wall. (b) Connected state with a constant density in a domain adjacent to the wall and a delta aggregation on the wall. It should be mentioned that any apparent defects in (a) or (b) are the result of some numerical error and intrinsic error involving particles preferring to arrange in hexagons and the geometry of the free swarm not allowing hexagonal packing to cover the area. (c) Energy of equilibria (4.1) as a function of the mass ratio; the lowest energy state corresponds to the connected equilibrium with $r_M = \gamma(g)$.

an equilibrium as checked by the velocity. If $\alpha(g) < r_M < \beta(g)$ then the solution fails to be an equilibrium as there will be points along Ω_1 with a horizontal velocity directed inwards. The curves α and β have been numerically approximated and shown in Figure 3.3(b).

One finds that if $r_M \in (\alpha(g), \beta(g))$ that the velocities on Ω_1 nearest the points $(0, \pm L)$ are the first to begin to point inwards. Figure 4.4 visualizes this idea for $g = 0.04 < \tilde{g}_c$ and various mass ratios. Notice that as $g \to 0$ then $\alpha \to 0$ and $\beta \to \infty$, which replicates the results found earlier

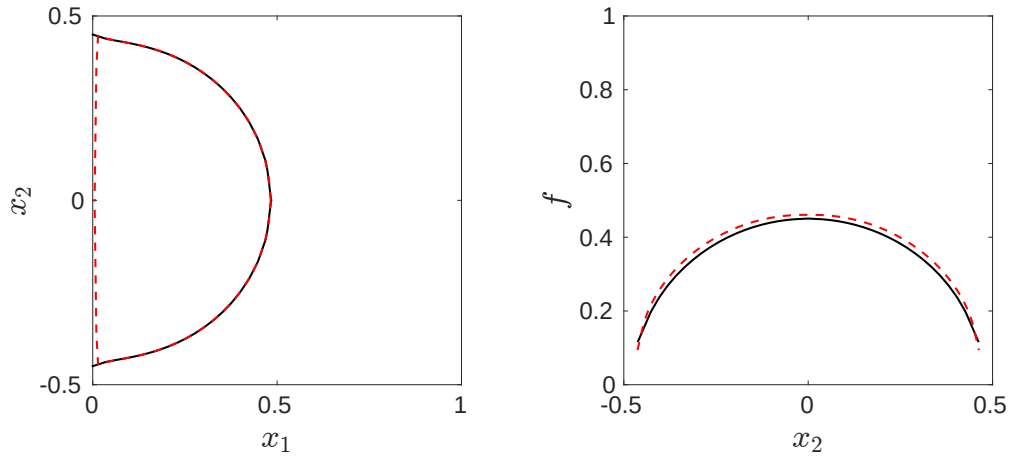

(a) (b)

Figure 4.3: Equilibria on the half-plane in two dimensions for $V(x_1, x_2) = gx_1$, with $g = 0.064$: the disconnected equilibria (4.1) approach a connected equilibrium state as the separation d_1 from the wall approaches 0 (or equivalently, r_M approaches the maximal mass ratio $\gamma(g)$). (a) The solid line represents the connected solution of (4.1). The dashed line shows a disconnected equilibrium with a mass ratio $r_M = 1.873 < \gamma(g)$; this is the disconnected state with the largest mass ratio that we were able to obtain in our numerical investigations. (b) Profile f of the density on the wall corresponding to the connected (solid line) and disconnected (dashed line) equilibria shown in plot (a).

without an external potential, namely that the only equilibria are the connected states.

Calculation of critical gravity g_c

We consider a particle at position $(\epsilon, 0)$ with $\epsilon > 0$. We get from (1.4b) that the velocity in the horizontal direction felt by this particle is

$$v_1 = -\int_{-L}^{L} \left(1 - \left(2\pi(\epsilon^2 + x_2^2)\right)^{-1}\right) \epsilon f(x_2) dx_2 - g.$$

To study the competition between social and gravitational forces one can focus just on the social velocity, defined by

$$v_1^s = -\int_{-L}^{L} \left(1 - \left(2\pi(\epsilon^2 + x_2^2)\right)^{-1}\right) \epsilon f(x_2) dx_2, \tag{4.14}$$

representing the velocity acting on the particle by interaction with the aggregation on the wall. With this notation, the horizontal velocity v_1 can be written as

$$v_1 = v_1^s - g. \tag{4.15}$$

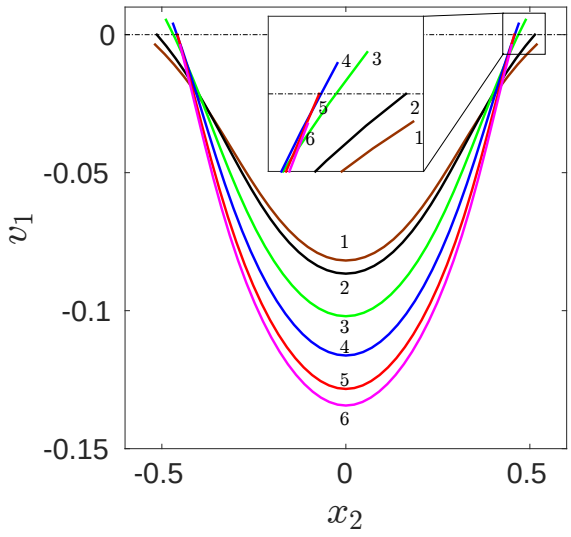

Figure 4.4: Horizontal velocity (before taking the projection (1.5)) along wall profile of solutions to (4.8) for $g = 0.04 < \tilde{g}_c$ and (1) $r_M = 1.531$, (2) $r_M = \beta(g) \approx 1.379$, (3) $r_M = 1.078$, (4) $r_M = 0.744$, (5) $r_M = \alpha(g) \approx 0.439$, (6) $r_M = 0.362$. Note the positive velocities for $r_M \in (\alpha(g), \beta(g))$, that is, in (3) and (4), indicating that mass would leave the wall and thus these solutions are not steady states. See also Figure 3.3(b).

Gravity is strong enough to yield negative horizontal velocity v_1 provided g is larger than the maximal social velocity. Consequently, we set

$$g_c = \lim_{\epsilon \to 0} v_1^s. \tag{4.16}$$

A more instructive and explicit formula can be derived by taking the limit directly in (4.14):

$$\lim_{\epsilon \to 0} v_1^s = \lim_{\epsilon \to 0} \int_{-L}^{L} \left(2\pi(\epsilon^2 + x_2^2)\right)^{-1} \epsilon f(x_2)\, \mathrm{d}x_2. \tag{4.17}$$

Assume that $f(x_2)$ has a convergent Taylor series centred on $x_2 = 0$:

$$f(x_2) = f(0) + \sum_{n=1}^{\infty} c_{2n} x_2^{2n}. \tag{4.18}$$

Note that we have used here the symmetry of the wall profile about $x_2 = 0$. Equations (4.17) and (4.18) then give

$$\lim_{\epsilon \to 0} v_1^s = f(0) \lim_{\epsilon \to 0} \int_{-L}^{L} \frac{\epsilon}{2\pi(\epsilon^2 + x_2^2)}\, \mathrm{d}x_2 + \lim_{\epsilon \to 0} \int_{-L}^{L} \sum_{n=1}^{\infty} \frac{\epsilon c_{2n} x_2^{2n}}{2\pi(\epsilon^2 + x_2^2)}\, \mathrm{d}x_2. \tag{4.19}$$

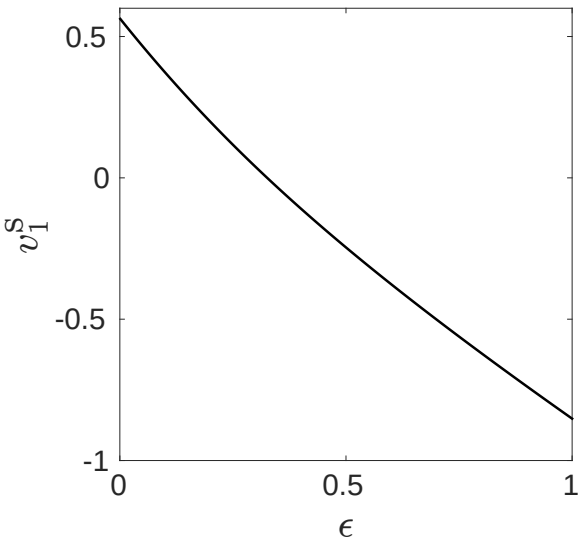

Figure 4.5: Social velocity (4.14) acting from the aggregation on the wall (see (4.10) and Figure 4.1(a)) on a particle at position $(\epsilon, 0)$.

Observe that

$$\begin{aligned}\left|\lim_{\epsilon\to 0}\epsilon\int_{-L}^{L}\sum_{n=1}^{\infty}\frac{c_{2n}x_2^{2n}}{2\pi(\epsilon^2+x_2^2)}\,\mathrm{d}x_2\right| &\leqslant \left|\lim_{\epsilon\to 0}\epsilon\int_{-L}^{L}\sum_{n=1}^{\infty}\frac{1}{2\pi}c_{2n}x_2^{2n-2}\,\mathrm{d}x_2\right|,\\ &\leqslant \frac{1}{2\pi}\left|\lim_{\epsilon\to 0}\epsilon\int_{-L}^{L}\sum_{n=1}^{\infty}2n(2n-1)c_{2n}x_2^{2n-2}\,\mathrm{d}x_2\right|,\\ &= 0,\end{aligned} \tag{4.20}$$

where we have assumed that $f''(x_2)$ has a convergent Taylor series as well.

Also, by an explicit calculation,

$$\lim_{\epsilon\to 0}\int_{-L}^{L}\frac{\epsilon}{2\pi(\epsilon^2+x_2^2)}\,\mathrm{d}x_2 = \frac{1}{2}. \tag{4.21}$$

With (4.19)-(4.21), (4.16) gives

$$g_c = \frac{1}{2}f(0). \tag{4.22}$$

Our numerical simulations yield $f(0) \approx 1.128$ (cf., Figure 4.1(a)), and hence we find $g_c \approx 0.564$. This value also agrees with Figure 4.5 (as it should).

4.2 On the disc of radius R

Here we consider the plain aggregation model (1.4) with the QANR potential in a bounded domain. That is, we consider the domain Ω defined by $(r, \theta) \in [0, R] \times [0, 2\pi)$ and search for equilibria that are radially symmetric. Figure 4.6 shows two different evolutions from initial states, showing a connected minimizer and a disconnected equilibrium that is not a minimizer. Through all our dynamical investigations we have found only radially symmetric steady states. Thus, though there could conceivably be solutions lacking radial symmetry, we search analytically for radially symmetric equilibria. This vastly simplifies the analytics and enables explicitly computable equilibria.

As we did with the QANR potential in the half-plane (Section 4.1), we assume that the free swarm component of any equilibrium we search for has a constant density of $2M$, so we are looking for equilibria $\bar{\rho}$ in the form of:

$$\bar{\rho}(r, \theta) = S\delta(r - R) + 2M\mathbb{1}_D(r, \theta), \tag{4.23}$$

where D is the region defined by $(r, \theta) \in [0, r^*] \times [0, 2\pi)$ and $\mathbb{1}_D$ is the characteristic function on D. We do not assume the annular form given by $(r, \theta) \in [r_1, r_2] \times [0, 2\pi)$, because we have not observed any such formations from dynamics, though this by no means rules them out. We are not presenting an exhaustive study of all possible equilibria.

We begin our construction with the mass condition (2.8a) which here takes the form,

$$M = 2\pi SR + 2M\pi {r^*}^2. \tag{4.24}$$

This determines S as a function of r^*. Notice from this that for $S \geqslant 0$ then we get the condition $r^* \leqslant \frac{1}{\sqrt{2\pi}}$ which is expected since if $r^* > \frac{1}{\sqrt{2\pi}}$ and $R > r^*$ then we are considering a domain where the free space minimizer can fit. As observed with the one boundary in Section 4.1 and no external potential, particles on the boundary can and will move off it. When $R < \frac{1}{\sqrt{2\pi}}$ then the domain constrains the possible equilibrium states and we see accumulations on the walls (see Figure 4.6). Then we consider $\Lambda(x)$ for equilibria (4.23),

$$\Lambda(x) = S\int_{\partial\Omega} K(x - y)\,\mathrm{d}y + 2M\int_D K(x - y)\,\mathrm{d}y. \tag{4.25}$$

We require $\Lambda(x) = \lambda_1$ on D and $\Lambda(x) = \lambda_2$ on $\partial\Omega$. In fact, because of the radial symmetry we can quickly infer that $\Lambda(x) = \lambda_2$ is necessarily satisfied on $\partial\Omega$. Evaluating $\Delta\Lambda(x)$, using $\Delta K(x) = 2 - \delta(x)$, we find

$$\Delta\Lambda(x) = 2\left(\int_{\partial\Omega} \rho(y)\,\mathrm{d}y + \int_D \rho(y)\,\mathrm{d}y - M\right).$$

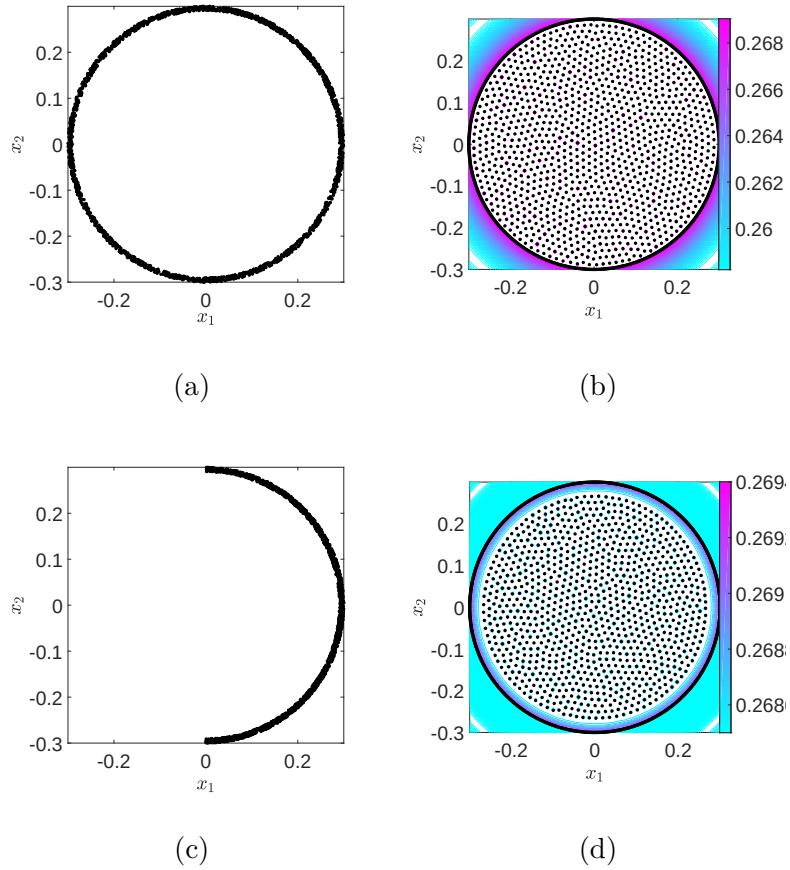

Figure 4.6: Dynamically achieved equilibria of the plain aggregation model with the QANR potential in a radially bounded domain. Here the boundary is at $R = 0.3$. (a) The initial condition for (b) where particles are initialized in an annular region of small width that is adjacent to the boundary. (b) The connected equilibrium (and indeed minimizer) obtained dynamically from evolving the initial condition in (a). We can see from the contour lines of $\Lambda(x)$ that it takes a constant value in the domain. Here we have $r_M \approx 1.4527$. (c) The initial condition for (d) where particles are initialized in a half-annular region of small width that is adjacent to the boundary. (d) A disconnected equilibrium obtained dynamically from evolving the initial condition in (c). We can see that $\Lambda(x)$ decreases away from the boundary accumulation and so this state is not a minimizer. Here we have $r_M \approx 1.0898$.

This is a rephrasing of the mass condition (4.24) and so already satisfied. So $\Delta\Lambda(x) = 0$ for $x \in D$ therefore $\Lambda(x)$ is harmonic on D. Then, because the radial symmetry gives us $\Lambda(x) = \lambda_1$ for $x \in \partial D$ and $\Lambda(x)$ is harmonic then we automatically get $\Lambda(x) = \lambda_1$ for all $x \in D$.

Lastly we need to check the unprojected velocity (1.1b) in the radial direction v_r on the boundary to ensure it is truly an equilibrium. Figure 4.7 shows the radial velocity as a function of the free swarm radius r^* for three choices of R. Here we see a critical radius $r_c = \frac{1}{2\sqrt{\pi}}$ where if $R < r_c$ then the radial velocity at the boundary is always positive and so outwards from the domain. Thus all

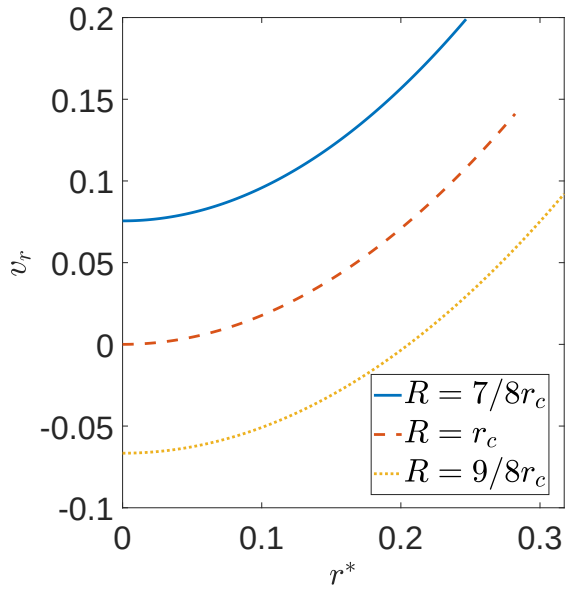

Figure 4.7: Radial velocity at $(R, 0)$ corresponding to forms (4.23). Here we have visualized the velocity for all possible r^* for the given R. If the radial velocity is positive (or zero) then the form (4.23) is an equilibrium.

states of the form (4.23) that have $R < r_c$ are indeed equilibria. However, we have not seen any such states dynamically and in fact we have only found equilibria from dynamics with a mass ratio greater than one.

Here we have then come to two main findings studying the plain aggregation model in a radial domain:

- Explicitly computable equilibria are possible even in two dimensions depending on the boundary geometry
- A continuum of equilibria have been found for this case with disconnected equilibria that are not minima of the energy

4.3 Equilibria solver in 2D

Here we describe the numerical method we used to find equilibria and subsequently what we compared against the particle method (see Figure 4.1 or Figure 4.2). This is a particularly important method in this chapter since we no longer had explicit solutions for equilibria, as we did in one dimension. Recall symmetry about $x_2 = 0$ so we need only focus on half the space but can extend

to the full space using symmetry. We now assume a solution of the form (4.1) where d_1, d_2, L, λ_1, λ_2, as well as the profiles $f(x_2)$ and $g(x_1)$ need to be determined. We define equispaced vertical and horizontal grids

$$y_i = \frac{L}{N_f} i, \quad 0 \leqslant i \leqslant N_f, \quad x_j = d_1 + \frac{d_2}{N_g} j, \quad 0 \leqslant j \leqslant N_g, \tag{4.26}$$

along with midpoints $y_i^* = \frac{1}{2}(y_{i-1} + y_i)$ for $1 \leqslant i \leqslant N_f$ and $x_j^* = \frac{1}{2}(x_{j-1} + x_j)$ for $1 \leqslant j \leqslant N_g$. We seek to find the $N_f + N_g$ variables

$$f(y_i^*) = f_i, \quad 1 \leqslant i \leqslant N_f, \quad g(x_j^*) = g_j, \quad 1 \leqslant j \leqslant N_g. \tag{4.27}$$

The profile density f and the free boundary g are then extended with a linear interpolant.

To solve for (4.8) we use observers at $(0, y_i)$ for $0 \leqslant i \leqslant N_f$, (x_j^*, g_j) for $1 \leqslant j \leqslant N_g$, $(d_1, 0)$, and $(d_1 + d_2, 0)$ – see Figure 4.8(a). We also have the mass condition (4.3) and the mass ratio condition (4.9). Together we have $N_f + N_g + 5$ conditions in total and $N_f + N_g + 5$ variables.

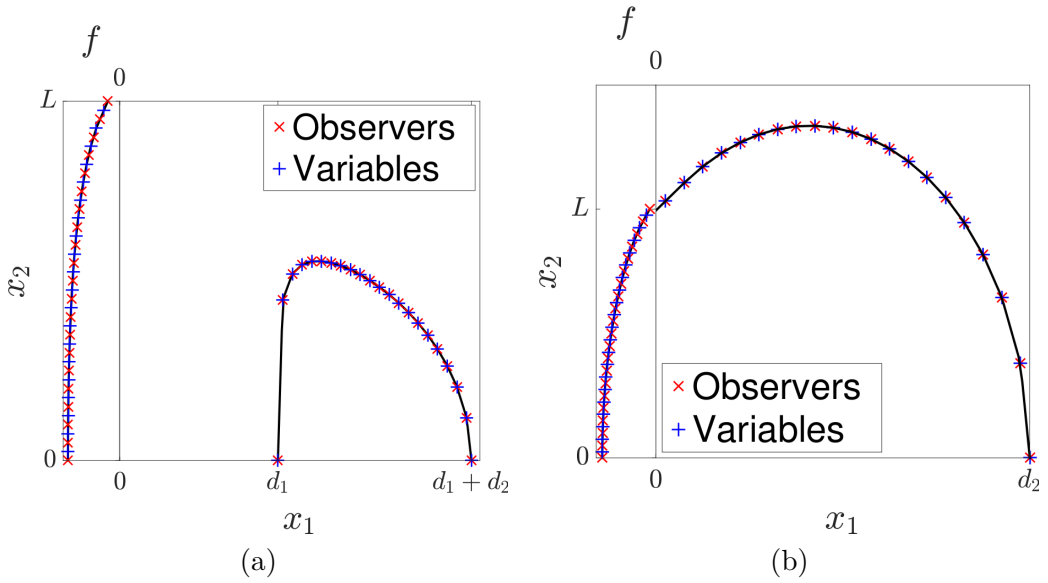

Figure 4.8: Abstracted (a) disconnected and (b) connected solutions presumed in the numerical solver in two dimensions showing locations of observers where we solve $\Lambda(x)$ to be a constant. Variables for the system are d_1, d_2, L, λ_1, λ_2, and $f(x_2)$ and $g(x_1)$ evaluated on the numerical grid (see (4.27)).

Connected case. The connected state implementation has the same prescription in dealing with $f(x_2)$ but differs for the free boundary g. First, we lose the point $(d_1, 0)$ as $d_1 = 0$ and we do not pin this edge now. Secondly, we drop the mass ratio condition and now we only have λ as $\lambda_1 = \lambda_2 =: \lambda$.

These are the only differences though and we wind up with $N_f + N_g + 4$ conditions and $N_f + N_g + 4$ variables – see Figure 4.8(b).

The system of equations is solved with MATLAB's `fsolve` using default settings and integrals are evaluated with MATLAB's `integral` or `integral2` for 1D and 2D integration respectively. When using `integral2` we use the iterated method setting.

Remark 4.3.1 (Mass and mass ratio constraints)**.** *In 1D the mass constraint* (3.2) *and the mass ratio constraint* (3.8) *are explicit, and we implement them directly in the numerics as additional conditions.*

In 2D recall that we work with the linear interpolants of f and g in which case, by using a numerical integrator, we can compute the necessary integrals for the mass condition (4.3) *and mass ratio condition* (4.9)*, namely*

$$\int_{-L}^{L} f(x_2)\,\mathrm{d}x_2, \qquad \textit{and} \qquad |D| = \int_{d_1}^{d_1+d_2} \int_{-g(x_1)}^{g(x_1)} \mathrm{d}x_2\,\mathrm{d}x_1.$$

Specifically, we used MATLAB's `integral` *and* `integral2` *to do the numerical integration. In the use of* `integral2` *we used the iterated method as described in the function's documentation.*

Chapter 5

Rectifying the model: Nonlinear diffusion

Up til now we have been highlighting the seemingly generic feature of model (1.4) to evolve into equilibria that are not energy minimizers, despite the model being an energy gradient system. This appears to be a defect in the model, as we would like the model to flow to a minimizer naturally. In the hope of rectifying this, we explore adding nonlinear diffusion such that we consider model (1.6). We will elaborate on this choice shortly, after we quickly remark about other possible solutions we considered

The first other possible solution to this problem is to consider an external potential that forces mass away from the walls. With enough repulsion away from the walls, mass would necessarily not be able to accumulate on the wall. Another possible solution is to introduce linear diffusion to the model. This has the same fundamental effect as the first other solution and indeed the same effect as nonlinear diffusion, in particular delta accumulations are precluded. Additionally, with linear diffusion we would expect the solution to no longer have compact support and from our explorations if a state only has a single component and it stays connected, then it almost certainly will evolve into a minimizer.

Both of the solutions above are undesirable when compared with using nonlinear diffusion. An external potential that forces mass away from the walls seems to avoid the issue by just constructing the problem in such a way that there is no hard boundary. Linear diffusion may still allow us to consider a hard boundary, but it causes us to lose the compactness of solutions. Using nonlinear diffusion preserves both the hard boundary interpretation and the compactness of solutions. We will be focusing mainly on the case with minimal diffusion since we want to preserve as much of the original model (1.4) as possible. Additionally, to simplify things, we do not consider an external potential.

To be specific, consider model (1.6) with ν replaced by ν^α (we note upfront that the exponent α is included for theoretical purposes; in numerical simulations we will always be considering $\alpha = 1$).

Also, for clarity, we add a subindex ν to solutions of the diffusive model. Hence, we consider:

$$\begin{cases} \partial_t \rho_\nu + \nabla \cdot (\rho_\nu v_\nu) = 0 \qquad \text{in } \Omega \times [0,T), \\ \qquad \text{with} \quad v_\nu = -\dfrac{\nu^\alpha\, m}{m-1} \nabla \rho_\nu^{m-1} - \nabla K * \rho_\nu - \nabla V, \\ v_\nu \cdot n_x = 0 \qquad \text{on } \partial\Omega \times [0,T), \\ \rho_\nu(0) = \rho^0 \qquad \text{on } \Omega. \end{cases} \tag{5.1}$$

Here, ρ_ν is an absolutely continuous probability measure, K is the interaction potential and V is the exogenous potential. The equation is set in a closed domain $\Omega \subset \mathbb{R}^d$ with smooth boundary, and n_x denotes the outward unit normal to $\partial\Omega$ at x. Also, $\nu > 0$ is the diffusion coefficient (with exponent $\alpha > 0$) and $m > 1$.

For convenience, we list below the energies corresponding to the two models we consider in this chapter. The energy of the plain aggregation model (see (2.3)) is:

$$E(\rho) \,=\, \frac{1}{2} \int_\Omega \int_\Omega K(x-y)\rho(x)\rho(y)\,\mathrm{d}x\,\mathrm{d}y + \int_\Omega V(x)\rho(x)\,\mathrm{d}x, \tag{5.2}$$

while the diffusive model (5.1) is the gradient flow of the energy (see (2.5)):

$$E_\nu(\rho) \,=\, \frac{\nu^\alpha}{m-1} \int_\Omega {\rho_\nu}^m(x)\,dx + \frac{1}{2} \int_\Omega \int_\Omega K(x-y)\rho_\nu(x)\rho_\nu(y)\,dxdy + \int_\Omega V(x)\rho_\nu(x)\,\mathrm{d}x. \tag{5.3}$$

Most of the results presented in this chapter have been reported in [46]. The author of this thesis would like to mention that my contribution to this paper was numerical evidence to support the analysis therein. The theoretical results established in [46] address the capability of model (5.1) to approximate the plain aggregation model (1.4). The first result shows that at each *fixed* $t > 0$, weak solutions of the diffusive model (5.1) converge to solutions of (1.4) in the zero diffusion limit. The second result studies the convergence of minimizers of the energy (5.3) associated to model (5.1) to minimizers of the energy (5.2) of the plain aggregation model. These results require different assumptions on the interaction potential, but they give us evidence that the diffusive model approximates well the plain aggregation model.

In particular, we have the following assumptions

(H1) K is symmetric, i.e., $K(x) = K(-x)$ for all $x \in \mathbb{R}^d$.

(H2) Either

(H2A) $\qquad K \in C^2(\Omega),\ K$ is bounded from below, and K is λ-convex for some $\lambda \in \mathbb{R}$,

or

(H2B) $$K \in L^1_{\text{loc}}(\Omega) \cap C^1(\Omega \setminus B_R(0)), R > 0,\ K \to +\infty \text{ as } |x| \to \infty,$$
there exists a function $K^a \in C(\Omega)$ so that $K^r := K - K^a$ is superharmonic,
and for $|x|$ large, K^r and K^a have at most quadratic growth.

(H3) Either

(H3A) $$V \in C^1(\Omega),\ |\nabla V(x)| \leqslant C(1 + |x|) \text{ for all } x \in \mathbb{R}^d, \text{ and } V \text{ is } \lambda\text{-convex},$$

or

(H3B) $V \in C(\Omega), V$ has at most quadratic growth, it is bounded from below, and V is either strictly increasing or translation invariant in every component.

(H4) $\Omega \subset \mathbb{R}^d$ is bounded, convex, and $\partial\Omega \in C^1$.

With these we state the theorems that were shown in [46]. These are:

Theorem 5.0.1. *Assume K, V, and Ω satisfy the hypotheses* (H1), (H2A), (H3A), *and* (H4). *Suppose $\rho_\nu(t)$ is a weak solution of* (5.1), *and $\rho(t)$ is a weak solution of* (1.4) *for all $t \in [0, T]$. Then there exist constants C, $\tilde{C} > 0$ such that*

$$d_W^2(\rho_\nu(t), \rho(t)) \leqslant \tilde{C}\nu^\beta\, t\, e^{Ct}$$

for all $t \in [0, T]$, where $\beta = \min\{\alpha - dm/(d+2),\ 1/(d+2)\}$, $\alpha > dm/(d+2)$, and d_W denotes the 2-Wasserstein metric.

Theorem 5.0.2. *Assume K and V satisfy the hypotheses* (H1), (H2B), *and* (H3B). *Also assume $\alpha > dm$. Let $\{\rho_\nu\}_{\nu>0} \subset \mathcal{P}_2(\mathbb{R}^d)$ be a sequence such that each ρ_ν is a minimizer of the energy E_ν. Then there exists $\rho \in \mathcal{P}_2(\mathbb{R}^d)$ such that, up to a subsequence, $\rho_\nu \to \rho$ in $\mathcal{P}_2(\mathbb{R}^d)$ as $\nu \to 0$, and ρ is a minimizer of E.*

We have stated these theorems for both context and reference. In this chapter we provide numerical validation of the theorems as well as show evidence that the theorems may hold true under relaxed assumptions. First we investigate the case of quadratic diffusion ($m = 2$) as this choice simplifies some of the work and explicit forms of equilibria can be found in the case with the QANR potential. Since the QANR potential only satisfies the conditions of Theorem 5.0.2 we also investigate a C^2-smoothed QANR potential (3.60). Regardless, we find that in both cases both results from the theorems are supported by what we found. Following this we visit the case of general nonlinear diffusion ($m > 1$) and see similar results. Almost all of our results here are in one

dimension though we briefly show some two-dimensional results with the QANR potential that are similar to those in one dimension.

Throughout these results we use the finite volume method developed in [24]. The method preserves the non-negativity of solutions as well as the energy gradient flow structure, and it has been demonstrated to capture accurately the long-time behaviour and equilibria of model (5.1). In particular, it works well for small diffusion values as in the present study, as it can deal robustly with metastable behaviour and large concentrations.

5.1 Quadratic diffusion

First we would like to go over known results in free space to understand what states we expect. Recall that the steady states of the QANR potential in free space are constant density, compact swarms while steady states of the smoothed version in free space are composed of a sum of delta masses. The QANR potential, and its C^1-smoothed version, were investigated in [40], with the addition of diffusive terms. The scope of the investigations there were much broader in fact, as the authors consider linear and nonlinear diffusion with power-law interaction potentials up to fourth order. Referencing the results in [41], it has been noted in [40] that when sufficiently small diffusion is added, steady states of multiple concentrations become multiple smoothed aggregates. Furthermore these states could possibly be continuous, piecewise smooth, and with compact support.

5.1.1 On the half-line $[0, \infty)$

Before we begin we note that the half-line is not bounded and so does not satisfy (H4), but the solutions we consider have compact support and so a large enough domain will be effectively equivalent to the half-line. The study here mostly involves the initial condition

$$\rho^0 = 4\ \mathbb{1}_{[0,0.25]},$$

where $\mathbb{1}_{[a,b]}$ denotes the characteristic function on $[a, b]$. We will also briefly study how the diffusive system (5.1) behaves when initialized near the previous unstable equilibria of the plain aggregation model, but we will make clear when we are considering this.

Dynamics with the C^2-smoothed QANR potential

In order to satisfy (H2A) consider the C^2-smoothed version of the QANR potential:

$$K_2^\epsilon(r) = \frac{1}{2}r^2 - \frac{1}{2}|r|_{\epsilon,2} \tag{5.4}$$

with

$$|r|_{\epsilon,2} = \begin{cases} -\frac{1}{8\epsilon^3}r^4 + \frac{3}{4\epsilon}r^2 + \frac{3}{8}\epsilon & r \leqslant \epsilon, \\ |r| & r > \epsilon. \end{cases} \tag{5.5}$$

We first present numerical support for Theorem 5.0.1, compare the 2-Wasserstein distance between the solutions to (5.1) and (1.4) (with the interaction potential given by (3.60)) and show that for fixed times, the distance decreases as ν decreases. Note that the estimate proved in Theorem 5.0.1 is based on Grönwall's lemma, meaning that for a fixed ν, the distance between the two solutions can potentially grow exponentially fast in time. For this reason the numerical check of Theorem 5.0.1 is restricted to relatively early times, as large times would require simulations with diffusion values that are too small for numerical purposes.

For early times, the diffusive and plain aggregation models are qualitatively similar (see Figure 5.1) and quantitatively, they remain close in the 2-Wasserstein metric (see Table 5.1). In both models we find that the initial mass begins separating, with some mass accumulating on, or near, the boundary and the rest moving away while remaining a single component. The notable difference is that the plain aggregation model forms delta accumulations of mass at the origin (Figure 5.1(b)), whereas the diffusive model forms instead a thin, sharp layer of mass next to it (Figure 5.1(a)). The latter is anticipated, as the measure-valued solutions of the diffusive model are absolutely continuous with respect to the Lebesgue measure.

Regarding the quantitative findings in Table 5.1, we see two general trends. First, the 2-Wasserstein distance at a fixed time decreases as ν decreases towards zero, in support of Theorem 5.0.1. Second, the 2-Wasserstein distance between the two solutions grows as solutions are evolved through time; at early times they do so at a slow rate, for growth at later times see Figure 5.3(a).

ν	$t = 0.5$	$t = 1$	$t = 5$
10^{-3}	2.1400e−2	3.1896e−2	8.6286e−2
10^{-4}	7.1776e−3	1.1110e−2	4.7896e−2
10^{-5}	3.8652e−3	7.5722e−3	3.3105e−2
10^{-6}	3.4619e−3	7.5057e−3	3.3048e−2
10^{-7}	3.4555e−3	7.5043e−3	3.2934e−2

Table 5.1: C^2-smoothed QANR potential: 2-Wasserstein distance $d_W(\rho_\nu(t), \rho(t))$ between solutions of the diffusive model and solutions of the plain aggregation model for various choices of ν and several early times.

The second major goal of these numerical simulations is to show that solutions of the diffusive model do not get trapped in equilibria that are not minimizers of the energy, as the plain aggregation model does. For this study we keep $\nu > 0$ fixed and observe the long time evolution of solutions $\rho_\nu(t)$ of the diffusive model. As expected, we find that the distance between solutions $\rho_\nu(t)$ and $\rho(t)$ grows in time, with the caveat that the two solutions begin to differ substantially, both qualitatively

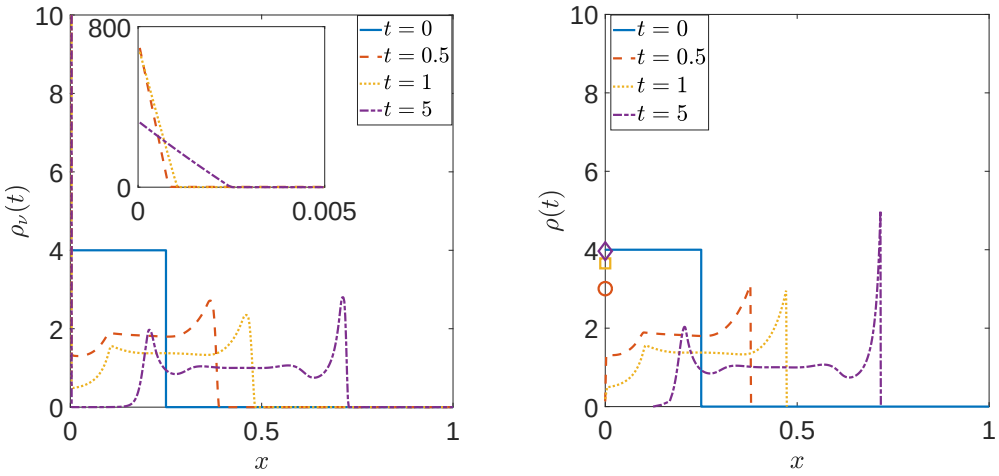

(a) (b)

Figure 5.1: Simulations with the C^2-smoothed QANR potential showing early time dynamics. (a) Snapshots of the diffusive model (5.1) with $\nu = 10^{-7}$. An insert has been included to show the layer of mass near the origin. (b) Snapshots of the plain aggregation model (1.4). Concentrations at the origin are represented as circle, square, and diamond markers for $t = 0.5$, $t = 1$, and $t = 5$ respectively. The masses of concentrations have been magnified 10 times for clarity.

and quantitatively, when mass near the origin in the diffusive model begins to move away from the boundary, into the interior of the domain. This mass transfer, a fundamental distinction between the two models, will be highlighted throughout the discussion below.

Figure 5.2(a) shows the onset of the mass transfer at $t = 10.9$ for simulations with $\nu = 10^{-7}$. Also, by $t = 12.5$ we see that mass has elongated away from the origin and has begun forming a new bump. The transfer of mass occurs repeatedly in the diffusive model as the solution evolves further through time, though less mass is transferred each time. Generally, this mass will either form a new bump or join with the next nearest bump. In contrast, Figure 5.2(b) shows that in the plain aggregation model the concentration at the origin does not change and the five bumps in the free swarm just become sharper, as overall they tend toward five delta concentrations.

Mass transfers are tightly linked to the 2-Wasserstein distance between solutions $\rho_\nu(t)$ and $\rho(t)$, as well as to the energy evolution of the diffusive model. Figure 5.3(a) shows the evolution in time of the distance between the two solutions, for various ν. In each plot we see a significant increase in the growth of the distance at exactly the times when mass first transfers away from the origin. Additionally we observe that decreasing ν keeps the distance between solutions smaller for longer times.

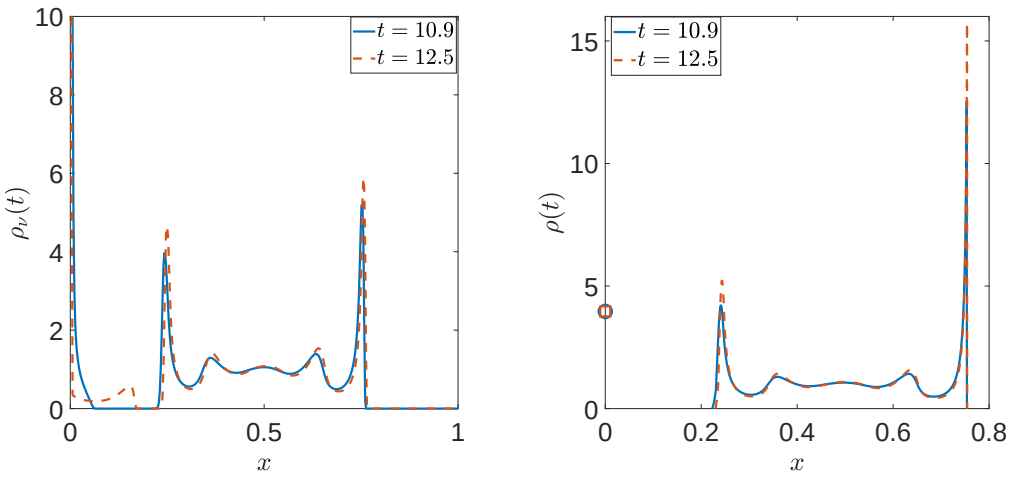

(a) (b)

Figure 5.2: Simulations with the C^2-smoothed QANR potential showing the first mass transfer from the boundary to the free swarm in the diffusive model. (a) Snapshots of the diffusive model (5.1) with $\nu = 10^{-7}$. (b) Snapshots of the plain aggregation model (1.4). Concentrations are represented as circle and square markers for $t = 10.9$ and $t = 12.5$ respectively. The masses of concentrations have been magnified 10 times for clarity.

Complementary to looking at the 2-Wasserstein distance, Figure 5.3(b) compares the energies of the diffusive model and of the plain aggregation model (see (5.3) and (5.2)). We observe that the energies are close, again, up until the first mass transfer occurs. The energy plots also show that the diffusive model enables solutions to reach lower energies where the plain aggregation model gets stuck at a higher energy that corresponds to an energetically unstable steady state.

With no mechanism to break apart the delta concentration at the boundary (see Figure 5.2(b)), the plain aggregation model evolves into a steady state $\bar{\rho}$ that consists of six delta concentrations (one at the origin and five in the interior) – see Figure 5.4(b). This steady state is *not* a minimizer of energy (5.2). This flaw of the plain aggregation model was demonstrated in Chapter 3. On the other hand, the mechanism of mass transfer in the diffusive model enables solutions $\rho_\nu(t)$ to bypass the unstable equilibrium $\bar{\rho}$ of the plain aggregation equation.

Figure 5.4(a) shows the 2-Wasserstein distance $d_W(\rho_\nu(t), \bar{\rho})$ between the solutions of the diffusive model and the unstable equilibrium of the plain aggregation model. The plots show that $d_W(\rho_\nu(t), \bar{\rho})$ achieves its minimum (i.e., the diffusive model comes nearest to the plain aggregation steady state) exactly at the times of the first mass transfer. The solutions $\rho_\nu(t)$ at these times, consisting of multiple smoothed aggregates, are shown in Figure 5.4(b). One can see indeed that the smaller the ν the closer the diffusive solutions pass by the plain aggregation equilibrium.

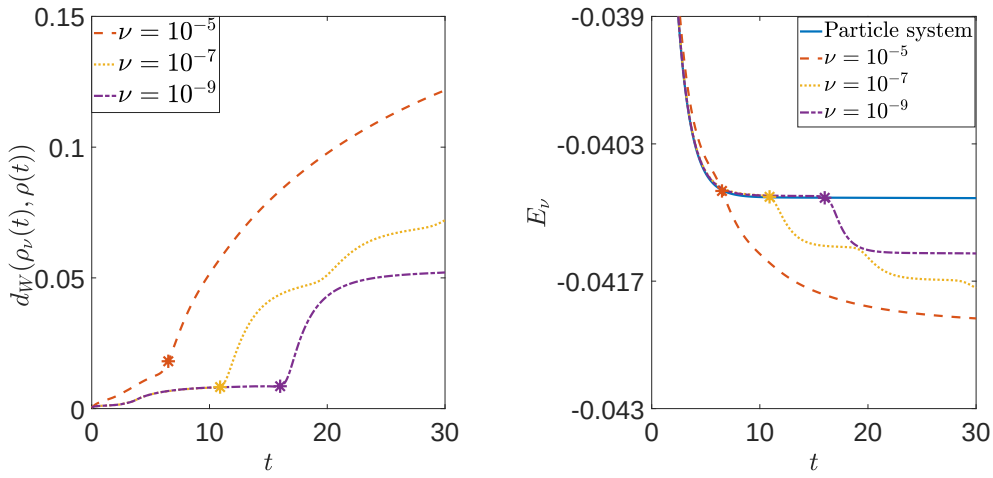

(a) (b)

Figure 5.3: Results with the C^2-smoothed QANR potential. (a) 2-Wasserstein distance between the diffusive and plain aggregation solutions for various choices of ν. (b) Energy (5.3) of solutions to the diffusive model through time for various choices of ν. Also included is the energy (5.2) of the solution to the particle model through time (solid line). Star markers have been placed at $t = 6.5$, $t = 10.9$, and $t = 16$ for $\nu = 10^{-5}$, $\nu = 10^{-7}$, and $\nu = 10^{-9}$ respectively, corresponding to the times of the first mass transfer.

It is expected that throughout their time evolution, solutions $\rho_\nu(t)$ of the diffusive model bypass other unstable equilibria of the plain aggregation model. This can be observed for instance in the staircase-like evolution of the energy for $\nu = 10^{-7}$ in Figure 5.3(b) (dotted line). The various plateaus of the energy correspond exactly to solutions being temporarily trapped near an unstable equilibria of the plain aggregation model (one could think of these configurations as metastable states for the diffusive model), while the drops in energy correspond to mass transfers. Finally, Figure 5.5 gives another viewpoint from which to see the diffusive model visits the plain aggregation equilibria.

Dynamics with the QANR potential

For early times we again find that the solutions of the diffusive and plain aggregation models remain qualitatively similar (see Figure 5.6): the initial density moves apart, with some mass staying near, or on, the origin and the rest spreading away from the wall. As with the C^2-smoothed QANR potential we find again that the diffusive model has a thin, sharp layer of mass near the origin where the plain aggregation model concentrates mass exactly at the origin. One notable difference

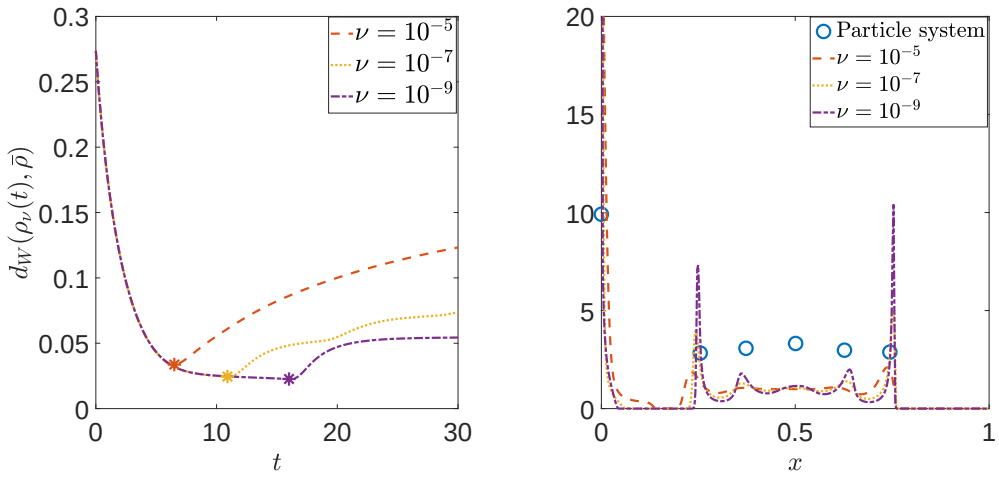

(a) (b)

Figure 5.4: Results with the C^2-smoothed QANR potential. (a) 2-Wasserstein distance between solutions to the diffusive model and the (unstable) equilibrium of the plain aggregation model, for various choices of ν. Markers have been placed at $t = 6.5$, $t = 10.9$, and $t = 16$ for $\nu = 10^{-5}$, $\nu = 10^{-7}$, and $\nu = 10^{-9}$ respectively, corresponding to the times of the first mass transfer (see also Figure 5.3); these times also correspond to when $\rho_\nu(t)$ is closest to $\bar{\rho}$. (b) Solutions to the diffusive model at the times marked in (a). The circles represent concentrations of the equilibrium $\bar{\rho}$, where they have been magnified 25 times for clarity.

from the C^2-smoothed QANR potential is that now the diffusive solution ρ_ν consists of only a single component for all tests we performed.

We also consider the 2-Wasserstein distance $d_W(\rho_\nu(t), \rho(t))$ between the two solutions and find similar results to the study with the C^2-smoothed QANR potential – see Table 5.2 and Figure 5.7(a). Specifically, we find that for fixed times the distance decreases as ν is decreased toward zero, suggesting that Theorem 5.0.1 may be refined to include less regular interaction potentials. We also find that the distance between the two solutions increases as time goes forward, with a faster growth rate at later times.

ν	$t = 0.1$	$t = 0.5$	$t = 3$
10^{-3}	6.8548e−3	2.4142e−2	6.6831e−2
10^{-4}	2.9493e−3	1.1424e−2	4.3318e−2
10^{-5}	2.3620e−3	8.9352e−3	3.7865e−2
10^{-6}	2.3166e−3	8.6382e−3	3.6588e−2
10^{-7}	2.3161e−3	8.6054e−3	3.6235e−2

Table 5.2: QANR potential: 2-Wasserstein distance $d_W(\rho_\nu(t), \rho(t))$ between solutions of the diffusive model and solutions of the plain aggregation model for various choices of ν at some early times.

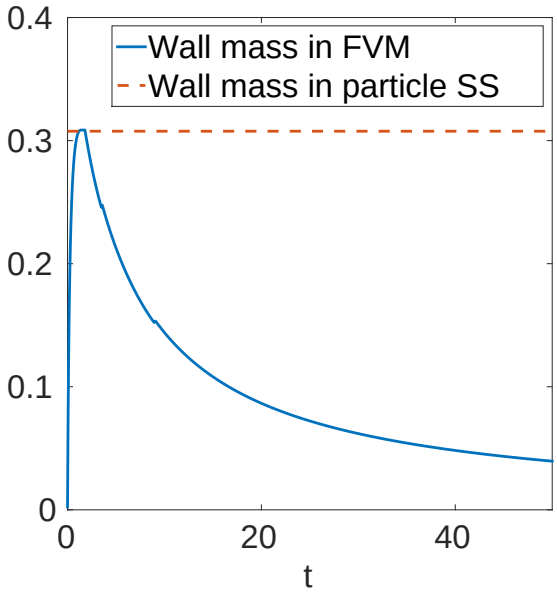

Figure 5.5: Showcasing the mass near the wall in the diffusive model (near in this context is just within some small distance relative to the swarm size). The particle steady state (SS) is achieved dynamically from the plain aggregation model. To note here is how the diffusive model first accumulates mass near the wall and peaks out exactly at the wall mass of the plain aggregation system before slowly losing mass as it flows away.

Figure 5.7(b) shows the energies of the diffusive and plain aggregation solutions. We find again that with diffusion, solutions achieve states of lower energy than the plain aggregation model. We do not see the same energy staircase pattern as in Figure 5.3(b) however. This is not unexpected actually, as the reason we observed the staircase pattern when considering the C^2-smoothed QANR potential was because the diffusive solution consisted of multiple disjoint components. The staircasing was highly linked to instances of mass from the origin gradually pulling away, leaving the origin, and moving to join the free swarm. Since with the QANR potential the diffusive solution does not form multiple disjoint components, there is no mass transfer and hence the mechanism for energy staircasing is missing.

We also find again that the diffusive model bypasses the unstable equilibrium of the plain aggregation model. Figure 5.8(a) shows that the solutions $\rho_\nu(t)$ of the diffusive model come near to the unstable equilibrium $\bar{\rho}$ of the plain aggregation model and decreasing ν causes this distance to decrease, though not as noticeably as for the smooth potential (Figure 5.4(a)). We have also included markers at times where $d_W(\rho_\nu(t), \bar{\rho})$ achieves its minimum though we do not see these times being significant to $d_W(\rho_\nu(t), \rho(t))$ in Figure 5.7(a) or to the energies of the diffusive model in Figure 5.7(b). We believe that, as for the energy staircasing, it is the lack of mass transfer of solutions that is the cause here. We also think that for the same reason the curves in Figures 5.7(a)

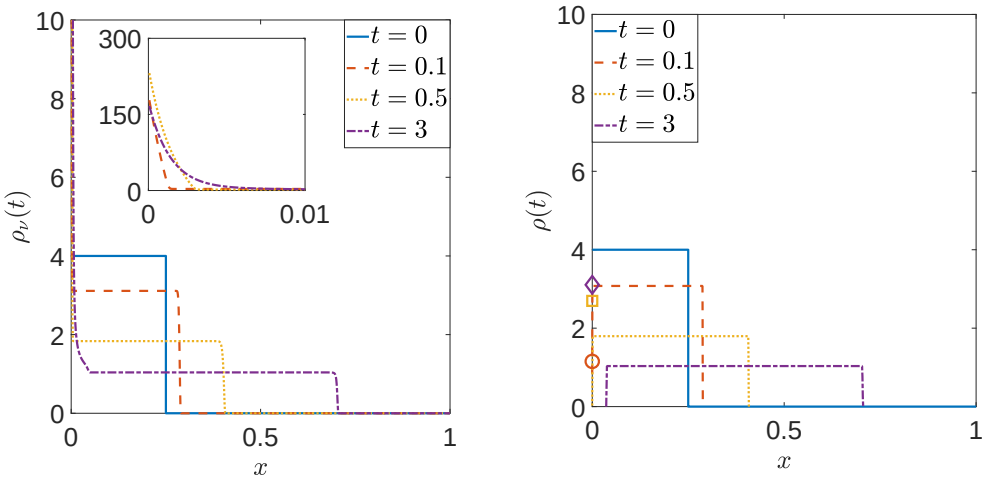

(a) (b)

Figure 5.6: Simulations with the QANR potential showing early time dynamics. (a) Snapshots of the diffusive model (5.1) with $\nu = 10^{-6}$. An insert has been included to show the layer of mass near the origin more clearly. (b) Snapshots of the plain aggregation model (1.4). Concentrations are represented as circle, square, and diamond markers for $t = 0.1$, $t = 0.5$, and $t = 3$ respectively. The masses of concentrations have been magnified 10 times for clarity.

and 5.8(a) are not as differentiated as they were with the C^2-smoothed potential (Figures 5.3 and 5.4).

Figure 5.8(b) shows the solutions $\rho_\nu(t)$ compared to the (unstable) equilibrium $\bar{\rho}$ of the plain aggregation model at times corresponding to the minima of $d_W(\rho_\nu(t), \bar{\rho})$, specifically $t = 6.9$, $t = 7.6$, and $t = 7.9$ for $\nu = 10^{-4}$, $\nu = 10^{-6}$, and $\nu = 10^{-8}$ respectively. Note that the solutions $\rho_\nu(t)$ match up with most of the free swarm component of $\bar{\rho}$. The major qualitative difference is again, that solutions of the diffusive model consist of a single component where the plain aggregation equilibria is formed of two disjoint parts.

Remark 5.1.1 (Initializing near an unstable equilibrium of the plain aggregation model)**.** *So far we have shown that, beginning from the same initial data, the diffusive model appears to visit unstable equilibria of the plain aggregation model but do not seem to be trapped in them. We further confirm now that the diffusive model indeed flows away from the unstable equilibria. To this end we initialize the diffusive model at an approximation of the unstable equilibrium shown in Figure 3.1(a). The delta accumulation at the origin is approximated by a thin, constant density component adjacent to the wall. Figure 5.9 shows the evolution of the diffusive model from this initial state, showing that the diffusive model flows away from the disconnected equilibrium of the plain aggregation model.*

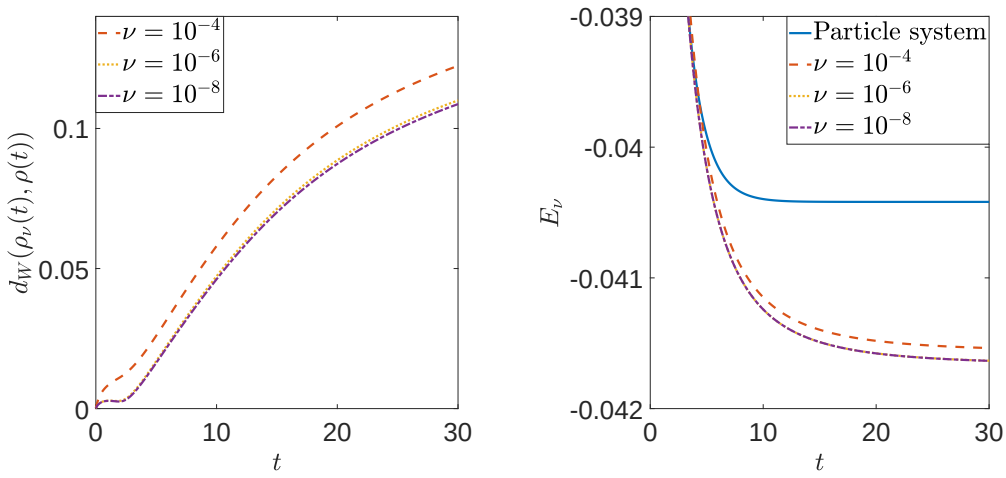

(a) (b)

Figure 5.7: Results with the QANR potential. (a) 2-Wasserstein distance between the diffusive and plain aggregation solutions for various choices of ν. (b) Energy (5.3) of solutions to the diffusive model through time for various choices of ν. Also included is the energy (5.2) of the solution to the particle model through time (solid line).

Convergence of energy minimizers for the QANR potential

We remark quickly that we only highlight the QANR potential here as it together with quadratic diffusion allows for explicitly computed equilibria. Recall that in the plain aggregation model, the minimizing equilibrium $\bar{\rho}^*$ of energy E (given by (5.2) with V=0) is the same as that for the problem in free space [44], i.e.,

$$\bar{\rho}^* = \mathbb{1}_{[0,1]}. \tag{5.6}$$

Note that this minimizer is unique up to translation. In addition, recal that there exists a one-parameter family of equilibria $\bar{\rho}$ that are not energy minimizers, composed of a concentration at the origin and a constant-valued, compact component away from the boundary. For this reason we added an asterisk superscript to the minimizer in (5.6), to distinguish it from the other (unstable) equilibria.

Though we do not assume the form of equilibria as we did with the plain aggregation model, there are some known results that guide our search. By the results in [21] and [41], as well as observations of our numerics, we assume that the equilibrium $\bar{\rho}_\nu$ is continuous, smooth on its support, and composed of a single component with compact support such that $\text{supp}(\bar{\rho}_\nu) = [0, L]$.

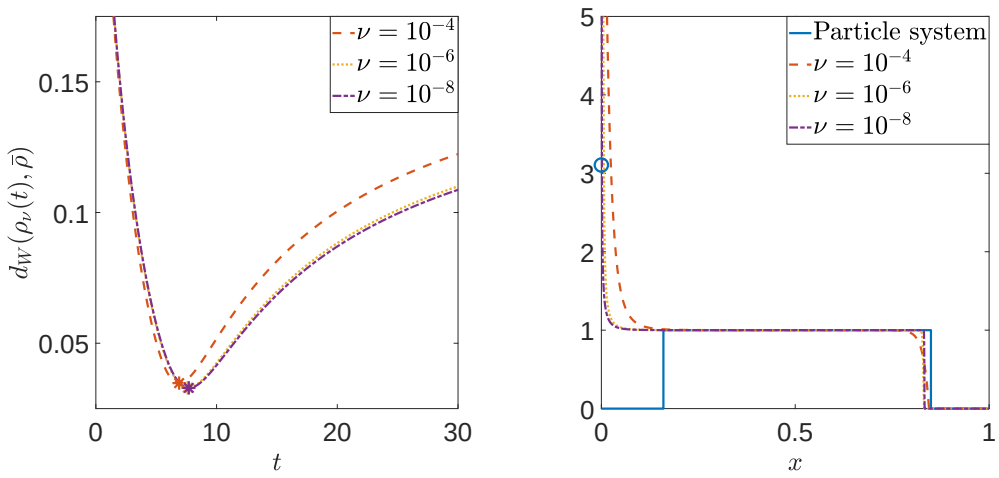

(a) (b)

Figure 5.8: Results with the QANR potential. (a) 2-Wasserstein distance between solutions to the diffusive model and the (unstable) equilibrium of the plain aggregation model, for various choices of ν. Markers have been placed at $t = 6.9$, $t = 7.6$, and $t = 7.9$ for $\nu = 10^{-4}$, $\nu = 10^{-6}$, and $\nu = 10^{-8}$ respectively, corresponding to the times when $d_W(\rho_\nu(t), \bar{\rho})$ achieves its minimum. (b) Solutions to the diffusive model at the times marked in (a), respectively for each ν. The solid line and the circle marker at origin (indicating a delta concentration) represents the unstable equilibrium $\bar{\rho}$ of the plain aggregation model. The concentration has been magnified 10 times for clarity.

We find equilibria $\bar{\rho}_\nu$ by looking for critical points of the energy E_ν by solving this problem's equilibrium condition (2.14). By an immediate calculation (see [10], also [45]), this becomes

$$\Lambda_\nu(x) = \lambda_\nu \qquad \text{for } x \in \operatorname{supp}(\bar{\rho}_\nu), \tag{5.7}$$

for some $\lambda_\nu \in \mathbb{R}$, where

$$\Lambda_\nu(x) = 2\nu\bar{\rho}_\nu(x) + K * \bar{\rho}_\nu. \tag{5.8}$$

Furthermore, if

$$\Lambda_\nu(x) \geqslant \lambda_\nu \qquad \text{for } x \notin \operatorname{supp}(\bar{\rho}_\nu), \tag{5.9}$$

then $\bar{\rho}_\nu$ is a local minimizer. The interpretation of (5.9) is that transporting mass from the support of $\bar{\rho}_\nu$ into its complement increases the total energy [10].

The approach we take is to solve $\Lambda_\nu'(x) = 0$ and $\Lambda_\nu''(x) = 0$ for $x \in \operatorname{supp}(\bar{\rho}_\nu)$ and then show that these equilibria must necessarily be local minimizers (i.e., satisfy (5.9)). We also note that we

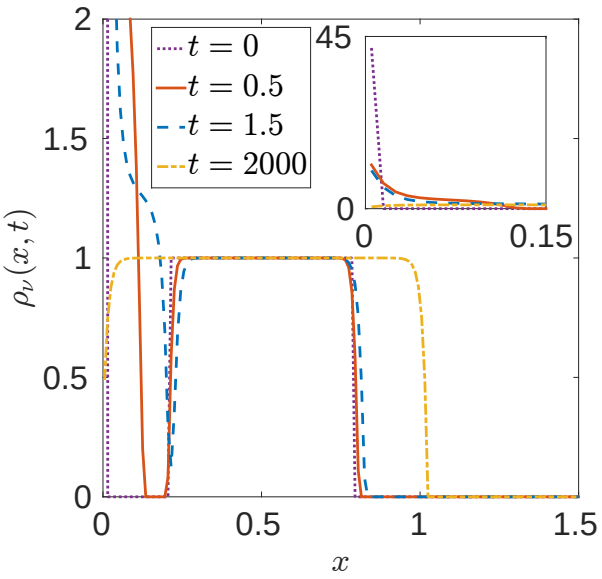

Figure 5.9: Evolution of the diffusive model (5.1) with no external potential when initialized near a (disconnected) non-minimizer equilibrium of the plain aggregation model (1.4) (see Figure 3.1(a)). Solutions to the diffusive model approach asymptotically a smoothed out version of the (connected) minimizer equilibrium of the plain aggregation model shown in Figure 3.1(b). Here we have $\nu = 10^{-4}$, with a zoom out near boundary shown in insert.

look for minimizers of unit mass ($\int_0^L \bar{\rho}_\nu(x)\,dx = 1$) that are continuous at the end of their support:

$$\lim_{x \nearrow L} \bar{\rho}_\nu(x) = 0. \tag{5.10}$$

From (5.8), one gets

$$\Lambda_\nu''(x) = 2\nu\bar{\rho}_\nu''(x) + 1 - \bar{\rho}_\nu(x). \tag{5.11}$$

Solving $\Lambda_\nu''(x) = 0$ is trivial and we get the general form of equilibria $\bar{\rho}_\nu$ to be

$$\bar{\rho}_\nu(x) = c_1 e^{\frac{x}{\sqrt{2\nu}}} + c_2 e^{-\frac{x}{\sqrt{2\nu}}} + 1, \qquad x \in [0, L]. \tag{5.12}$$

We cannot, however, explicitly solve for the unknowns c_1, c_2, and L and we resort to obtaining them by numerically solving the remaining three conditions: $\Lambda_\nu' = 0$ in $[0, L]$, the unit mass condition, and continuity at L given by (5.10). We point out that $\Lambda_\nu(x)$ is continuous and that $\Lambda_\nu''(x) = 1 > 0$ for $x \notin \text{supp}(\bar{\rho}_\nu)$. The strict convexity of Λ_ν outside $\text{supp}(\bar{\rho}_\nu)$, combined with (5.7), implies that (5.9) necessarily holds, so the equilibria (5.12) are in fact minimizers of the energy.

Remark 5.1.2 (Solving for the constants c_1, c_2, and L)**.** *We find the constants c_1, c_2, and L as functions of ν through a continuation method. The problem is to find c_1, c_2, and L for a given ν such that $\Lambda'_\nu(x) = 0$, the mass of the profile is 1, and the profile is continuous, which we can write as a nonlinear system of equations $F(c_1, c_2, L) = 0$. We do not write the equations here as it is an elementary exercise to find them.*

To begin the continuation we find an initial point by solving $F(c_1, c_2, L) = 0$ using MATLAB's fsolve with $\nu = 1$ and initial guess $(c_1, c_2, L) = (1, 1, 1)$. For $\nu = 1$ we see the system is relatively well conditioned (see Figure 5.10(a)) and we can compare the result of this procedure to the steady state obtained dynamically via the finite volume code (see Figure 5.11), which we can argue further is a minimizer because of the profile of $\Lambda(x)$. The checks on first-order optimality and residuals are both reasonable for $\nu = 1$ (see Figures 5.10(b) and 5.13(b)). After obtaining this initial solution we then change ν and re-solve the nonlinear system using the previous solution as the initial guess.

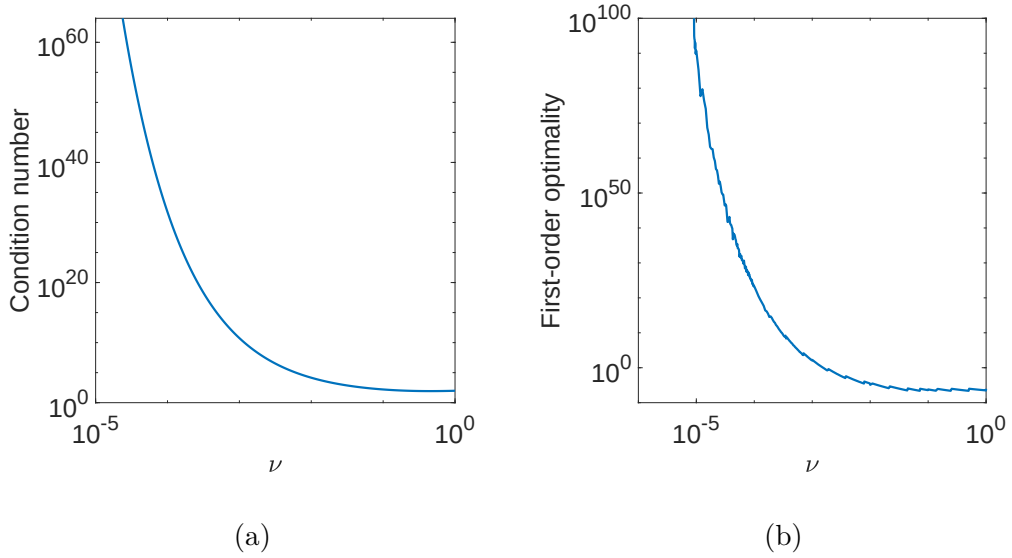

(a) (b)

Figure 5.10: (a) Calculated condition numbers of the nonlinear system using the found solutions. (b) Check of the first-order optimality of the solution for the given ν.

Due to the focus on the magnitude of ν, we chose a non-uniform grid that ranges from $\nu = 1$ to $\nu = 10^{-6}$ with 100 equidistant jumps within each magnitude. Then with the solution for $\nu = 1$, we move down the grid re-converging whenever we change ν. Figure 5.12 shows the solution curves $c_1(\nu)$, $c_2(\nu)$, and $L(\nu)$ along with the changes observed in the constants during the solution of the nonlinear system for the given ν. Note that the changes are relatively small for c_2 and L whereas c_1 experiences very small changes in magnitude, while the values themselves are very small as well (see Figure 5.13(a)). See also Figure 5.13(b) for the residuals in the numerical solution.

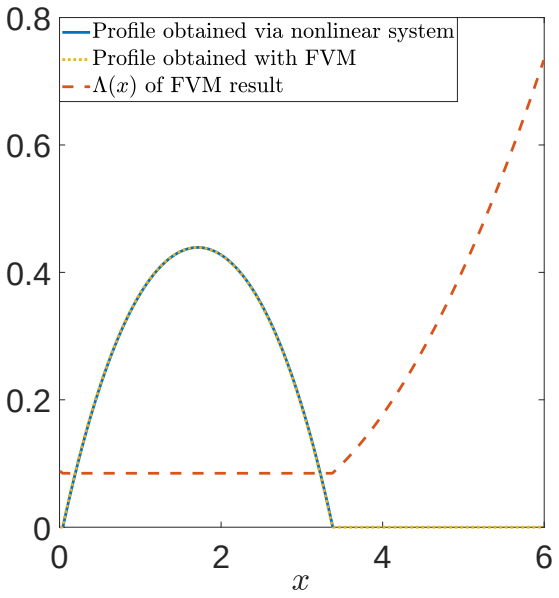

Figure 5.11: Comparing the result of the solution of the numeric method versus results from the finite volume code (FVM).

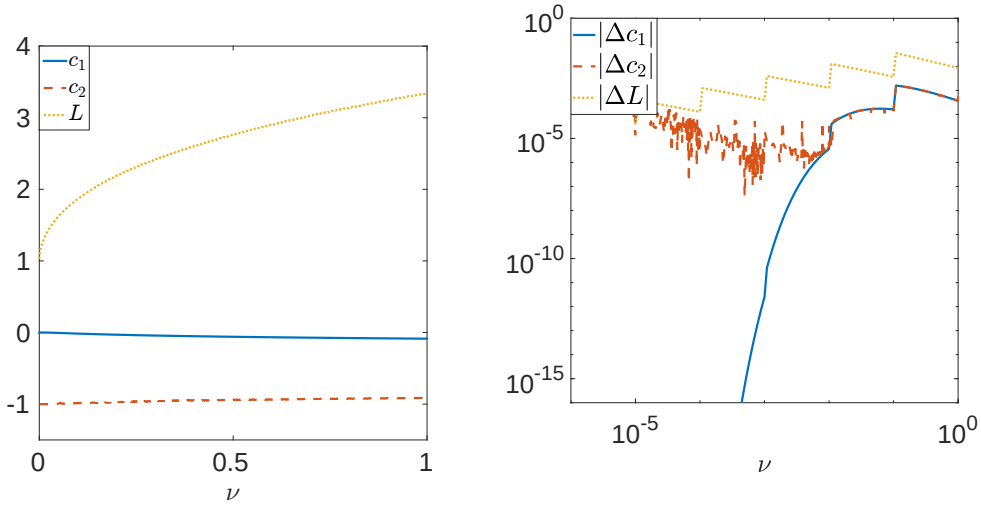

(a) (b)

Figure 5.12: (a) Numerically calculated c_1, c_2, and L as functions of ν. (b) Changes in c_1, c_2, and L that occurred during solution of nonlinear system with the given ν.

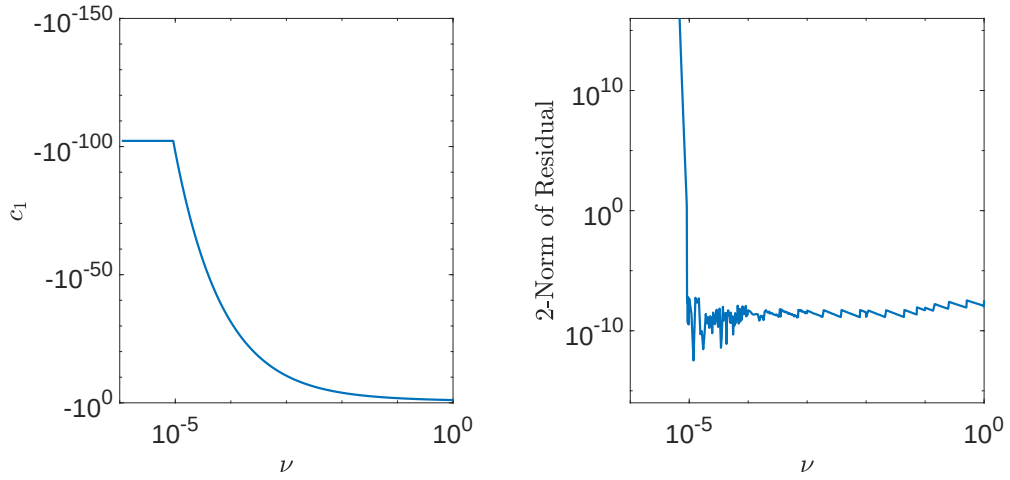

(a) (b)

Figure 5.13: (a) Logarithmic perspective of the values of c_1 as a function of ν. (b) Residuals for the solution $c_1(\nu)$, $c_2(\nu)$, and $L(\nu)$ of the nonlinear system with the given ν.

Looking at Figures 5.10, 5.12 and 5.13, one might expect indeed some ill-behaviour as ν decreases. Even $\nu = 10^{-5}$ is ambitious in fact, but the solution appears to be solved according to the residuals (Figure 5.13(b)). Additionally the result for $\nu = 10^{-5}$ both matches with observed steady states of the finite volume method and appears to converge towards the minimizer of the system without diffusion, as expected by Theorem 1.2. Trying to get to $\nu = 10^{-6}$ seems to not be possible as the system becomes too ill-conditioned, and very apparent defects in the profile arise in these solutions (see Figure 5.14(b)).

.

Next we compare the minimizers (5.12) of E_ν with the minimizer (5.6) of E for the plain aggregation model. Figure 5.15(a) shows that $\bar{\rho}_\nu$ qualitatively approach $\bar{\rho}^*$, while Figure 5.15(b) provides direct quantitative numerical evidence for Theorem 5.0.2, namely that minimizers of E_ν approach (in the 2-Wasserstein metric) minimizers of E in the zero diffusion limit.

Figure 5.12(a) shows the numerically calculated values of c_1, c_2, and L as functions of ν (the lowest ν for which such results have been obtained is $\nu = 10^{-5}$). Observe that L tends to 1 as ν tends to zero which is in agreement with the minimizer (5.6) of the plain aggregation model. Furthermore notice that c_1 and c_2 approach 0 and -1, respectively, in the zero diffusion limit. As explained below, this yields the following pointwise limit of $\bar{\rho}_\nu(x)$ as $\nu \to 0$:

$$\lim_{\nu\to 0} \bar{\rho}_\nu(x) = 0 \quad \text{for } x = 0,\ x = L, \qquad \text{and} \qquad \lim_{\nu\to 0} \bar{\rho}_\nu(x) = 1 \quad \text{for } x \in (0, L), \tag{5.13}$$

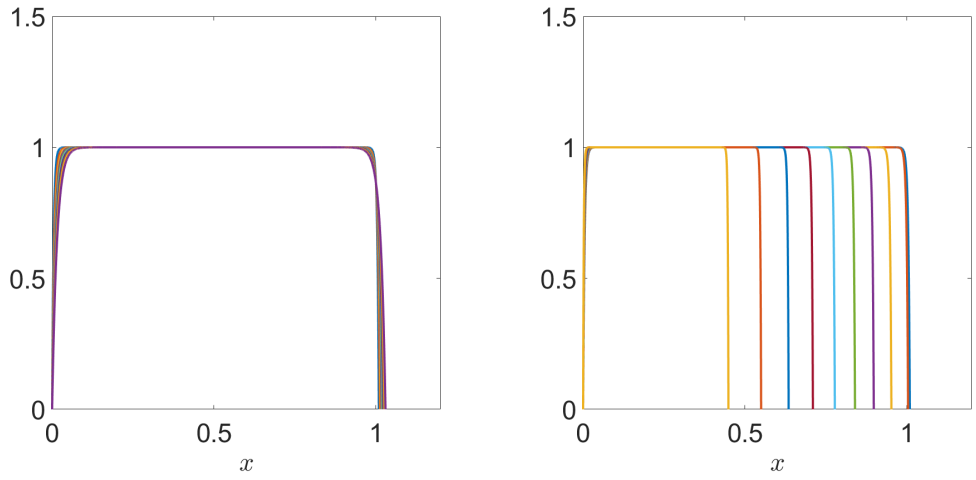

(a) (b)

Figure 5.14: (a) Profiles of the solution with ν taking on 10 equidistant values between 10^{-4} and 10^{-5}. Though difficult to see, the profile with the largest support has the largest ν and the profile with the smallest support has the smallest ν. Observe the general coarsening towards the minimizer of the non-diffusive system. (b) Profiles of the solution with ν taking on 10 equidistant values between 10^{-5} and 10^{-6}. The profile with the largest support has the largest ν and the profile with the smallest support has the smallest ν. It is at this point that the results of the numerical method diverge from observations from the finite volume method.

consistent with the limiting behaviour of minimizers shown in Figure 5.15(a).

The pointwise limit at $x = 0$ can be inferred immediately from (5.12) and $c_1 \to 0$, $c_2 \to -1$ as $\nu \to 0$ (Figure 5.12(a)). Furthermore, since c_2 approaches a finite value as $\nu \to 0$, at strictly positive x in the support of $\bar{\rho}_\nu$ we have:

$$\lim_{\nu \to 0} \bar{\rho}_\nu(x) = \lim_{\nu \to 0} c_1 e^{\frac{x}{\sqrt{2\nu}}} + 1, \qquad \text{for } x \in (0, L]. \tag{5.14}$$

In Figure 5.12(b) we explore the behaviour of $c_1 e^{\frac{x}{\sqrt{2\nu}}}$ as ν tends to zero, at $x = L$ and $x = L - 10^{-2}$, that is, at the end of the support, as well as very close to it. We find the two pointwise limits to be -1 and 0 respectively. From this observation and (5.14) we conclude (5.13), also noting that if $\lim_{\nu \to 0} c_1 e^{\frac{x}{\sqrt{2\nu}}} = 0$ for x arbitrarily close to L then the limit is also zero for all $0 < x < L$.

Finally, it should be remarked that the values of ν for which we have calculated numerically c_1, c_2, and L are not coincidental. These are all the values (less than 1) for which we can reasonably solve the system of nonlinear equations to find the constants. As ν decreases one finds that the condition number of the system becomes unmanageable beyond $\nu = 10^{-5}$, when the numerical method fails and defects in the solution profile are visibly apparent. It should be also noted that

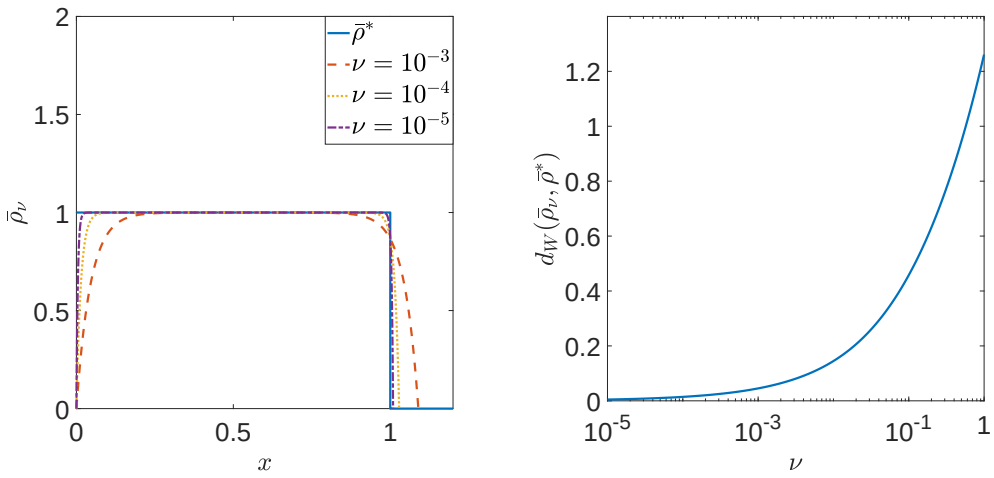

(a) (b)

Figure 5.15: (a) Comparison between the energy minimizer $\bar{\rho}^*$ of the plain aggregation model (see (5.6)) and minimizers $\bar{\rho}_\nu$ of the diffusive model (see (5.12)) for various ν. (b) The 2-Wasserstein distance between the minimizers $\bar{\rho}_\nu$ and $\bar{\rho}^*$ as a function of ν.

while the system becomes ill-conditioned, any results shown in the paper have been compared satisfactorily versus the results from other methods, namely the finite volume method, so that we are confident in what has been reported here.

Remark 5.1.3 (Linear exogeneous potential: $V(x) = gx$)**.** *So far we have only investigated the case with no external potential. The case with an external potential has been studied as well, though the case with the smoothed QANR potential is more complicated so we neglect that entirely. The case with the QANR potential is fairly simple and explicit forms of equilibria can be calculated similarly to the case with no external potential. Additionally we perform a similar test as in Remark 5.1.1. Figure 5.16(a) shows the diffusive model initialized near a disconnected equilibrium of the plain aggregation model. Just as in Figure 5.9, we see that the diffusive model flows away from the disconnected equilibrium towards a regularized version of the connected minimizer of the plain aggregation model (see Figure 3.2(b)). Figure 5.16(b) shows explicitly calculated equilibria of the diffusive model and Figure 5.16(c) shows a calculation of the mass in the boundary layer near the wall, highlighting how the mass in the boundary layer approaches the mass of the delta accumulation in the connected minimizer of the plain aggregation model.*

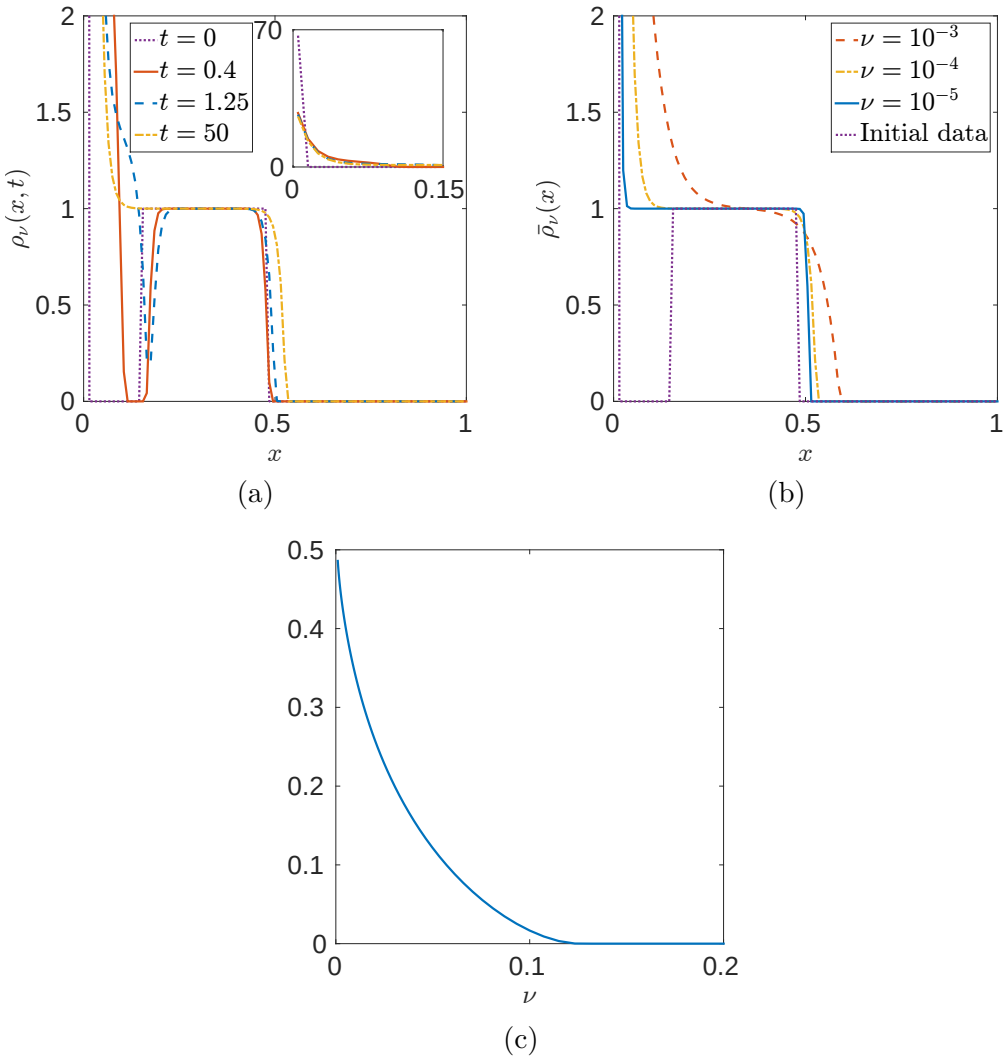

Figure 5.16: (a) Evolution of the diffusive model (5.1) on the half-line with $V(x) = gx$ when initialized near a (disconnected) non-minimizer equilibrium of the plain aggregation model (1.4) (see Figure 3.2(a)). Solutions to the diffusive model approach asymptotically a smoothed out version of the (connected) minimizer equilibrium of the plain aggregation model shown in Figure 3.2(b). Here we have $\nu = 10^{-4}$, with a zoom out near boundary shown in insert. (b) Showcasing some explicitly calculated equilibria of the diffusive model with $V(x) = gx$. (c) Calculation of mass in the boundary layer adjacent to the wall for the explicitly calculated equilibria shown in (b). Note that as $\nu \to 0$ we see the mass in the boundary layer approach the mass of the accumulation of the connected minimizer of the plain aggregation model (Figure 3.2(b)).

5.1.2 On the half-plane $[0, \infty) \times (-\infty, \infty)$

A natural extension of the previous results is to consider higher dimensions, and while this case is definitely more complicated we can still come to some conclusions about the diffusive model in two dimensions. We repeat the tests performed in Remark 5.1.1 and Remark 5.1.3, specifically we initialize the diffusive model near a disconnected equilibrium of the plain aggregation model and see how the diffusive model evolves.

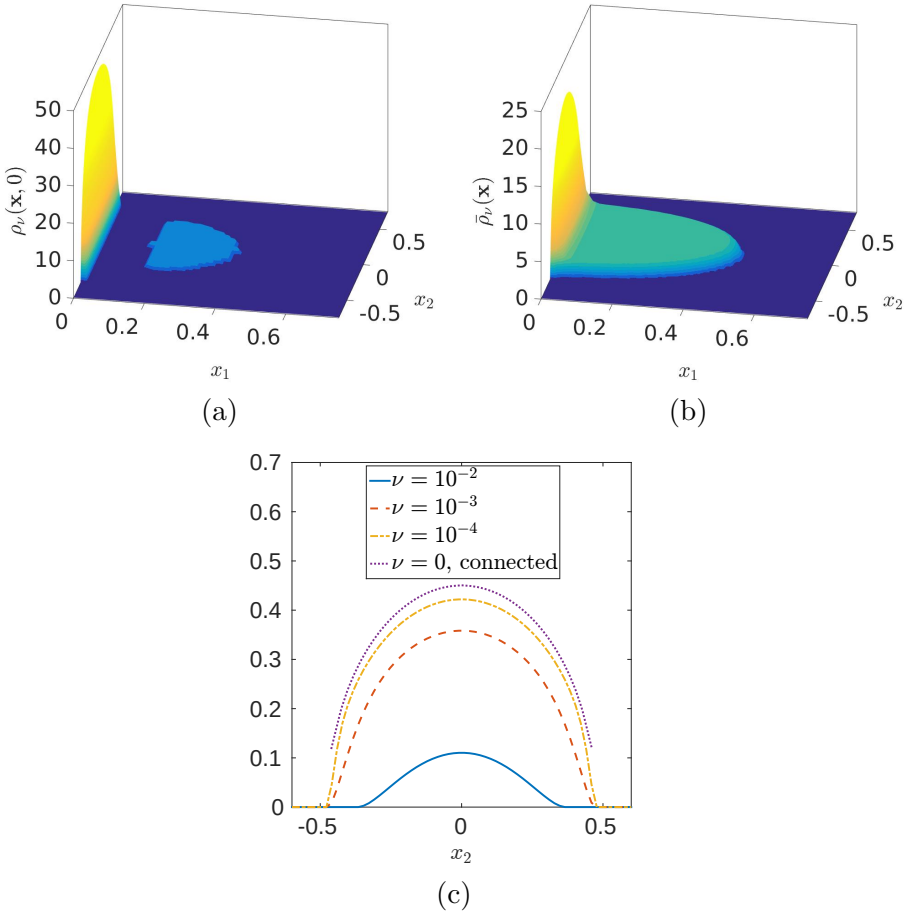

Figure 5.17: Evolution of the diffusive model (5.1) on the half-plane with $V(x_1, x_2) = gx_1$ when initialized near a (disconnected) non-minimizer equilibrium of the plain aggregation model (1.4) (see Figure 4.2(a)). Solutions to the diffusive model approach asymptotically a smoothed out version of the (connected) minimizer equilibrium of the plain aggregation model shown in Figure 4.2(b). Here we have $\nu = 10^{-4}$. (a) The initial state of the diffusive model. (b) The observed steady state of the diffusive model resulted from the initial state in (a). (c) A visualization of the mass in the boundary layer of observed steady states of the diffusive model. Here we sum masses in the x_1 direction and compare them to the wall profile $f(x_2)$ of the (connected) stable equilibrium from Figure 4.2(b).

Figures 5.17(a) and (b) show the results of this test while Figure 5.17(c) gives evidence that the mass near the boundary in the diffusive model concentrates in a manner that approximates the accumulation on the boundary of the connected minimizer of the plain aggregation equation.

5.2 General nonlinear diffusion

Having now shown that quadratic diffusion has at least some capacity to regularize the plain aggregation model, a natural extension is to consider more general nonlinear diffusion. In this section we consider $m = 1.5$ and $m = 3$ and present results that very much mirror those of the quadratic diffusion (see Section 5.1), highlighting what differences there are. We repeat the same dynamical tests as with quadratic diffusion and discuss briefly the calculations of equilibria.

In the following we consider starting from the same initial density as with the quadratic diffusion tests, namely $\rho^0 = 4\,\mathbb{1}_{[0,0.25]}$. Note that in Theorem 5.0.1 we have an explicit upper bound for the convergence rate of $d_W^2(\rho_\nu(t), \rho(t))$ at fixed times, as $\nu \to 0$. The rate (not necessarily sharp) is ν^β, where β depends on m and the dimension d such that

$$m_1 < m_2 \quad \Longrightarrow \quad \beta_1 \geqslant \beta_2.$$

Therefore, we expect better convergence at fixed times for lower values of m.

Figure 5.18 below shows the early time dynamics for $m = 1.5$ and $m = 3$; also see Figure 5.1 (for $m = 2$). A key distinction is that the approximation is better for decreasing m – note the boundary layer at the origin which gets steeper and narrower with decreasing m and hence better approximates the Dirac accumulation on the boundary in the plain aggregation model. Aside from the general observation we made above (rate of convergence ν^β which improves with lowering m), a formal argument for this fact is that at high concentrations ρ, the diffusion ρ^m decreases with m. Also, as shown below, at later times diffusive solutions with lower values of m capture more sharply the interior delta aggregations of the plain aggregation model.

The observation in the paragraph above is also confirmed at later times. Indeed, Figure 5.19 below (see also Figure 5.2 for $m = 2$) shows how lower values of m capture more sharply the delta aggregations in the plain aggregation model.

The evolution of $d_W(\rho_\nu(t), \rho(t))$ for $m = 1.5$ and $m = 3$ is shown in Figure 5.20 – see also Figure 5.3 for $m = 2$. The stars correspond to the times of the first mass transfer from the boundary. As anticipated, the transfer occurs faster for larger values of m (where there is more diffusion). This fact is also illustrated in the energy plot in Figure 5.21: the energy staircasing gets accelerated by increasing m (more diffusion, faster mass transfers). Finally, as shown by Figure 5.22 below, the minimum distance between the diffusive solution and the equilibrium of the plain aggregation model occurs faster for larger m. On the other hand, these minimum distances decrease with lowering m as we can see in Figure 5.23.

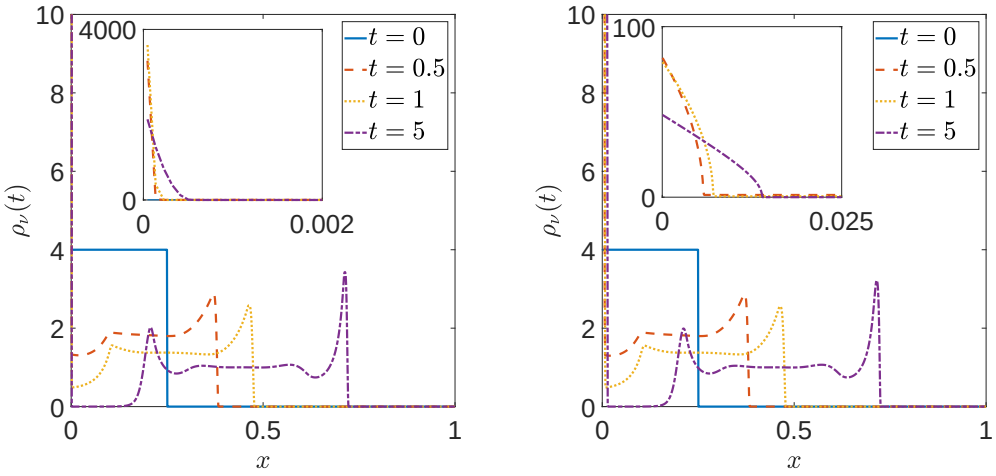

(a) m = 1.5 (b) m=3

Figure 5.18: Simulations with the C^2-smoothed QANR potential showing early time dynamics for $\nu = 10^{-7}$. The approximation by nonlinear diffusion improves with decreasing m: the boundary layer near the origin gets steeper with decreasing m and better approximates the Dirac accumulation at the origin in the plain aggregation model.

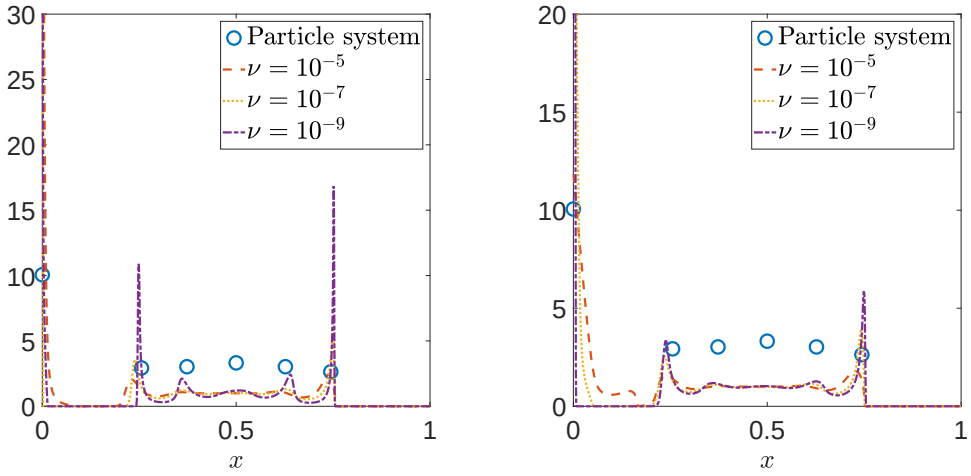

(a) m = 1.5 (b) m=3

Figure 5.19: Results with the C^2-smoothed QANR potential. Solutions of the diffusive model at the times when $\rho_\nu(t)$ is closest to $\bar{\rho}$. The approximation by nonlinear diffusion gets sharper with decreasing m.

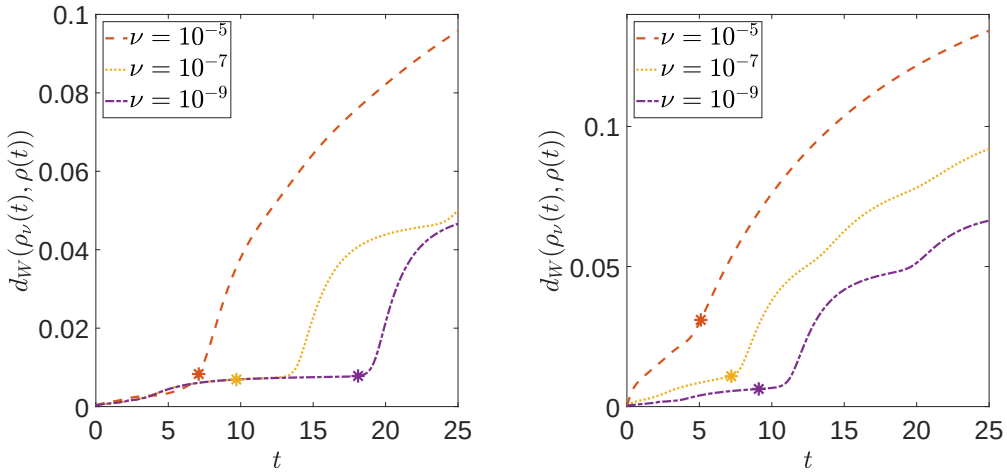

(a) m = 1.5 (b) m=3

Figure 5.20: Results with the C^2-smoothed QANR potential. The stars correspond to the times of the first mass transfer from the boundary at origin. Larger m correspond to faster mass transfers (as there is more diffusion).

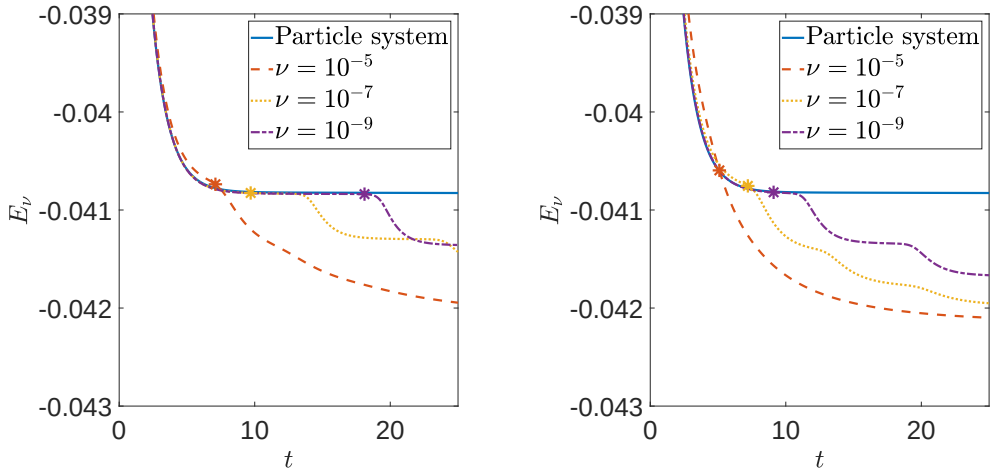

(a) m = 1.5 (b) m=3

Figure 5.21: Time evolution of the energy with the C^2-smoothed QANR potential. The stars correspond to the times of the first mass transfer from the boundary. The energy staircasing gets accelerated by increasing m (more diffusion, faster mass transfers).

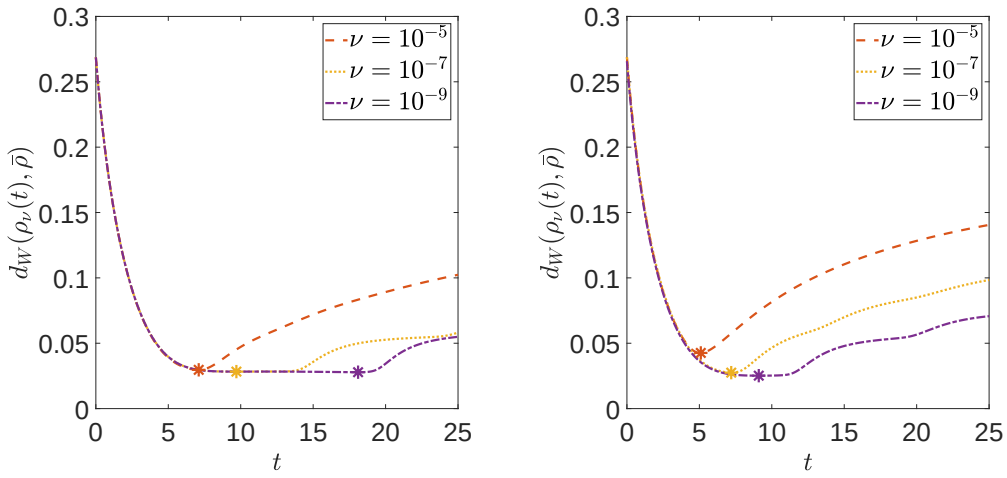

(a) m = 1.5 (b) m=3

Figure 5.22: Distance between the solutions of the diffusive model and the unstable equilibrium of the plain aggregation model. The minimum distances (achieved at times indicated by stars) occur faster for larger m. On the other hand, these minimum distances decrease with lowering m.

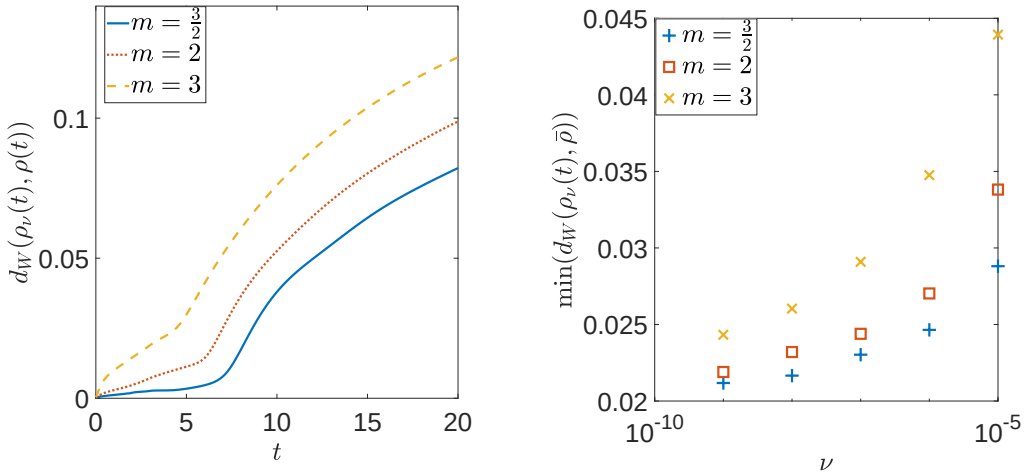

(a) (b)

Figure 5.23: Results for various values of the exponent m. (a) Decreasing m improves the approximation by nonlinear diffusion for fixed ν (here $\nu = 10^{-5}$). (b) By decreasing m, the solutions of the diffusive model pass more closely by the unstable equilibrium of the plain aggregation model.

These numerical results further support Theorem 5.0.1 and suggest that any nonlinear diffusion with $m > 1$ will regularize the model in essentially the same ways that we have thus far discovered with quadratic diffusion.

Chapter 6

Conclusion and future directions

Summary of findings

What have we shown in this thesis? Simply, we have conclusively demonstrated that the widely used plain aggregation model in domains with boundaries (1.4) can dynamically achieve equilibria that are not minimizers of the energy. One could view this is as a deficiency of the model because the model can be formulated as an energy gradient flow! Intuition then leads one to expect steady states of the model should be minimizers of the energy. We showed this a generic phenomenon as in both one and two dimensions such equilibria are observed dynamically from non-trivial initial conditions for a variety of interaction potentials and boundary geometries. Furthermore we showed that equilibria can be numerically calculated using the variational framework in [10]. These equilibria can be explicitly calculated in some cases.

In Chapter 3 we established a significant result in one dimension when considering the primarily investigated interaction potential of this thesis, namely the QANR potential (see Section 3.1). We found numerical and analytical evidence suggesting that equilibria which are not energy minima are the overwhelming majority of achieved states from any evolution of an initial condition where agents interact with a boundary.

Though not as thoroughly researched, we also investigated a C^1-smoothed version of the QANR potential (see Section 3.2) which exhibits delta accumulations as equilibria in free space. We explicitly computed equilibria and could characterize their stability, showing that there were indeed equilibria that were not minimizers of the energy. These states were observed dynamically from initial conditions concentrated near the boundary. Finally we showcased a Morse-type interaction potential (see Section 3.3) where similar findings were made and even though it is not reported in this thesis, the author would point out here that many other interaction potentials were simulated and in every case one could find energetically unstable equilibria.

In Chapter 4 we studied just the QANR potential in two dimensions with both a single boundary, acting as a "floor" which the external potential acted to move agents towards, and a radial boundary to simulate a confined domain as was studied in one dimension on the line segment $[-x^*, x^*]$. Though

the analysis is more complicated and we had to resort to numerically calculating equilibria in most cases, again energetically unstable equilibria were found from non-trivial initial conditions.

Having highlighted a deficiency with the plain aggregation model, we then proposed a rectification of this. Namely we studied the diffusive model (1.6) in Chapter 5 which is the plain aggregation model with nonlinear diffusion introduced. We numerically showed that the diffusive model does rectify the plain aggregation model. In particular, evolution of the diffusive model will approach, but not equilibrate towards, the unstable equilibria found with the plain aggregation model. We also found that the minimizers of the diffusive model approach the minimizers of the plain aggregation model in the zero diffusion limit ($\nu \to 0$). All the numerical investigations in Chapter 5 are further reinforced by analytic findings in [46].

Future directions of research

Throughout the author's work on this thesis, a number of interesting tangents arose that were only briefly investigated and not reported here. Indeed the space for research of swarming models in the presence of boundaries is still quite fertile. We will only touch on two here, as they refer to material introduced here and the second is of particular importance with regards to the goal of the rectification proposed by way of nonlinear diffusion.

Solution forms with the C^1-smoothed QANR potential. Throughout the investigations of the plain aggregation model we found that the free swarm typically has the same form as the minimizer in free space. That is, except for the study of the C^1-smoothed QANR potential. It is unique amongst the interaction potentials studied as only it gave rise to solutions with free swarm components structurally different from free space equilibria.

In Section 3.2 we presented some dynamically observed equilibria that were entirely composed of delta accumulations. Recall as well that the free space minimizer of the C^1-smoothed QANR potential is a sum of delta accumulations. However, through our dynamical investigations we came across approximate steady states that were not entirely composed of delta accumulations (see Figure 6.1). The point of interest here is that there appears to be some particles that have not formed as a delta accumulation near the boundary at $x = 0$. This seems to suggest that in this case, part of the swarm away from the boundary is not a delta accumulation. It may also be the case that some very slow dynamics are present.

On the rectification of the plain aggregation model with nonlinear diffusion. Though we have shown how the diffusive model flows away from unstable equilibria of the plain aggregation model, we have not been able to argue whether the steady states of the diffusive model are energy minima or not for all cases of ν. Through the author's investigations, the diffusive model does flow into energy minima as long as the observed steady states are composed of a single component. However, if the diffusive model forms multiple disconnected components then the author has not been able to

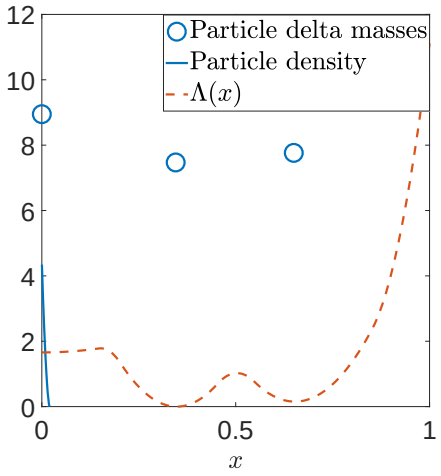

Figure 6.1: Dynamic simulations using the particle method for the C^1-smoothed QANR potential with $\epsilon = 0.2$. $\Lambda(x)$ is shown, though it has been vertically shifted and magnified for clarity. Additionally, the masses of the deltas have been magnified 25 times for clarity as well. Approximate steady state at $t = 100$ from an equidistant distribution of particles in the region $[0, 0.5]$. Note that this state seems to have a small portion near the boundary that is a classical density and seems like it could be in equilibrium, given the profile of $\Lambda(x)$.

show conclusively that the observed steady states are energy minima. Indeed some cases show that $\Lambda(x)$ seems to decrease away from the mass near the wall, while in some other cases $\Lambda(x)$ seems to increase away from the mass near the wall (see Figure 6.2).

Now, these considerations so far are just for the smoothed QANR potentials. The QANR potential with the diffusive model appears to form single component steady states which are energy minima (see Figure 5.8). With this acknowledgement, the author would like to point out next steps they would take in order to investigate whether the C^1-smoothed QANR potential with the diffusive model evolves into energy minima or not.

The first thing to point out is that the concavity of $\Lambda(x)$ for $x \notin \operatorname{supp} \rho$ can still be characterized by how much mass is within ϵ of the given point x as could be done in the plain aggregation model. Indeed, for $x \notin \operatorname{supp}(\rho)$ we get

$$\Lambda''(x) = M - \frac{1}{2\epsilon} \int_{-\epsilon}^{\epsilon} \rho(y)\, \mathrm{d}y.$$

As $\Lambda(x)$ is C^1 when considering the C^1-smoothed QANR potential, understanding the concavity of $\Lambda(x)$ could reveal whether equilibria are minimizers or not. One additional thing that may be worthwhile to consider in tandem with this might be the evolution of $\Lambda(x)$ itself. That is it may be

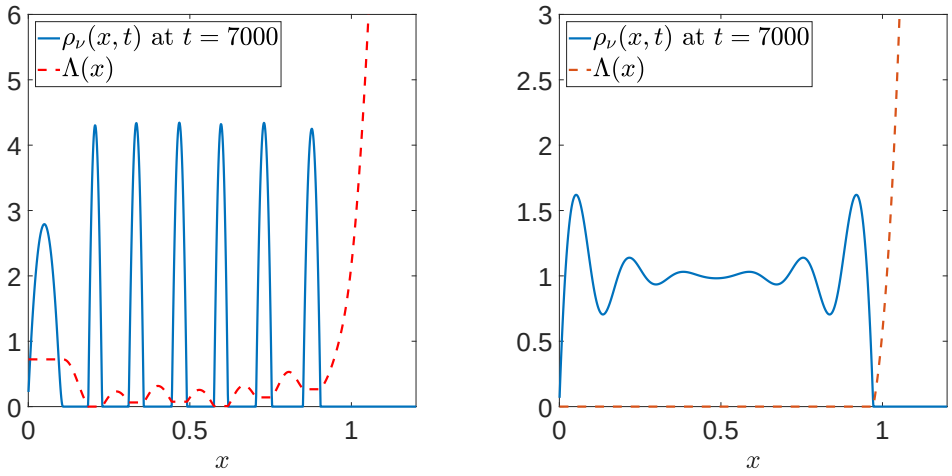

(a) (b)

Figure 6.2: Long time dynamics of the diffusive model (1.6) with the C^1-smoothed QANR potential and $\epsilon = 0.1$. Both states were initialized at a constant density state in $[0, 0.5]$ with total mass 1. (a) A multi-component approximate steady state with $\nu = 10^{-5}$. Note $\Lambda(x)$ appears to decrease away from the first bump suggesting that this is not a minimizer. (b) A single-component approximate steady state with $\nu = 10^{-4}$. Note $\Lambda(x)$ increases away from the component, suggesting that this is a minimizer.

worthwhile to consider

$$\frac{\mathrm{d}\Lambda}{\mathrm{d}t} = \int K(x-y)(\rho(y)\Lambda_{yy}(y) + \rho_y(y)\Lambda_y(y))\,\mathrm{d}y.$$

One might be able to argue whether if $\Lambda(x)$ is concave between compact swarms then can $\Lambda(x)$ ever become convex? And if so, how can it?

Bibliography

[1] L. Ambrosio, N. Gigli, and G. Savaré. *Gradient Flows in Metric Spaces and in the Space of Probability Measures*. Lectures in Mathematics ETH Zürich. Birkhäuser Verlag, Basel, 2005.

[2] D. Balagué, J. A. Carrillo, T. Laurent, and G. Raoul. Dimensionality of local minimizers of the interaction energy. *Arch. Ration. Mech. Anal.*, 209(3):1055–1088, 2013.

[3] D. Balagué, J. A. Carrillo, T. Laurent, and G. Raoul. Nonlocal interactions by repulsive-attractive potentials: Radial ins/stability. *Phys. D*, 260:5–25, 2013.

[4] J. M. Ball. Dynamic energy minimization and phase transformations in solids. In *ICIAM 91 (Washington, DC, 1991)*, pages 3–14. SIAM, Philadelphia, PA, 1992.

[5] J. M. Ball, P. J. Holmes, R. D. James, R. L. Pego, and P. J. Swart. On the dynamics of fine structure. *J. Nonlinear Sci.*, 1(1):17–70, 1991.

[6] J. Bedrossian, A. L. Bertozzi, and N. Rodriguez. Local and global well-posedness for aggregation equations and patlak-keller-segel models with degenerate diffusion. *Nonlinearity*, 24(6):1683–1714, 2011.

[7] J.-D. Benamou and Y. Brenier. A computational fluid mechanics solution to the Monge-Kantorovich mass transfer problem. *Numer. Math.*, 84(3):375–393, 2000.

[8] A. J. Bernoff, M. R. D'Orsogna, L. Edelstein-Keshet, and C. M. Topaz. Locust dynamics: Behavioral phase change and swarming. *PLoS Comput. Biol.*, 8(8):e1002642, 11, 2012.

[9] A. J. Bernoff, A. J. Leverentz, and C. M. Topaz. Asymptotic dynamics of attractive-repulsive swarms. *SIAM J. Appl. Dyn. Syst.*, 8(3):880–908, 2009.

[10] A. J. Bernoff and C. M. Topaz. A primer of swarm equilibria. *SIAM J. Appl. Dyn. Syst.*, 10(1):212–250, 2011.

[11] A. L. Bertozzi, J. A. Carrillo, and T. Laurent. Blow-up in multidimensional aggregation equations with mildly singular interaction kernels. *Nonlinearity*, 22(3):683–710, 2009.

[12] A. L. Bertozzi and Y. Huang. Self-similar blowup solutions to an aggregation equation in $\mathbb{R}^n$. *SIAM J. Appl. Math.*, 70(7):2582–2603, 2010.

[13] A. L. Bertozzi, T. Kolokolnikov, H. Sun, and D. Uminsky. A theory of complex patterns arising from 2D particle interactions. *Phys. Rev. E, Rapid Communications*, 84:015203(R), 2011.

[14] A. L. Bertozzi and T. Laurent. Finite-time blow-up of solutions of an aggregation equation in $\mathbf{R}^n$. *Comm. Math. Phys.*, 274(3):717–735, 2007.

[15] A. L. Bertozzi, T. Laurent, and F. Léger. Aggregation and spreading via the newtonian potential: The dynamics of patch solutions. *Math. Models Methods Appl. Sci.*, 22(Supp. 1):1140005, 2012.

[16] A. L. Bertozzi, M. A. Lewis, and C. M. Topaz. A nonlocal continuum model for biological aggregation. *Bull. Math. Bio.*, 68:1601–1623, 2006.

[17] A. L. Bertozzi and D. Slepčev. Existence and uniqueness of solutions to an aggregation equation with degenerate diffusion. *Commun. Pure Appl. Anal.*, 9(6):1617–1637, 2010.

[18] M. Bodnar and J. J. L. Velazquez. An integro-differential equation arising as a limit of individual cell-based models. *J. Differential Equations*, 222(2):341–380, 2006.

[19] M. Burger and M. Di Francesco. Large time behavior of nonlocal aggregation models with nonlinear diffusion. *Netw. Heterog. Media*, 3(4):749–785, 2008.

[20] M. Burger, M. Di Francesco, and M. Franek. Stationary states of quadratic diffusion equations with long-range attraction. *Comm. Math. Sci.*, 11(3):709–738, 2013.

[21] M. Burger, R. C. Fetecau, and Y. Huang. Stationary states and asymptotic behavior of aggregation models with nonlinear local repulsion. *SIAM J. Appl. Dyn. Syst.*, 13(1):397–424, 2014.

[22] S. Camazine, J-L. Deneubourg, N. R. Franks, J. Sneyd, G. Theraulaz, and E. Bonabeau. *Self-organization in Biological Systems*. Princeton Studies in Complexity. Princeton University Press, Princeton, NJ, 2003. Reprint of the 2001 original.

[23] J. A. Cañizo, J. A. Carrillo, and F. S. Patacchini. Existence of compactly supported global minimisers for the interaction energy. *Arch. Ration. Mech. Anal.*, 217(3):1197–1217, 2015.

[24] J. A. Carrillo, A. Chertock, and Y. Huang. A finite-volume method for nonlinear nonlocal equations with a gradient flow structure. *Commun. Comput. Phys.*, 17(1):233–258, 2015.

[25] J. A. Carrillo, M. Di Francesco, A. Figalli, T. Laurent, and D. Slepčev. Global-in-time weak measure solutions and finite-time aggregation for nonlocal interaction equations. *Duke Math. J.*, 156(2):229–271, 2011.

[26] J. A. Carrillo, S. Hittmeir, B. Volzone, and Y. Yao. Nonlinear aggregation-diffusion equations: Radial symmetry and long time asymptotics. *preprint arXiv:1603.07767*, 2017.

[27] J. A. Carrillo, R. J. McCann, and C. Villani. Contractions in the 2-Wasserstein length space and thermalization of granular media. *Arch. Ration. Mech. Anal.*, 179(2):217–263, 2006.

[28] J. A. Carrillo, D. Slepčev, and L. Wu. Nonlocal-interaction equations on uniformly prox-regular sets. *Discrete Contin. Dyn. Syst. Ser. A*, 36(3):1209–1247, 2016.

[29] L. Chayes, I. Kim, and Y. Yao. An aggregation equation with degenerate diffusion: Qualitative property of solutions. *SIAM J. Math. Anal.*, 45(5):2995–3018, 2013.

[30] R. Choksi, R. C. Fetecau, and I. Topaloglu. On minimizers of interaction functionals with competing attractive and repulsive potentials. *Ann. Inst. H. Poincaré Anal. Non Linéaire*, 32(6):1283–1305, 2015.

[31] J. Cortés. Discontinuous dynamical systems: A tutorial on solutions, nonsmooth analysis, and stability. *IEEE Control Syst. Mag.*, 28(3):36–73, 2008.

[32] J. Crank. *The Mathematics of Diffusion*. Oxford University Press, 2 edition, 1979.

[33] Q. Du and P. Zhang. Existence of weak solutions to some vortex density models. *SIAM J. Math. Anal.*, 34(6):1279–1299, 2003.

[34] W. E. Dynamics of vortex liquids in Ginzburg-Landau theories with applications to superconductivity. *Physical Review B*, 50(2), 1994.

[35] L. Edelstein-Keshet and A. Mogilner. A non-local model for a swarm. *J. Math. Biol.*, 38:534–570, 1999.

[36] R. Eftimie, G. de Vries, and M. A. Lewis. Complex spatial group patterns result from different animal communication mechanisms. *Proceedings of the National Academy of Sciences*, 104(17):6974–6979, 2007.

[37] M. Egerstedt and M. Ji. Distributed coordination control of multi-agent systems while preserving connectedness. *IEEE Trans. Robot.*, 23(4):693–703, 2007.

[38] L. C. Evans. *Partial Differential Equations*, volume 19 of *Graduate Studies in Mathematics*. American Mathematical Society, Providence, RI, second edition, 2010.

[39] J. H. M. Evers and T. Kolokolnikov. Metastable states for an aggregation model with noise. *SIAM J. Appl. Dyn. Syst.*, 15(4):2213–2226, 2016.

[40] K. Fellner and B. D. Hughes. Continuum models of cohesive stochastic swarms: The effect of motility on aggregation patterns. *Phys. D*, 260:26–48, 2013.

[41] K. Fellner and G. Raoul. Stable stationary states of non-local interaction equations. *Math. Models Methods Appl. Sci.*, 20(12):2267–2291, 2010.

[42] A. E. Fernando, K. A. Landman, and M. J. Simpson. Nonlinear diffusion and exclusion processes with contact interactions. *Phys. Rev. E*, 81(1), 2010.

[43] R. C. Fetecau and Y. Huang. Equilibria of biological aggregations with nonlocal repulsive-attractive interactions. *Phys. D*, 260:49–64, 2013.

[44] R. C. Fetecau, Y. Huang, and T. Kolokolnikov. Swarm dynamics and equilibria for a nonlocal aggregation model. *Nonlinearity*, 24(10):2681–2716, 2011.

[45] R. C. Fetecau and M. Kovacic. Swarm equilibria in domains with boundaries. *SIAM J. Appl. Dyn. Syst.*, 16(3):1260–1308, 2017.

[46] R. C. Fetecau, M. Kovacic, and I. Topaloglu. Swarming in domains with boundaries: Approximation and regularization by nonlinear diffusion. *Discrete Contin. Dyn. Syst. Ser. B*, 2018. (accepted); arXiv preprint http://arxiv.org/abs/1711.03622.

[47] A. F. Filippov. *Differential Equations with Discontinuous Righthand Sides*, volume 18 of *Mathematics and its Applications (Soviet Series)*. Kluwer Academic Publishers Group, Dordrecht, 1988. Translated from the Russian.

[48] J. M. Haile. *Molecular Dynamics Simulation: Elementary Methods*. John Wiley and Sons, Inc., New York, 1992.

[49] D. Holm and V. Putkaradze. Aggregation of finite-size particles with variable mobility. *Phys Rev Lett.*, 95:226106, 2005.

[50] D. Holm and V. Putkaradze. Formation of clumps and patches in self-aggregation of finite-size particles. *Physica D.*, 220(2):183–196, 2006.

[51] P. J. Holmes and P. J. Swart. Energy minimization and the formation of microstructure in dynamic anti-plane shear. *Arch. Rational Mech. Anal.*, 121(1):37–85, 1992.

[52] B. D. Hughes. *Random Walks and Random Environments*, volume 1. Oxford University Press, 1995.

[53] B. D. Hughes, K. A. Landman, and C. J. Penington. Building macroscale models from microscale probabilistic models: A general probabilistic approach for nonlinear diffusion and multi-species phenomena. *Phys. Rev. E*, 84:1–12, 2011.

[54] B. D. Hughes, K. A. Landman, and M. J. Simpson. Multi-species simple exclusion processes. *Physica A: Statistical Mechanics and its Applications*, 388(4):399–406, 2009.

[55] A. Huth and C. Wissel. The simulation of fish schools in comparison with experimental data. *Ecological Modelling*, 75-76:135d–146, 1994. State-of-the-Art in Ecological Modelling: Proceedings of ISEM's 8th International Conference.

[56] G. Kaib. Stationary states of an aggregation equation with degenerate diffusion and bounded attractive potential. *SIAM J. Math. Anal.*, 49(1):272–296, 2017.

[57] R. J. McCann. Existence and uniqueness of monotone measure-preserving maps. *Duke Math. J.*, 80(2):309–323, 1995.

[58] S. Motsch and E. Tadmor. Heterophilious dynamics enhances consensus. *SIAM Review*, 56:577–621, 2014.

[59] D. Pita, B. A. Moore, L. P. Tyrrell, and E. Fernández-Juricic. Vision in two cyprinid fish: implications for collective behavior. *PeerJ*, 3:e1113, August 2015.

[60] Z. Qian, X. E. Cheng, and Y. Q. Chen. Automatically detect and track multiple fish swimming in shallow water with frequent occlusion. *PLOS ONE*, 9(9):1–12, 2014.

[61] R. Simione, D. Slepčev, and I. Topaloglu. Existence of ground states of nonlocal-interaction energies. *J. Stat. Phys.*, 159(4):972–986, 2015.

[62] D. Slepčev and L. Wu. Nonlocal interaction equations in environments with heterogeneities and boundaries. *Comm. Partial Differential Equations*, 40(7):1241–1281, 2015.

[63] G. Toscani. One-dimensional kinetic models of granular flows. *M2AN Math. Model. Numer. Anal.*, 34(6):1277–1291, 2000.

[64] C. Villani. *Topics in Optimal Transportation*, volume 58 of *Graduate Studies in Mathematics*. American Mathematical Society, Providence, RI, 2003.

[65] Y. Zhang. On continuity equations in space-time domains. *arXiv preprint https://arxiv.org/abs/1701.06237*, 2017.

Appendix A

Morse Potential - Explicit System

We provide below the six equations derived from (3.66). The four equations that ensure $\Lambda(x) = \lambda_2$ for $x \in [d_1, d_1 + d_2]$ are:

$$\frac{C}{L^{-2}+\mu^2}\exp\left(\frac{d_1}{L}\right)\Big(-\frac{1}{L}\cos(\mu d_1)-\mu\sin(\mu d_1)\Big)$$
$$+\frac{D}{L^{-2}+\mu^2}\exp\left(\frac{d_1}{L}\right)\Big(-\frac{1}{L}\sin(\mu d_1)+\mu\cos(\mu d_1)\Big)+\frac{L\lambda_2}{\epsilon}\exp\left(\frac{d_1}{L}\right)+S=0,$$
$$\frac{C}{1+\mu^2}\exp(d_1)\Big(-\cos(\mu d_1)-\mu\sin(\mu d_1)\Big)$$
$$+\frac{D}{1+\mu^2}\exp(d_1)\Big(-\sin(\mu d_1)+\mu\cos(\mu d_1)\Big)+\frac{\lambda_2}{\epsilon}\exp(d_1)+S=0,$$
$$\frac{C}{L^{-2}+\mu^2}\exp\left(-\frac{d_1+d_2}{L}\right)\Big(-\frac{1}{L}\cos(\mu(d_1+d_2))+\mu\sin(\mu(d_1+d_2))\Big)$$
$$+\frac{D}{L^{-2}+\mu^2}\exp\left(-\frac{d_1+d_2}{L}\right)\Big(-\frac{1}{L}\sin(\mu(d_1+d_2))-\mu\cos(\mu(d_1+d_2))\Big)$$
$$+\frac{L\lambda_2}{\epsilon}\exp\left(\frac{-(d_1+d_2)}{L}\right)=0,$$
$$\frac{C}{1+\mu^2}\exp(-(d_1+d_2))\Big(-\cos(\mu(d_1+d_2))+\mu\sin(\mu(d_1+d_2))\Big)$$
$$+\frac{D}{1+\mu^2}\exp(-(d_1+d_2))\Big(-\sin(\mu(d_1+d_2))-\mu\cos(\mu(d_1+d_2))\Big)+\frac{\lambda_2}{\epsilon}\exp(-(d_1+d_2))=0.$$

The equation that ensures $\Lambda(0) = \lambda_1$ is

$$
\begin{aligned}
&- GL\Big(\frac{C}{L^{-2}+\mu^2}\exp\left(-\frac{y}{L}\right)\Big(-\frac{1}{L}\cos(\mu y)+\mu\sin(\mu y)\Big)\\
&\quad+\frac{D}{L^{-2}+\mu^2}\exp\left(-\frac{y}{L}\right)\Big(-\frac{1}{L}\sin(\mu y)-\mu\cos(\mu y)\Big)\\
&\quad+\frac{L\lambda_2}{\epsilon}\exp\left(-\frac{y}{L}\right)\Big)\Big|_{y=d_1}^{y=d_1+d_2}+\Big(\frac{C}{1+\mu^2}\exp(-y)\Big(-\cos(\mu y)+\mu\sin(\mu y)\Big)\\
&\quad+\frac{D}{1+\mu^2}\exp(-y)\Big(-\sin(\mu y)-\mu\cos(\mu y)\Big)+\frac{\lambda_2}{\epsilon}\exp(-y)\Big)\Big|_{y=d_1}^{y=d_1+d_2}+S(1-GL)=\lambda_1.
\end{aligned}
$$

Finally, the mass constraint equation gives

$$
S+\frac{C}{\mu}(\sin(\mu(d_1+d_2))-\sin(\mu d_1))-\frac{D}{\mu}(\cos(\mu(d_1+d_2))-\cos(\mu d_1))-\frac{\lambda_2 d_2}{\epsilon}=M.
$$